Mechanisms of Fracture and Friction of Crustal Rock in Simulated Geologic Environments

B. K. Atkinson, N. J. Price, S. M. Dennis

P. G. Meredith, D. MacDonald, and R. F. Holloway

Imperial College of Science and Technology
Geology Department
London SW7 2BP
Great Britain

USGS Contract No. 14-08-0001-18325

Supported by the Earthquake Hazards Reduction Program

OPEN-FILE No. 81-277

U. S. Geological Survey
OPEN FILE REPORT

IMPERIAL COLLEGE OF SCIENCE AND TECHNOLOGY

Department of Geology, Royal School of Mines
Prince Consort Road, London SW7 2BP
Telephone: 01-589 5111 Telex: 261503

MECHANISMS OF FRACTURE AND FRICTION OF CRUSTAL ROCK IN SIMULATED GEOLOGIC ENVIRONMENTS

Final (second semi-annual) technical report for FY 1980 to the managers of the US National Earthquake Hazards Reduction Program.

by

B.K. ATKINSON and N.J. PRICE (Principal Investigators)
with contributions by
S.M. DENNIS, P.G. MEREDITH, D. MACDONALD, R.F. HOLLOWAY

Sponsored by the US Geological Survey under
Contract No.: 14-08-0001-18325
Contract effective: 1 October 1979 - 30 September 1980
Amount of contract: $84,000
Date of report: 1 November 1980

MECHANISMS OF FRACTURE AND FRICTION OF CRUSTAL ROCK IN SIMULATED GEOLOGIC ENVIRONMENTS

Contract No: 14-08-0001-18325

Principal Investigators: B. K. ATKINSON, N. J. PRICE

Additional Contributions by: S. M. DENNIS, P.G. MEREDITH, D. MACDONALD, and R.F. HOLLOWAY

IMPERIAL COLLEGE OF SCIENCE AND TECHNOLOGY
GEOLOGY DEPARTMENT
LONDON SW7 2BP
GREAT BRITAIN

01-589-5111 X 1683, X 1690

Investigations

1. Construction of apparatus for high-temperature (up to 500°C) and high-pressure (up to 3 kbar) apparatus for fracture mechanics studies of critical stress intensity factors and subcritical (stress corrosion) crack growth in crustal rocks.

2. Fracture mechanics experiments and associated acoustic emission studies of stress corrosion crack growth in granites and basalts.

3. Study of thermal and stress cycling on fracture and acoustic emission properties of rock.

4. Experimental study of influence of pore water on sliding properties of faults in granites and basalts at conditions of temperature and pressure typical of the upper 15 km of the earth's crust.

5. Identification of active mechanisms of deformation in the above experiments and construction of fracture and friction deformation mechanism maps.

Results

1. We have constructed 3 new pieces of apparatus for fracture mechanics experiments. (a) double torsion environmental cell for deforming rock plates in vacuum or vapour environments to 500°C, (b) short rod apparatus for tests on cores at ambient humidity to 300°C, and (c) internally pressurized thick-walled cylinder apparatus for tests to 3 kbar and 500°C. All three pieces of

1. REPORT SUMMARY

CONTENTS

2. SUBCRITICAL CRACK PROPAGATION IN ROCK: THEORY, EXPERIMENTAL RESULTS AND APPLICATIONS

B.K. Atkinson

ABSTRACT

The micromechanisms of tensile fracture are reviewed, with particular emphasis on the influence of chemical effects on fracture controlled by pre-existing cracks (stress corrosion). A fracture mechanism map for quartz is constructed using a combination of theoretical insights and experimental data. The manner in which stress corrosion will modify the predictions of fracture mechanism maps is discussed by reviewing the numerous theories of stress corrosion. Experimental data are presented on stress corrosion in tensile deformation of quartz, quartz rocks, calcite rocks, basaltic rocks, granitic rocks and other geological materials. Although the experimental evidence for stress corrosion is overwhelming, very few data were obtained under conditions that simulate those in the bulk of the earth's crust and so the extent of its geophysical significance is yet to be fully established. Examples are given, however, of how invoking stress corrosion as a rate-controlling deformation mechanism sheds new light on extremely diverse geophysical phenomena, such as: predicting the strength and sliding friction properties of rocks, modelling earthquake rupture, the stability of hot, dry rock geothermal reservoirs, stimulation of oil and gas reservoirs, the crack-seal mechanism of rock deformation and low stress dilatancy, fracture mechanics of lunar rocks, magmatic intrusions and the relaxation of internal stresses in rock.

apparatus are designed to be used in measurements of crack propagation parameters for mode I deformation (tensile). Acoustic emission can be monitored simultaneously with other parameters relevant to the test.

2. Additional apparatus development has been done to enable the measurement of mode II (in-plane shear) crack propagation parameters. Two methods have been chosen: (a) one based on a double direct shear specimen for tests at ambient pressure, and (b) one based on a modification to the analysis of post-failure stress/displacement data from triaxial tests suggested by Rice (Proc. Int. School of Physics 'Enrico Fermi', LXXVIII, 1979).

3. Double torsion experiments to study stress corrosion and acoustic emission of Whin Sill dolerite gave the following results for n (stress corrosion index, $V = \alpha K_I^n$) n_E (event rate index, $dN_E/dt = \beta K_I^{n_E}$), and n_R (ring-down rate index, $dN_R/dt \cong \gamma K_I^{n_R}$). Crack velocity is V, stress intensity factor is K_I, α, β and γ are constants, N_R and N_E are number of ring-down counts and events, respectively, and t is time.

	Air, 20°C, 30%RH	H_2O, 20°C	H_2O, 75°C
n	31.2 (0.990)	29.0 (0.992)	28.4 (0.995)
n_E	31.1 (0.984)	29.1 (0.977)	
n_R	32.9 (0.981)	29.9 (0.973)	

Figures in brackets are correlation coefficients.

The activation enthalpy for crack propagation determined by two different methods gave the following results: 30.4±1.9 kJ.mole^{-1} and 34 to 47.6 kJ.mole^{-1}. K_{Ic} for this dolerite was 3.28±0.1 MN.m^{-3}/2.

As we have found for other materials the rate of acoustic emission is a good guide to the crack velocity.

4. Short rod tests have been run on a variety of rock types at 20°C and ambient humidity to check out the validity of this test for rock and to get an idea of K_{Ic} values for materials on which no data existed before this study. Some results are given here. Where possible they are compared with results for double torsion experiments.

Material	K_{Ic} ($MN.m^{-3/2}$) SR	DT
Westerley granite	1.62±.08	1.74
Whin Sill dolerite	2.96±.19	3.28
Black gabbro	2.73±.40	2.88
Pink granite	1.53±.17	1.66
Icelandic Tholeiite	0.87±.06	
Serpentinized dunite	1.39±.38	
Arkansas novaculite	1.77±.25	1.34
Oughtibridge gannister	1.39±.27	
Penant sandstone	1.97±.06	
Tennessee sandstone	0.79±.05	0.45
Carrara marble	0.82±.04	0.64
Solnhofen limestone	1.09±.06	1.06

5. Acoustic emission was monitored from thermal and stress cycled Westerley granite. Also stress intensity factor /crack velocity diagrams were determined for heat treated granite.

On increasing the maximum temperature of heat treatment the microcrack density increases and K_{Ic} decreases. The most marked change in these properties occurs between 200°C and 300°C. During stress cycling the Kaiser effect is only observed up to a specific fraction of K_{Ic}, thereafter there is an anomalous increase in the acoustic emission that suggests the release of locked-in, residual strain energy. With increasing heat-treatment there is a reduction in the stress intensity factor required to obtain a given crack velocity.

6. Preliminary estimates of critical strain energy release rate in mode II deformation for granite are of the order $10^4 J.m^{-2}$.

7. A fracture mechanism map for quartz has been constructed. It may be inferred from this diagram that the propagation of pre-existing cracks by stress corrosion will be the most important mechanism of tensile failure in the upper 15-20 km of the earth's crust.

8. A study of the influence of pore water on the fracture and sliding friction strength of Westerley granite shows that at 20°C the presence of water has little effect. i.e. the so-called Rehbinder effects are not very important. The following results were obtained from stress relaxation experiments on dry and wet, intact and initially pre-faulted specimens at 300°C and 400°C and under a pore water pressure of 200 bars or 1 kbar at a fixed effective

confining pressure of 1.5 kbar.

(a) Dry granite shows no reduction in sliding stress at strain rates down to $10^{-12}s^{-1}$.

(b) The sliding stress on wetting is reduced at strain rates below ca. $10^{-7}s^{-1}$, but not by as much as Tennessee sandstone or Mojave quartzite.

(c) Increasing pore fluid pressure at constant effective pressure substantially increases the rate of stress relaxation.

(d) Values of the stress exponent, n, where strain rate $\propto$ (stress)^n are as follows:

P_{H_2O}	n
200 bars	25
1000 bars	6

(e) The activation enthalpy for frictional sliding of wet specimens of Westerley granite from 300°C to 400°C, varied from 20 - 45 kJ.mole^{-1}.

These results do not support a model in which the rate of sliding of wet specimens is controlled by pressure solution. An alternative model based on stress corrosion has been developed which is a more satisfactory fit to these data.

Similar work is now under way on a Tholeiitic basalt. Additionally, textural studies of specimens deformed in constant strain rate mode to total strains of ca. 3-5% are being performed.

Reports

ATKINSON, B.K. 1980. An outline proposal of some aims, strategies and objectives in earthquake prediction. In Proceedings 2nd Workshop on European Earthquake Prediction Programme jointly organised by European Space Agency and Parliamentary Assembly of the Council of Europe, Strasbourg, 1980, 135-155.

ATKINSON, B.K. 1980. Fracture Mechanics modelling of earthquake generating processes. In Proceedings of an Interdisciplinary Conference on Earthquake Prediction Research in the N. Anatolian Fault Zone, Istanbul, 1980 (in press)

ATKINSON, B.K. and Avdis, V. 1980. Fracture Mechanics parameters of some rock-forming minerals determined with an indentation technique. Int. J. Rock Mech. Min. Sci. and Geomech. Abstr. (in press).

Norton, M.G. and ATKINSON, B.K. 1980. Stress-dependent morphological features on fracture surfaces of quartz and glass. Tectonophysics (in press).

ATKINSON, B.K. 1980. Review of subcritical crack propagation in rock. Proc. 26th International Geological Congress, Paris, 1980. (To be published in J. Struct. Geol.)

ATKINSON, B.K. and Rawlings, R.D. 1980. Acoustic emission during stress corrosion cracking in rocks. Proc. 3rd Maurice Ewing Symposium on Earthquake Prediction, New York, 1980. Geophysical Union (in press).

ATKINSON, B.K. and Meredith, P.G. 1980. Stress corrosion of quartz: Influence of chemical environment. Tectonophysics (in press).

Meredith, P.G. and ATKINSON, B.K. 1980. Stress corrosion and acoustic emission of Whin Sill dolerite (in preparation)

Dennis, S.M. and ATKINSON, B.K. 1980. The influence of pore fluids on the sliding of faulted surfaces of Westerley granite under simulated geologic environments (in prep.)

Dennis, P.F. and ATKINSON, B.K. 1980. Flow and fracture deformation mechanism maps for quartz (in preparation)

ATKINSON, B.K. 1981. Earthquake precursors. Physics in Technology 12.

ATKINSON, B.K. 1980. How to take the shock out of earthquakes. The Guardian, 25 September.

INTRODUCTION

The fracture mechanics description of crack propagation (Irwin, 1958) allocates a key role to the stress intensity factor, K, which is a measure of a body's resistance to fracture. Fracture propagation problems can be analysed in terms of the three stress intensity factors, K_I, K_{II} and K_{III}, which pertain to the three fundamental modes of crack propagation. These are: mode I - tensile; mode II - in-plane shear; mode III - anti-plane shear. For a two-dimensional plane crack of any mode the stress intensity factor is given by

$$K = Y\sigma_a a^{\frac{1}{2}} \qquad (1)$$

where Y is a geometrical constant, σ_a is the remote applied stress and a is a characteristic crack length.

If the stress intensity factor is raised above a critical value, K_c, which is a material constant, then the crack will propagate at velocities approaching those of sound in the medium. For many materials such as oxides and silicates, however, crack propagation can occur at much lower values of K than K_c. A variety of environmentally dependent mechanisms, noteably stress corrosion, can facilitate this stable, quasistatic subcritical crack propagation. It occurs at velocities which decrease as K is lowered to some threshold value, K_o, below which no crack propagation is observed.

In recent years there has been a rapid increase in the number of experimental studies designed to advance our understanding of subcritical crack propagation in rocks. The impetus for this has come from both the extensive work of materials scientists, who have analysed the premature failure of structural engineering components in terms of subcritical crack propagation, and the growing awareness amongst earth scientists that subcritical crack growth can explain many previously puzzling problems in geophysics.

This paper has four main sections. In the first I will outline the complexities of subcritical failure in rocks and present a fracture mechanism map for quartz to illustrate some of these phenomena. In the second section the current state of modelling some aspects of subcritical failure at a theoretical level is reviewed. The third section presents the findings of experimental studies of subcritical crack propagation in rocks. The emphasis here is on results, as experimental methods are to be reviewed elsewhere (Atkinson, 1981). The fourth section contains a number of illustrations of the potential importance of subcritical cracking in geophysical phenomena.

To a very large extent this work concentrates on results for mode I, tensile crack propagation under the influence of stress corrosion. This arises mainly because the vast majority of experimental results pertain to this mode. However, not only is this mode of fracture in itself of fundamental importance in the fracture of rocks in the earth, but in addition there is no obvious physico chemical

reason why the form of the law to describe processes such as stress corrosion, but not necessarily the parameters, should depend on mode (Das and Scholz, 1980).

MICROMECHANISMS OF FRACTURE

Following Ashby and others (Ashby et al., 1979; Gandhi and Ashby, 1979) we can identify four main micromechanisms of tensile crack propagation for materials that cleave. I consider here only those mechanisms leading to fracture after relatively modest plastic flow (<10%). Fractures after large strain (10 - 100%) without cleavage are not considered.

Fracture controlled by pre-existing cracks

If a brittle solid contains a crack or a flaw it may propagate at stresses which are lower than that required for slip or twinning on any crystallographic system. Fracture occurs at a stress, σ_f, given by

$$\sigma_f \simeq \left(\frac{E\ G_c}{\pi\ c} \right)^{\frac{1}{2}} \qquad (2)$$

where E is Young's modulus, 2c is the pre-existing crack length and G_c is the critical strain energy release rate ($G_c = K_I^2(1-\nu^2)/E$ for plane strain, where ν = Poisson's ratio). Because the stress at fracture is less than the yield stress of even the softest slip or twinning system no general plasticity is possible. There may, however, be local plasticity at the crack tip. Gandhi and Ashby (1979) call this mechanism cleavage 1. Note that the fracture strength

of a body is determined by the largest crack it contains.

Fracture controlled by cracks generated through micro-plasticity.

If pre-existing cracks are very small or absent, then the stress can reach the level required to initiate slip or twinning. Provided that slip or twinning only occurs on a limited number of independent systems (less than 5) and the total bulk plastic strain is less than about 1% then internal stresses are generated which can nucleate cracks. This most commonly occurs when slip or twinning dislocations pile up at grain boundaries. Cracks that are nucleated in this way generally have a length which is proportional to the grain size, d, because this is the wavelength of the internal stresses. We can envisage that if the stress for twinning or slip on the softest system exceeds σ^* where

$$\sigma^* \simeq \left(\frac{E\ G_c}{\pi d} \right)^{\frac{1}{2}} \qquad (3)$$

then a crack will propagate as soon as it is formed and fracture will occur at the stress for the onset of micro-plasticity, σ_y. If, however, σ^* is greater than σ_y then a crack nucleated by slip or twinning will not immediately propagate and the stress will have to be raised even further before macroscopic fracture occurs. Gandhi and Ashby (1979) call this mechanism cleavage 2.

Both cleavage 1 and cleavage 2 are mechanisms of fracture

that occur at very low plastic strains (<1%). If the temperature is raised then the flow stress falls until general plasticity or creep is possible. Fracture can still occur under these conditions, however, as described below.

Fracture controlled by cracks generated through general plasticity/grain boundary sliding

Substantial plastic strain (1-10%) precedes fracture by this mechanism. The plasticity blunts small pre-existing cracks and effectively raises the resistance to fracture, G_c. Significant general plasticity or grain boundary sliding can then generate larger grain boundary cracks or cause a pre-existing crack to grow in a stable manner, until its increased length, coupled with the higher stress caused by work-hardening cause it to propagate unstably as a cleavage crack. Gandhi and Ashby (1979) term this mechanism cleavage 3.

At this point it is important to note that because of the delicate balance between the stress required to cause a mineral grain to cleave and the stress required to cause brittle grain boundary cracking it is not always an easy matter to predict which will predominate under any given set of conditions. This balance can be upset by small changes in temperature, impurity content, cement mineralogy and rock texture. The dominant fracture path is best determined from experiments. If brittle intergranular fracture occurs, then Gandhi and Ashby (1979) refer to it as B.I.F.1,2 or 3.

Intergranular creep fracture

The fourth mechanism of fracture that we will consider occurs at high temperatures and low stresses. Failure under these conditions is always by intergranular creep fracture (Gandhi and Ashby, 1979). Voids or wedge cracks nucleate and grow (Söderberg, 1972) on grain or phase boundaries. Nucleation is probably controlled by dislocation creep but when cracks are small growth is by local diffusion; the rate of diffusion being controlled by dislocation creep in the surrounding grains (Ashby et al., 1979). The linking of voids or cracks leads to a relatively low (<10%) - ductility fracture after long periods of creep deformation.

Fracture Mechanism Map

Experimental results and theoretical descriptions of these fracture mechanisms can be combined to aid the construction of a fracture mechanism map for specific materials as described by Ashby et al. (1979) and Gandhi and Ashby (1979). These maps are analogous to plastic flow deformation mechanism maps and indeed are partly based on them. They show the environmental conditions under which different mechanisms of fracture are dominant; i.e. produce failure in the shortest time.

In Figure 1 I show a typical fracture mechanism map for quartz. The method of constructing this figure is outlined in the Appendix. Note, however, that it is based on a new plastic deformation fracture mechanism map derived for quartz

by P. Dennis (personal communication, 1980). The top of Figure 2 is truncated by the stress required for fracture at the ideal strength, i.e. the stress required to overcome the interatomic forces in a perfect crystal.

This is given by

$$\sigma_{ideal} \simeq E/10 \qquad (4)$$

A field is shown on this diagram labelled dynamic fracture which is for the mechanism active at the highest stresses. This field cuts off all other fields of lower stress mechanisms and is the region where even the initial loading must be described in terms of the propagation of an elastic wave through the material.

The map could have superimposed on it contours of time-to-failure or crack velocity but the paucity of data precludes such a refinement at this stage.

One may infer from the fracture mechanism map that for the upper 20 km, or so, of the earth's crust, cleavage (B.I.F.) 1 will be the most important fracture mechanism. For this reason I will concentrate on this mechanism in the ensuing discussion.

Influence of Chemical Effects on Fracture

There are a number of different ways in which the action

of the environment or the chemistry of the phases involved can help lower the barriers to crack propagation. Consider the influence of these variables on cleavage/B.I.F. 1 in quartz.

(a) The presence of liquid water, water vapour or some other reactive species in the crack tip environment can facilitate crack propagation by promoting weakening reactions. For the quartz/water system reactions of the form

$$(\text{-Si-O-Si-}) + H_2O \rightarrow \left(\text{-Si-OH}\cdot\text{HO-Si-}\right) \qquad (5)$$

may occur. The strong silicon-oxygen bonds are replaced with much weaker hydrogen bonds (Scholz, 1972; Martin, 1972; Swain et al., 1973; Atkinson, 1979; Atkinson and Meredith, 1981). This phenomena is known as <u>stress corrosion</u>.

(b) Some solids contain dissolved chemical impurities, such as structurally bound water in quartz, which can have a degrading effect on strength if present in sufficient quantities. During crack propagation stress directed diffusion of these chemical impurities to crack tips may occur, where they can take part in weakening reactions, thus facilitating crack extension (Schwartz and Mukherjee, 1974). In addition, the difference in chemical potential between the highly stressed atoms of the crack tip and those in the bulk of the solid can lead to a concentration gradient of vacancies at the crack tip. The diffusion of vacancies to the crack tip will then

control the crack propagation rate as described by Stevens and Dutton (1971). These diffusion-based mechanisms are only likely to be important at relatively high homologous temperatures.

(c) If the chemical environment contains species which can undergo ion exchange with species in the solid phase, and if there is a gross mis-match in the size of these different species then lattice strains can result from ion exchange which can facilitate crack extension, e.g. exchange of H^+ for Na^+ in silicate glasses (Wiederhorn, 1978).

Atkinson(1979) has suggested that for quartz at least the most important of these effects is stress corrosion at low homologous temperatures.The overwhelming proportion of data on subcritical crack propagation in rocks relates to this phenomenon. I shall concentrate on this aspect of subcritical crack propagation in the rest of this paper.

THEORETICAL BACKGROUND TO STRESS CORROSION

Observations on stress corrosion in a wide range of glasses, oxides and silicates are broadly consistent with a schematic stress intensity factor (K_I)/crack velocity (v) diagram shown in Fig. 2 for mode I crack propagation.

In this diagram K_{Ic} is the critical stress intensity factor and K_o is a threshold stress intensity factor below which no appreciable crack growth occurs. K_o is not commonly

observed even at very low velocities - but consideration of the properties of materials suggests it must exist. In region 1, v is apparently controlled by stress corrosion reactions. At higher K_I values in region 2 the transport of reactive species to the crack tip is believed to be rate controlling. At yet higher K_I values v is controlled by some poorly understood, thermally activated process that is comparatively (but not totally) insensitive to the chemical character of the environment.

The influence of increasing the partial pressure or concentration of water in the environment is as shown. Increasing temperature also tends to shift the K_I-v curves towards the top left hand of the diagram. The influence of hydrostatic pressure is not known. It might be expected that increasing the pressure on a water bearing environment would enhance the rate of stress corrosion because the water molecules become more concentrated and chemical corrosion reactions are enhanced. The limited evidence available from work on metals (Dehart and Liebowitz, 1968) suggests that in some materials, at least, stress corrosion is suppressed by pressure. In some cases K_o may be increased by application of pressure (Gerberich, 1974). Furthermore, Kranz's (1980) study of the influence of pressure on static fatigue of granite can be interpreted to show that increasing pressure decreases the rate of stress corrosion primarily by increasing the activation enthalpy required for the stress corrosion process. Secondary effects might include a retardation of the rate at which corrosive species can reach crack tips by decreasing crack wall spacing under pressure.

As an aside it is worth noting that even for silicate glasses the stress corrosion explanation for the schematic K_I-v curves of Figure 2 is not universally accepted. Marsh (1964), Wiedmann and Holloway (1974) and Williams and Marshall (1975) have suggested that plastic flow may be an alternative explanation - even at ambient temperatures. The latter two authors have attempted to put their ideas into quantitative form. However, it has yet to be shown that the theories of Wiedmann and Holloway (1974) and Williams and Marshall (1975) are consistent with the huge volume of data on the environmental dependence of crack velocity even in silicate glasses. Until then these ideas should be viewed with caution, especially in the light of the marked success of chemical theories of fracture (see later) in accounting for experimental observations of environmentally dependent subcritical cracking (Wiederhorn, 1974; 1978). Moreover, even allowing that plastic flow may be of minor significance in low-temperature subcritical cracking of some minerals, such as calcite or galena, all the available evidence (Martin and Durham, 1975; Dunning et al., 1980) suggests that low-temperature subcritical crack propagation in quartz is <u>not</u> accompanied by plastic flow.

There have been numerous attempts to develop theoretical descriptions of K_I-v curves in terms of chemically assisted stress corrosion processes. The early theories have been reviewed by Anderson and Grew (1977) and will not be repeated here (see also Atkinson, 1979). I will concentrate on the most widely used expressions and those that have been most

recently published.

The two most commonly used equations to describe stress corrosion data are Charles' (1958) power law

$$v = v_o \exp(-\Delta H/RT) K_I^n \tag{6}$$

and the Wiederhorn and Bolz (1970) equation

$$v = v_o' \exp\left[(-\Delta H + 2V^* K_I/(\pi\rho)^{\frac{1}{2}}\right]/RT \tag{7}$$

where v is the crack velocity, v_o and v_o' are pre-exponential factors, ΔH is an activation enthalpy, V^* is an 'activation volume', ρ is the radius of curvature of the crack tip, R is the gas constant, n is a material constant known as the stress corrosion index, T is the absolute temperature and R is the gas constant. Equation (7) is based on the Charles and Hillig (1962) formulation for stress corrosion based upon reaction rate theory and continuum mechanics. Empirical data on stress corrosion are often fit to the equation

$$v = v_o' \exp(-\Delta H + \beta K_I)/RT \tag{8}$$

where β is an experimentally determined constant and equation (8) is identical with equation (7) when $V^* = (\beta/2)(\pi\rho)^{\frac{1}{2}}$.

Although equations 6, 7 and 8 have been widely used in studies of glasses and ceramics, the Charles equation (6)

has been used most commonly in studies of rocks and minerals. In part this is because the Wiederhorn and Bolz equation can only be used to describe region 1 of the schematic K_I-v curve. Charles' equation on the other hand can be used with appropriate changes in v_o, ΔH and n, to describe all three regions of the schematic K_I-v curve. Furthermore, these two theories of stress corrosion are still largely empirical and because n in equation (6) is often large (usually >10) then it is virtually impossible in practice to distinguish between equations (6) and (8).

In an attempt to model chemically enhanced subcritical cracking at the atomic level Lawn (1975) and Lawn and Wilshaw (1975) developed a two-stage description of crack propagation in which reactive species must first be transported to the crack tip before reactions can occur there to facilitate crack extension. The slowest of these two steps, reaction and transport, will control the rate of the overall process. The central idea in crack advance is of an ideally brittle fracture crack in which sequential bond rupture occurs via the lateral motion of atomic kinks along the crack front. For the case when solid/vapour reactions limit the crack velocity (v_r) Lawn found that

$$v_r = V(T)\left[\frac{p_a^o}{p_a}\right]^{\eta/2} \exp\left(-U_o^*/kT\right) \exp\left(G/2N_a kT\right) \qquad (9)$$

where G is the strain energy release rate, V(T) is a slowly

varying temperature-dependent term, p_a^o is the vapour pressure at the crack mouth, p_a^s is the vapour pressure in some reference state, η is the number of molecules of environmental species reacting with one bond in the solid to produce a weakened state, U_o^* is a collection of various uncertainty energy constants, k is Boltzmann's constant, and N_a is the surface density of crack plane bonds. For transport limited crack velocity (v_t) Lawn (1975) obtains

$$v_t = \kappa a_o p_a^o \; / \; \eta N_a (2\pi m k T)^{\frac{1}{2}} \qquad (10)$$

where κ is an attenuation factor associated with the increasing incidence of retarding, diffuse molecule wall collisions as the gas approaches the crack tip, a_o is the lattice spacing, representing the reaction cross section per unit width of crack front presented to the impinging gas molecules by the crack tip bonds, m is the molecular mass of the gaseous species.

These latter equations can account quite well for stress corrosion crack growth in the sapphire/water vapour system (Lawn, 1975). As it stands, however, Lawn's atomistic theory would not be able to account for more complex behaviour, such as shown by polycrystalline, polyphase ceramics and rocks, or more complex chemical effects. In principle, however, Lawn's approach can be extended to include these more complex phenomena. It becomes necessary to rewrite the total energy function of the system to suit the appropriate

new system variables and to identify the various mechanisms which contribute to the overall crack growth process, and then determining the conditions under which each mechanism might assume a rate-controlling role.

Brown (1979) has recently taken the analysis of subcritical crack growth an important stage further. He noted that no existing theory can account in a unified manner for all three stages of the schematic K_I-$\dot{v}$ curve. Approaching the problem of slow crack growth in terms of steady state multibarrier kinetics (network theory) Brown (1979) derived a general equation that does account for all three regions of a K_I-v curve and from which specialized expressions can be developed for the crack velocity in specific cases.

From the hypotheses that (a) subcritical crack growth consists of ℓ competitive rate processes, each of which is composed of n_j sequential steps ($j = 1,2,3 \ldots\ldots\ldots,\ell$), (b) the crack advances by the generation and movement of double kinks along the crack front, which itself is more like a band, a number of kink steps wide, than a line, Brown (1979) obtains

$$v = \# \lambda_k^2 (kT/h) \sum_{j=1}^{\ell} \left\{ \frac{1 - \exp(\Delta G_j / RT)}{(C_{1,j} k/h) + \sum_{g=2}^{m_j} [\theta_{g,j} a_{g,j} \exp(\Delta G^{\ddagger}_{g,j} / RT)]} \right\}^{-1}$$

where # is the steady state number of active double kinks per unit length of crack band, λ_k is the average step size of a double kink, and h is Planck's constant. The set of n_j

sequential steps is perceived as a collection of m_j sequential subsets each of which corresponds uniquely to a different rate process in the series. $\theta_{g,j}$ = the number of sequential steps corresponding to the g th subset both in the j th set. $a_{g,j}$'s are dimensionless parameters which lump appropriate geometric factors, reactant concentrations raised to the powers of their respective orders of reaction, stoichiometric constants and conversion factors corresponding to the g th subset of the j th sequence. $\Delta G^{\ddagger}_{g,j}$ are the Gibbs free energies of activation for forward steps in the g th subset. $(-\Delta G_j)$ is the free energy driving force for the entire j th sequence. $c_{1,j}$ is a parameter that relates to gaseous diffusion processes (transport of reactive species to crack tip through an interadjacent, stagnant gas film) where one m_j is arbitrarily designated the subset for which g = 1. It depends on thickness of the stagnant gas film, the order of the stress-sensitive bond-rupturing reactions, the collision cross section and molecular weight of both reactant species and inert gas species, Avagadro's number, the mole fraction of reactant species and the average step size of a double kink.

Equation (11) is very general and was specialized for selected cases in order to obtain $\dot{v} = \dot{v}(K)$ relations. To do this odd j suffixes were arbitrarily assigned to those sequences which include mass transport of a key reactant or product species between the environment and crack tip. Even j suffixes correspond to those processes that occur wholly within the solid, at and/or near the crack tip, that

are comparatively unaffected by the environment, ℓ is set <4. Subcritical crack growth was classified according to five general environments: (1) inert gas or liquid, or vacuum, (2) dilute reactive gas, (3) dilute reactive liquid, (4) concentrated reactive gas, and (5) concentrated reactive liquid. The number of $v = v(K)$ relations that can be obtained from equation (11), even with $\ell \leq 4$ is enormous, but study of a wide range of empirical data suggests that certain simplifications are possible. A specific expression for $v = v(K)$ that fits a wide variety of mechanisms and types of environment was found by Brown (1979) to be

$$v = \Omega_0 \exp(-\Omega_1 K_I) + \frac{\Omega_2 \exp(\Omega_3 K_I)\left\{1-\exp\left[-L(K_I-K_I^*)\right]\right\}}{1+\Omega_4 \exp(-\Omega_3 K_I)} \quad (12)$$

where K_I is the mode I stress intensity factor, K_I^* is a threshold stress intensity factor, L is a constant and the Ω's are lumped constants that have theoretic definitions that correspond to specific cases and conditions. For more details see Brown (1979). One advantage of this approach is that many different transport mechanisms to the crack tip can be included in Ω_4, for example, stress independent, bulk, solid state diffusion or surface diffusion.

For many materials where values can be assigned to the constants Ω, such as porcelain in water, soda-lime-silicate glass in octanol, there is excellent agreement between the theory and experimental results for all three regions of the

K_I-v curve. However, to assign values to the constants Ω can be a formidable task and at least at present is not really feasible for studies of rocks. Although Brown's (1979) theory clearly has substantial scope for future application in geophysics there is at present too much guesswork involved in assigning values to the constants in equation (12) for rocks.

Thomson has recently developed Lawn and Wilshaw's (1975) ideas a stage further (Thomson, 1980; Fuller and Thomson, 1980) and attempted to provide a more satisfactory theoretical framework. He addresses the problem of fracture at an atomically sharp crack assisted by the adsorption of a gaseous chemical species which lowers the energy of bond breaking. He obtained a general statistical mechanical description of brittle crack growth in terms of chemical absolute reaction rate theory that leads to certain general conclusions. The most important one is that chemically assisted fracture should be a widespread phenomena, associated with the lowering of the surface energy of the material by the external environment. However, steric or size effects can restrict the external molecules from entering the cohesive region where chemical reactions occur and a variety of complex chemical effects can occur at crack tip to strengthen the crack or to slow down its growth. Thus the details of environmentally assisted fracture will vary widely from one system to another. Despite the enormous literature on fracture there is little in the way of an appropriate data base with which to check the specific quantitative predictions

of Thomson and to throw light on the specific chemical processes involved.

Krausz (1978) has developed a theory of stress corrosion cracking based on deformation kinetics theory that amplifies some aspects of Lawn and Wilshaw's (1975) work and anticipates some of Brown's (1979) conclusions. This chemical kinetic approach shows that regions 1 and 2 of the schematic K_I-v curve are associated with two consecutive energy barriers in parallel with a single energy barrier associated with region 3 behaviour. He obtained the following expression for the crack velocity

$$v = n_c a \frac{1-\frac{kT}{h}({}_1k_1)^{-1}}{\{k(1)\}^{-1} + \{k(2)\}^{-1}} + n_p a_o k(3) \qquad (13)$$

where $k(1)$, $k(2)$ and $k(3)$ are the single rate constants that describe the behaviour in regions 1, 2 and 3. These must be determined by theoretical analysis in conjunction with appropriate experiments to clarify which of the rate constants associated with the forward or backward consecutive barriers in regions 1 and 2 actually dominate $k(1)$ and $k(2)$ for specific combinations of material and environment. At each bond breaking event the crack will propagate by a multiple integer (n_c) of the atomic distance (a_o). m_p is the number of bonds broken in unit crack advance during the region 3 mechanism and this may be different to that during crossing of the consecutive energy barrier, n_c. ${}_1k_1$ is an elemental rate constant associated with the threshold region barrier.

One interesting conclusion of Krausz's work is that as long as the mechanism of the consecutive processes in regions 1 and 2 does not change, then the threshold stress intensity is independent of temperature.

I have already alluded to the suggestion of Stevens and Dutton (1971) that at relatively high homologous temperatures slow crack growth in some materials may be facilitated by mass transport processes such as volume or surface diffusion or vapour phase transport. For example, Stevens and Dutton (1971) show that surface diffusion and vapour phase transport may control the high-temperature static fatigue of alumina in a dry environment, even though at low temperatures in water vapour crack propagation may well be controlled by stress corrosion. Unfortunately, there are too few experimental data points to constrain the theoretical predictions for ceramics. There is no pertinent data for rocks. However, the general implication of Stevens and Dutton's work, that mechanisms of fracture are dominant over different ranges of environmental conditions is entirely consistent with the view of fracture that I have sought to present in this article.

Unfortunately, the more recent of theories described in this section are only easily applicable to certain simple, model systems such as soda-lime silicate glass/water or alumina/water. The complexities of subcritical cracking in polyphase, polycrystalline rocks which have complicated

microstructures, cements, fabrics and chemistry at present cannot easily be analysed in these terms. A full description of subcritical cracking of rocks in terms of fundamental processes is certain to be highly complex. Evans and Graham (1975) have used acoustic emission amplitude studies to construct a model of macro-crack propagation in single phase polycrystalline ceramics that takes into account some of the complexities of microstructure, but this sort of work is still in its infancy.

Under these circumstances, and considering the relatively limited data available on subcritical cracking of rocks compared to that of model materials, such as silicate glasses, the continued use is justified of the relatively simple and semi-empirical Charles power law (equation 6) to describe stress corrosion results for geological materials. Not only has this equation certain advantages (described above) but it is also the equation that is most often favoured by experimentalists who have studied stress corrosion in rocks.

EXPERIMENTAL STUDIES OF STRESS CORROSION IN GEOLOGICAL MATERIALS

Quartz

Static fatigue of quartz in wet environments was studied by Scholz (1972), Martin (1972) and Martin and Durham (1975), but their results were not reported in terms of fracture mechanics parameters. Temperatures up to 250^{o}C were investigated in the two latter papers. Some of their data are given in Table 1. Swain et al. (1973) used a Hertzian indentation

technique to explore the influence of rate of loading, physical state and concentration of corrosive agent on the strength of quartz.

Atkinson (1979) was the first to report stress corrosion data on quartz in terms of K_I-v diagrams. The double torsion testing method (Williams and Evans, 1973) was used in this study to investigate the influence of liquid water and water vapour on crack propagation at temperatures from 20° to 80°C. values obtained for the stress corrosion index and the activation enthalpy for crack propagation are shown in Table 1. Crack growth rates as slow as 10^{-9}m.s^{-1} were studied without any firm evidence of a stress corrosion limit. All of Atkinson's (1979) data pertain to region 1 of the schematic K_I-v curve (Figure 2). Using the theory of Lawn (1975) a plateau (region 2) in the K_I-v curve for quartz ($\underline{a}$ plane $\perp$ $\underline{r}$ in 68% RH) was calculated to lie at 4×10^{-4}m.s^{-1} or just outside the range of experimental data.

Further work on the stress corrosion of quartz has been reported in terms of K_I-v diagrams by Bruner (1979). He used double cantilever beam specimens at room temperature in water vapour. In Figure 3 is shown a synoptic diagram that includes the results of Bruner (1979) and some of the results of Atkinson (1979). Crystallographic orientation can clearly exert a pronounced influence on crack propagation rates in this material, especially at slow crack velocities. This point was also inferred by Scholz (1972) from his static fatigue experiments. Note that the plateau in the experimental K_I-v curves (region 2) in Figure 3 is in good agreement with

Atkinson's (1979) theoretical prediction.

Atkinson and Meredith (1981) have shown that the pH of the aqueous environment can strongly influence the rate of crack propagation at room temperature. This influence is greatest at low values of K_I and diminishes as K_I is raised (Figure 4). At very high values of K_I close to K_{Ic} no significant influence of pH on crack propagation rates is observed. This is interpreted in terms of a two stage model as follows. At low crack velocities the crack tip environment is open to modification by the external environment through diffusion of chemical species along the crack between the bulk fluid and the crack tip. Chemical differences between the crack tip and the bulk fluid are not long sustained and the crack tip environment is controlled by the chemical composition of the bulk fluid. At high crack velocities (ca. $10^{-2}m.s^{-1}$) transport of chemical species from the bulk fluid to the crack tip environment cannot keep pace with the creation of new sources of reactive ions in fresh crack surfaces. In this case the composition of the crack tip solution is controlled primarily by the chemical composition of the fresh crack surfaces. The greater the availability of OH^- ions, the faster is the rate of crack propagation, for a given value of K_I.

As mentioned earlier, electron microscope studies (Martin and Durham, 1975; Dunning et al., 1980) have shown that chemically enhanced crack growth is not accompanied by any significant plastic deformation, at least at temperatures

up to 250°C. In Martin and Durham's (1975) study, however, Dauphiné twins were observed in experiments at 125°C and above. It is possible that Dauphiné twins are produced in advance of crack propagation in contact-loaded quartz (see Hartley and Wilshaw, 1973) but the very small atomic motions that this involves serve merely to efficiently accommodate the local elastic strain that accumulates in elastically anisotropic quartz.

Hartley and Wilshaw (1973) have interpreted their Hertzian indentation studies to show that intrinsic water in the quartz structure may promote strength reduction at temperatures above 520°C by stress-assisted diffusion of lattice water to crack tips. The role of OH^- ions in the silica lattice, however, is markedly affected by annealing.

No systematic attempt has been made here to identify data pertaining to synthetic or natural quartz. There is some suggestion, however, that some types of natural Brazilian quartz may have markedly different mechanical properties to synthetic quartz (Norton and Atkinson, 1981).

Quartz rocks

A K_I-v diagram has been published by Atkinson (1980) for stress corrosion of double torsion specimens of Arkansas Novaculite in liquid water at temperatures of 20°-80°C. This Novaculite is a microcrystalline almost pure quartz rock

with a mean grain size of approximately 10 micrometres. The stress corrosion index was somewhat greater than for any orientation of single crystals of quartz yet studied but the activation enthalpy was comparable to that of quartz (see Table 1). Crack velocity data were obtained in the range from 10^{-4} to 10^{-10} m.s^{-1}. All data pertain to region 1 of the schematic K_I-v curve and no stress corrosion limit was observed.

Peck (1980) has noted a 15-20% reduction in fracture energy determined for double cantilever beam specimens of Sioux quartzite in tap water compared to that in air of ambient humidity. This was attributed to stress corrosion effects.

Calcite rocks

Henry (1978) and Henry and Paquet (1976) have reported stress corrosion data for a marble and a micrite in liquid water containing dissolved $CaCO_3$, and in moist air. These workers also used the double torsion testing method. They found that there was a strong orientation dependence of K_I-v data for marble; the trends in the data had approximately the same slope, but their position in K_I-v space varied substantially with orientation. The stress corrosion index for micrite in air was markedly different to that for micrite in liquid water (Table 1). These data for calcite rocks showed the trimodal pattern familiar from work on silicate

glasses and illustrated schematically in Figure 2. Most unusually, however, at very low K_I values an apparently anomalous region of behaviour was encountered. As K_I was lowered at the slow velocity end of region 1 behaviour there appeared a second, constant crack velocity, plateau region. On lowering K_I further still this was followed by another region where crack velocity decreases with decrease in K_I at much the same rate as for region 1 behaviour. This apparently anomalous region may be ascribed to relatively poor data obscuring a threshold stress intensity. There is a considerable scatter to the Henry and Paquet (1976) results. Alternatively, if the effect is real then it may result from complex chemical reactions between solid and solution or to the onset of plastic deformation as a significant contributor to crack growth processes.

For a given stress intensity factor the rate of crack propagation in micrite is generally increased on raising the pH of the corrosive medium above 7 (Henry, 1978). Activation enthalpies for crack propagation in micrite at temperatures from 20° to 85°C were found to be temperature dependent by Henry (1978). These data are given in Table 1.

Basaltic rocks

To date, all experiments run on basaltic rocks have used the double torsion testing method. Some details of crack growth in basaltic rocks are presented in Figure 5 and

Table 1. Stress corrosion crack velocity/K_I curves for Black gabbro in liquid water and in air of 30% R.H. at 20°C were found by Atkinson and Rawlings (1979a, b; 1981) to have the trimodal form characteristic of the behaviour shown by glasses and ceramics (see Figure 2). Crack growth was followed down to velocities of ca. 10^{-9}m.s.$^{-1}$ (0.54 K_{Ic}) without encountering a stress corrosion limit.

Waza et al. (1980) studied subcritical crack growth in relatively porous (6%) Kinosaki basalt. The porous nature of the basalt may explain why it was apparently much weaker (K_{Ic} = 1.1 MN.m$^{-3/2}$) than the coarser grained Black gabbro (K_{Ic} = 2.88 MN.m$^{-3/2}$). Because only a few data points are reported by Waza et al. (1980) only very approximate values can be assigned to the stress corrosion index (Table 1). Another basalt, Murata basalt, has been tested by Sano and Ogino (1980). For this material K_{Ic} was in excess of 2 MN.m$^{-3/2}$. Stress corrosion data for Whin Sill dolerite have been determined by Meredith and Atkinson (1981).

Crack velocity/K_I curves for a lunar analogue basaltic glass at water vapour pressures of 1.33 KPa and 0.13 Pa have been reported by Soga et al (1979). They found that in common with other glasses increasing the partial pressure of water vapour at constant K_I dramatically enhances the rate of crack propagation. The basaltic glass was made from Ralston intrusive. Stress corrosion data for the crystalline form of this rock are reported in Atkinson et al (1980).

Granitic rocks

Figure 6 shows a synoptic diagram of most of the available stress corrosion data for granitic rocks. Values of the stress corrosion index and testing conditions can be found in Table 1. With the exception of Wilkins' (1980) fracture statistics approach all other workers on granitic rocks have used the double torsion method.

One especially interesting feature of Figure 6 is the absence of a stress corrosion limit in Lac du Bonnet granite even at crack velocities as slow as 10^{-11}m.s^{-1}.

It can be inferred from Swanson's (1980) data for Westerley Granite in toluene that as crack velocity is raised above approximately 10^{-3}m.s^{-1} there is a gentle reduction in the slope of the K_I-v curve. This could mean that region 2 behaviour (see schematic K_I-v curve, Figure 2) is being approached. The gentle slope change observed for granite contrasts with the rather abrupt change noted for silicate glasses and some ceramics. Because the crack "tip" in granite consists of many secondary cracks at these velocities (Swanson, 1980) the gradual change in slope may be explained as a result of the differential onset of region 2 behaviour for different secondary cracks. The conditions for the onset of this behaviour will depend on crystallographic orientation, on the nature of the host mineral, and on the degree of intra- and inter-granular character to the crack path.

There is some spread in the range of results for Westerley granite. This is probably due to differences in testing techniques because when different blocks of Westerley granite are tested in the same laboratory using identical testing techniques then relatively similar results are obtained. For example, compare curves labelled a and b in Figure 6 for air of 30% R.H. (Atkinson and Rawlings, 1981; Atkinson et al., 1980). The uncertainty in measuring K_I and v is approximately 2.5% and 15%, respectively.

Microscopic studies of the crack path during stress corrosion in Westerley granite have shown that there is a decrease in the ratio of transgranular to intergranular fracturing as crack propagation rates are reduced (Swanson, 1980; Atkinson and Rawlings, 1981).

In room temperature time-to-failure tests on Barre granite with moist air as the stress corrosion agent Kranz (1980) found that static fatigue is inhibited by the application of confining pressure. This effect was attributed to an increase in the activation enthalpy required for the stress corrosion process, to a change in the rate that corrosive water vapour could reach the crack tips and a decrease in crack interaction prior to the onset of tertiary creep. An increased amount of inelastic deformation also occurs on raising the pressure before the rock becomes unstable. This is due to the formation of longer and more numerous microcracks, although the crack angle and length spectra are

grossly similar at the onset of tertiary creep for each pressure.

Only very approximate values can be quoted for the stress corrosion index of Yugawara andesite (see Table 1) determined by Waza et al (1980) in double torsion experiments because of the paucity of data points reported. Sano and Ogino's (1980) double torsion experiments on Oshima granite are discussed in the following section on acoustic emission (see also Table 1).

Other geological materials

Time-to-failure tests have been conducted by Schmidt (1976) on oil shale from Anvil Points Colorado in distilled water, air of 7% R.H. and in dry argon. Schmidt concluded that stress corrosion can reduce the time-to-failure in this material provided that K_I is greater than $0.8K_{Ic}$. Because these tests never lasted for longer than 123 hours it is of course possible that stress corrosion can occur at yet lower levels of K_{Ic}, but at rates which are so slow that failure will result after weeks, months or years rather than a few hours.

Wiederhorn (1968) has obtained K_I-v curves for stress corrosion of $(10\bar{1}2)$ fractures in sapphire in the presence of water vapour. These data spanned a range of velocities from 10^{-8} to 10^{-4} m.s^{-1} and showed all the features of the schematic K_I-v curve (Figure 2). The most striking aspect of these data is that the plateau, or transport-controlled region (region 2) is shifted dramatically to higher crack velocities.

on raising the pressure of water vapour. For example, region 2 behaviour occurs at ca. $7 \times 10^{-7} m.s^{-1}$ under water vapour pressures of 2.4 $N.m^{-2}$, but on raising the pressure to 300 $N.m^{-2}$ region 2 is shifted to ca. $7 \times 10^{-5} m.s^{-1}$. Lawn's (1975) atomistic theory can account for the qualitative features of these results on sapphire.

Acoustic emission and Stress corrosion

A substantial body of literature exists on acoustic emissions during subcritical crack growth in ceramics (e.g. Evans and Linzer, 1973). These transient elastic waves often have frequencies between 100 kHz and 1 MHz. A few years ago Anderson and Grew (1977) surveyed the available literature and arrived at the conclusion that experiments had not yet satisfactorily answered the question of whether rocks undergo slow crack growth without acoustic emission. Since that time there have been a number of reports that have shown clearly that not only do rocks show acoustic emission during stress corrosion but that the characteristics of these emissions can be related to the mechanisms of crack growth and hence to parameters such as stress intensity factor, crack velocity and the 'humidity' at the crack tip. Acoustic emission, therefore, is an excellent means of remotely monitoring the characteristics of stress corrosion crack growth in rocks.

In an early study, Scholz (1972) showed that the rate

of microfracturing, estimated from the rate of acoustic emission, of single crystals of quartz is proportional to crack velocity. Byerlee and Peselnick (1970), however, were unable to detect with their instruments acoustic emission from slow crack growth in glass.

Atkinson and Rawlings (1979a, b; 1981) have made an extensive study of acoustic emission during stress corrosion in double torsion plates of Westerley granite and Black gabbro. Acoustic emissions were observed in the range of frequencies from 100 kHz to greater than 1 MHz. A spectral peak occurred in the region of 200 kHz and so further monitoring of emissions was restricted to the bandwidth 100 kHz - 350 kHz. In both granite and gabbro significant acoustic emission accompanies crack propagation at even the slowest crack velocities observed (10^{-9} m.s^{-1}). The acoustic emission rate was directly proportional to the crack velocity and could be used as an indirect measure of this parameter. For example, see Figure 7. In addition, amplitude distributions, measured by the parameter b, show distinctive shifts with increase in stress (see Figure 8). The amplitude distribution parameter, b, is given by

$$n(V) = (V/V_o)^{-b} \qquad (14)$$

where n(V) is the fraction of the emission population whose peak amplitude exceeds amplitude V and V_o is the lowest detectable amplitude. Furthermore, both the acoustic emission

rate and the amplitude distribution are sensitive to the details of the mechanism of crack propagation which is controlled by stress intensity factor and crack tip 'humidity.'

An especially interesting feature of Figure 8 is that the trends in the amplitude distributions do not seem sensitive to rock type.

Swanson (1980) has used acoustic emission location techniques to pin-point the source of emissions in double torsion tests on Westerley granite. He found that subsidiary microcracking ahead of the main fracture occurred at crack velocities greater than 10^{-5}m.s^{-1}, but not at lower velocities. Both macrocrack and microcrack extension was probably controlled by stress corrosion. The results of Atkinson and Rawlings (1981) can be interpreted to show that the majority of acoustic emission from crack growth in double torsion plates of Westerley granite and Black gabbro over the range of velocities 10^{-4} to 10^{-9}m.s^{-1} occurs by extention of the macrocrack.

Sano and Ogino (1980) have also noted that acoustic emission rate in rock shows a close relation with the growth rate of cracks in double torsion plates. They studied the behaviour of Murata basalt and Oshima granite. In these studies a tendency was observed for the dominant frequency (in the range 100 kHz to 1MHz) to decrease with increase in

crack velocity. In contrast to this, acoustic emission studies during uniaxial compressive experiments on Ralston intrusive (basalt), Westerley granite and pyrophyllite showed an enhancement of high frequency spectral components in events prior to failure, i.e. as stress or crack velocity increases (Granryd et al., 1980).

An important aspect of the results of these laboratory acoustic emission studies lies in their potential application as a means of monitoring stress corrosion in the earth. Acoustic emissions with frequencies in the range 0.5 to 5 kHz have been detected with deeply buried geophones in seismically active areas (Teng and Henyey, 1981). See also Weeks et al. (1978). Propagating fractures in petroleum reservoir rocks have also been monitored with arrays of acoustic emission transducers (Shuck and Keech, 1977). Because these emissions occur on a time - scale measured in seconds or minutes, rather than the much longer time scale associated with low frequency seismic events, a large enough number of events can be recorded in a reasonable time so as to establish statistically meaningful changes in amplitude and frequency distributions and seismicity rates.

SOME GEOPHYSICAL APPLICATIONS OF SUBCRITICAL CRACK GROWTH DATA.

In this section I will briefly discuss some areas of geophysics in which I believe subcritical crack growth data can be important. This list is not exhaustive but has been chosen in order to show the potential of using the insights provided by a fracture mechanics description of subcritical

crack growth in analysing geophysical phenomena.

Prediction of time- and rate-dependent failure and friction properties of rocks

In principle, integration of the area under a crack velocity/stress intensity factor diagram can provide all the information needed to predict the time- and rate-dependent fracture strength of rocks. In practice, the problem is made more difficult by complex stress states and mixed mode crack growth problems and some simplifying assumptions are necessary.

For the simplest case of pure mode I fracture propagation the influence of stress rate on fracture stress (σ_f) can be approximated by (Evans and Johnston, 1975)

$$\sigma_f = \left[2\dot{\sigma}\ (n_1+1)/A_1 Y^{n_1}(n_1-2)\, a_i^{(n_1-2)/2}\right]^{1/(n_1+1)} \qquad (15)$$

where a_i is the initial flaw size, $\dot{\sigma}$ is the stress rate, Y is a geometrical constant and A_1, n_1 are constants in the equation $v = A_1 K_1^{n_1}$ describing the region 1 stress corrosion behaviour of the material. Atkinson (1980) has used this equation successfully to predict the influence of stress (strain) rate on the tensile fracture stress of Arkansas Novaculite in water at 20°C. It was found that at a strain rate faster than $\sim 6 \times 10^{-5}$ s^{-1} stress corrosion does not appreciably influence the tensile fracture stress, but at lower strain rates there is a monotonic reduction in strength from a maximum

value of $72MN.m^{-2}$ in the absence of stress corrosion effects to approximately $40MN.m^{-2}$ at a strain rate of $10^{-10}s^{-1}$.

The time-to-failure (t_f) at a constant tensile stress (σ) is also given by a similar integration of the K_I-v diagram (Evans, 1972). It is found that

$$t_f = 2/\sigma^2 Y^2 \int_{K_{Ii}}^{K_{Ic}} (K_I/v.)\ dK_I \qquad (16)$$

where K_{Ii} is the stress intensity factor associated with the initial flaw size.

Henry and Paquet (1976) have used equations based on (15) and (16) to predict the influence of tensile stress on time-to-failure and strain rate on tensile fracture stress of calcite rocks.

Das and Scholz (1980) have developed a simple theoretical approach to predicting the time-to-failure of an earthquake rupture subject to stress corrosion. Provided that the static stress drop is independent of time then time-to-failure is given by

$$t_f = (X_o/v_o)(2/n_1-2) \qquad (17)$$

where X_o is the earthquake rupture radius and v_o the rupture velocity at the threshold stress intensity, and n_1 is the stress corrosion index for region 1 behaviour. Note that

here the time-to-failure depends only on the initial conditions and n_1 and not on the final conditions as in the analysis of Evans (1972).

Workers at the Cooperative Institute for Research in Environmental Science (Mizutani et al., 1977; Soga et al., 1979) have developed an equation that is a reasonably good predictor of the ultimate compressive strength of rocks as a function of (stress) strain rate, water vapour pressure and temperature. They assumed that brittle failure in rocks occurs by the interaction of numerous small cracks that form parallel to the loading axis under the influence of the applied stress and the moisture content at crack tips. If the stress is applied at a slow rate and moisture is abundant at crack tips then the cracks will grow to be large and coalesce into a failure plane at low stress. If the stress is applied rapidly and the moisture content is low then the existing cracks will not relieve the stress concentrations and many new small cracks are formed. In the latter case failure occurs by the coalescence of a larger number of smaller cracks. Assuming that for a given crack configuration (size, shape and distribution) the rock will fail at a stress (σ_u) when the cracks have reached an average critical length and that the crack growth is governed by an activated mechanism (stress corrosion by water), then

$$\sigma_u = D\{(\ell n\dot{\sigma} - \ell n\ T - n\ \ell n\ p_{H_2O} - B)RT + U\} \qquad (18)$$

where $\dot{\sigma}$ = applied stress rate, p_{H_2O} is the partial pressure

of water, n = the order of the chemical reaction in stress corrosion ($\simeq$1 in this case), R and T are the gas constant and the absolute temperature, respectively, U is the activation energy for stress corrosion and D and B are constants that depend on activation volume, initial crack configuration and rock type.

The ultimate strengths of basalt, granite and quartz as a function of strain rate, temperature and water vapour partial pressure are well described by this equation.

Scholz (1968) and Cruden (1970) have developed theories of creep in brittle rocks on the basis of stress corrosion theory. Cruden criticised Scholz's theory on a number of grounds including the form of the equation used to describe static fatigue by stress corrosion and the oversimplified view of the stress distribution in the rock and the assumed uniformity of physical and chemical properties of elements of the rock. The importance of Cruden's work is that his theory could explain the different creep behaviour of Carrara marble and Penant sandstone in terms of differing stress corrosion behaviour and crack length distributions.

Anderson and Tiernan (1980) have produced a simple stress corrosion model of aseismic creep in fault zones which is envisaged as a slow breaking and reforming of asperities which are in contact along a fault plane. Thus macroscopic creep deformation measured at the surface actually consists of relatively slow rupturing on a microscopic scale.

The creep rate measured at the surface ($\dot{e}_{creep}$) is given by the time required for cracks to grow a length, δ, through asperities (δ being a characteristic distance for asperity disruption) and cause them to transfer their loads to neighbouring asperities which are on the average, separated by a distance $\bar{R}$. The creep rate is crudely given by

$$\dot{e}_{creep} = v \left(\frac{1}{\varepsilon} \cdot \frac{\delta}{\bar{R}}\right) \tag{19}$$

where v is the microscopic crack growth velocity, ε is the strain resulting from stress relaxation in the fault zone and $\delta/\bar{R}$ may reasonably be expected to vary between 1.0 and 0.1.

Modelling earthquake rupture

There have been numerous suggestions that stress corrosion may play an important role in various time-dependent earthquake phenomena (Scholz, 1972; Martin, 1972; Bonafede et al., 1976; Atkinson, 1979, 1980; Rice, 1979; Rudnicki, 1980). Recently, however, Das and Scholz (1980) have taken these speculations an important stage further and developed a simple, yet extremely comprehensive theory of shallow earthquake rupture based upon stress corrosion crack growth of a two dimensional circular crack. This theory manages to predict virtually the whole gamut of observed earthquake phenomena (slow earthquakes, multiple events, delayed multiple events, postseismic rupture growth and afterslip, foreshocks and aftershocks). The theory also predicts that there must

be a nucleation stage prior to an earthquake and predicts its form.

Das and Scholz (1980) obtain their results by combining two simple, but fundamental concepts. Firstly, from fracture mechanics

$$K = C\Delta\tau\sqrt{x} \tag{20}$$

and secondly, from stress corrosion theory

$$K = K_o\left(\frac{\dot{X}}{v_o}\right)^{1/n} \tag{21}$$

where K is the stress intensity factor, $\Delta\tau$ is the stress drop, X is the rupture length and $\dot{X}$ the rupture velocity, C is a geometrical factor and K_o, v_o, n are material constants. K_o and n are the stress corrosion limit and stress corrosion index respectively.

A very important insight that is incorporated into Das and Scholz's model is that a major fault is not an homogeneous surface; a point that has been strongly emphasized by geologists. The applied stress, and hence K, and the material properties K_o and n will be functions of position on the fault plane. To avoid the complexities of considering earthquake rupture as a stochastic growth process Das and Scholz consider only gross inhomogeneities, termed barriers (after Das and Aki, 1977b).

For a detailed discussion of this model the reader is

referred to the original papers. Only a brief outline is given here.

Tectonic stress is believed to increase in the earth's crust at a very slow rate and it is released when an earthquake occurs. This is equivalent to an increase in K until K_c is reached and the earthquake initiates. Stress corrosion theory, however, suggests a fracture criterion that is incompatible with this simplistic model. It predicts that propagation of the earthquake fault begins when $K = K_o$ and it quasi-statically accelerates as K approaches K_c. Thus, on this model an earthquake must be preceded by some precursory slip.

The size of a nucleation zone and the time scale of the process depend only upon n and K_o and their spatial distribution on the fault surface. Das and Scholz (1980) estimate the time from which the crack starts growing subcritically to that when it reaches instability, the nucleation time (t_f) from equation (17). Estimates of the time-to-failure, velocity and rupture size immediately (1 second) before failure for physically reasonable values of X_o, and v_o and n from Atkinson (1979) leads to the conclusion that the majority of rupture growth occurs in the last few hours before an earthquake. This may explain why precursory slip on earthquake faults is not more commonly observed. An example of earthquake rupture growth by stress corrosion is shown in Figure 9.

Some of the limitations to the Das and Scholz theory are

as follows. Firstly, it assumes that stress corrosion influences crack growth in modes II and III. Although stress corrosion has only been observed in crack growth in mode I there is no obvious reason why mode II and III should not show the same phenomena. Secondly, the simple form of the K-v curve used by Das and Scholz, which is the basis of their predictions, can be due to mechanisms other than stress corrosion, although this would not materially alter their results. Thirdly, their analysis assumes only one large crack and their somewhat pessimistic view of earthquake precursors is based on that. In nature many smaller cracks might be involved in subcritical growth and the subsequent strain change might be sufficiently large to be measurable at the surface. Furthermore, quasi static growth of numerous smaller ruptures or microscopic grain size level cracks may lead to the development of other precursory phenomena of sufficiently large magnitude that they can be observed. Finally, under conditions where free water is absent and stress corrosion is presumably impossible earthquake patterns will not be predictable on the basis of the above model. This is presumably the case with many deep focus earthquakes which only rarely are accompanied by aftershocks.

One of the beauties of invoking stress corrosion crack growth as a necessary precondition for rupture in the earth's crust is that the difference between so-called 'aseismic' and seismic fault zones also becomes clear. The difference

between seismic and aseismic fault segments is merely a difference in spatial/temporal variation in material properties and environment along fault zones. Moreover, the difference between "slow" and "normal" earthquakes, multiple event earthquakes, delayed multiple event earthquakes and aftershocks is also largely one of scale.

Stability of hot, dry rock geothermal reservoirs

The extraction of thermal energy from hot, initially dry rocks at depth in the earth's crust involves in theory the creation of a large quasi-vertical crack in these rocks by hydrofracturing. To extract the heat from the rock cold water is circulated within the crack while it is held open by the water pressure exceeding the local horizontal stress in the rock. The cold water gains heat from the large surface area of rock and the heated water is pumped to the surface where it can be used.

The Los Alamos Scientific Laboratory project for the development of dry rock geothermal reservoirs in New Mexico is following a similar scheme to the above. The Cornwall hot, dry rock project also has the same guiding philosophy.

For a given size of hydrofracture the volume of the crack will increase linearly with the differential pressure which is given by

$$\Delta P = P_{fluid} - \sigma_3 \qquad (22)$$

where P_{fluid} is the fluid pressure in the hydrofracture, and σ_3 is the horizontal stress in the rock, assuming the crack to be vertical. The volume of the crack and hence the flow of water and energy yield are limited by the maximum fluid pressure which the crack can sustain without growing appreciably in size during the proposed lifetime of the geothermal well, (Demarest, 1976). If the proposed life of the well is measured in tens of years then in this context an appreciable amount of crack growth would be hundreds of metres (based upon the Los Alamos experiments). Thus, in order that the energy yield of the geothermal reservoir should not be seriously degraded, ΔP must not attain a value that leads to crack propagation by stress corrosion of ca. 10 metres. yr^{-1} ($\simeq 3 \times 10^{-7} m.s^{-1}$).

Demarest (1976) notes that the stress intensity factor governing crack growth in artificial geothermal systems such as the above is given by

$$K_I = \Delta P (2/\pi)^{\frac{1}{2}} (a)^{\frac{1}{2}} \qquad (23)$$

where a is the radius of the circular crack and K_I is the mode I stress intensity factor. He also points out that stress corrosion crack growth can occur at stress intensity factors less than that required to rapidly propagate the initial hydrofracture and thus degrade the energy yield of the geothermal well.

A typical reservoir rock is likely to be granite (e.g. Cornwall, New Mexico). From the data for stress

corrosion in Westerley granite (Atkinson and Rawlings, 1981) we can estimate the value of K_I which will produce a crack velocity of 10^{-7}m.s^{-1}. This is approximately 1.12 MN.m$^{-3/2}$ for liquid water at 20^{o}C.

The working down-hole environment of an initially dry rock geothermal well, such as that at Los Alamos, involves pressurized water at a temperature of ca. 200^{o}C and depths of 2 - 5 km. One can predict that an increase in temperature of ca. 200^{o}C should increase the rate of crack propagation in granite by approximately one order of magnitude based upon observations of the temperature dependence of stress corrosion in quartz (Atkinson, 1979) and novaculite (Atkinson, 1980). The increased water pressure at these depths may tend to inhibit stress corrosion and thus this figure is probably an upper bound. Using these figures a crack velocity of 10^{-7}m.s^{-1} would be achieved with a stress intensity factor of ca. 1 MN.m$^{-3/2}$.

Taking K_I for fast hydrofracturing equal to K_{Ic} leads to the conclusion that the K_I in the geothermal well should not exceed approximately 0.6 of the K_I to cause hydrofracturing. If stress corrosion were much more rapid than predicted by these calculations then it could place a serious constraint on the extraction of energy from hot, initially dry rocks.

Stimulation of oil and gas reservoirs

So called 'tight', i.e. impervious geological formations bearing oil and gas are often stimulated to increase production by hydrofracturing. Pressurized water may be pumped into these artificial fractures in order to force out the less dense oil and gas. Stress corrosion growth of these induced fractures could occur in a manner described in the previous section. If these fractures ran into "loose", highly permeable strata or zones of high fluid conductivity, such as faults, then the integrity of the oil or gas reservoir could be breached and wasteful loss of energy reserves occur.

Crack-seal mechanism of rock deformation and low stress dilatancy

Mineralized extension cracks and fissures are common in rocks that have been tectonically deformed in the upper 30 km of the earth's crust. Such silicate- or carbonate-filled extension fissures can apparently give rise to quite large finite strains (Ramsay, 1980). A mechanism whereby these extension veins are formed by an accretionary process has been described by Ramsay (1980). This process involves many cycles of (i) formation of a narrow tensile fracture as a result of fluid pressure build up to the point where the tensile strength of the rock is exceeded, and (ii) filling of the open space by crystalline material deposited from the fluid phase, perhaps by pressure solution transfer of

material from the bulk rock to the low pressure vein. Ramsay (1980) describes this process as the crack-seal mechanism of rock deformation.

Extensional mineralized veins are also commonly associated with some fault zones. Sibson (1980) has described the fluid pressure build up around normal, reverse and thrust faults that leads to a form of low stress dilatancy of the host rock. This process is essentially the same as Ramsay's crack-seal cycles.

As we have seen in previous sections, if the stress rate is relatively slow then subcritical crack growth of hydraulically opened extensional fractures can occur at stresses substantially below that required to initiate hydraulic fracturing if the stress rate is rapid. Caution should therefore be exercised in using these widespread geological features to infer stress levels during their formation. Any such estimates are likely to be upper bounds.

Fracture mechanics of lunar rocks

The available evidence concerning the nonhydrostatic shape of the moon, the remarkably deep moonquakes and the existence of mascons strongly suggest that the lunar interior has both a high strength and a high viscosity (Mizutani et al., 1977). Furthermore, the lunar lithosphere and surface are at a high vacuum and so free water is generally absent. The temperature/depth profile in the moon, however, is thought to have been extremely high (Anderson and Hanks,

1972; Duba et al., 1976). How can one reconcile the apparently high strength of the lunar lithosphere for periods of the order of 10^9 years with the inference that the temperature may have been abnormally high by terrestrial standards?

Following Martin (1972) and Mizutani et al. (1977) these observations can be reconciled by noting that all the available evidence on stress corrosion (see earlier sections) suggests that the stress required to maintain a given crack growth rate is higher the lower is the concentration of liquid water or water vapour. Mizutani et al. (1977) have shown by experiments that the compressive strength of lunar rock analogues increases with an increase in the hardness of the vacuum of the test environment at a rate of approximately 20 MPa per order of magnitude of water vapour pressure. This has approximately the same effect as raising the strain rate by one order of magnitude. It was also noted by Mizutani et al. (1977) that the higher the vacuum the less was the influence of temperature on strength reduction. See also the results of Soga et al. (1979) on crack propagation studies in analogues of lunar glass under vacuum. These results confirm the implications of internal friction studies of lunar and terrestrial rocks under high vacuum (e.g. Tittmann et al., 1973).

Thus, the apparently high strength of the lunar lithosphere can be ascribed to the absence of water and hence to the absence of stress corrosion. Soga et al. (1979) have

attempted to illustrate this by constructing a partial deformation mechanism map for lunar rocks which modifies an earlier one produced by Verrall and O'Connell (1979) by incorporating the influence of water vapour pressure on rock strength.

Magmatic intrusions

Anderson and Grew (1977) have proposed that an important type of upwards magma transport through the earth's lithosphere involves fluid (magma)- filled cracks and that growth of these cracks due to stress corrosion under the influence of volatiles can control the movement of the magma. They also note that the chemistry of the intruding fluid and volatiles relative to the rock of the crack tip may be a rate-determining factor. A variety of acids have been found in natural magmas. At magmatic temperature (>600^{o}C) and low pressures, HCl and HF are weakly dissociated. However, a cooling fumarolic gas rich in HCl will become strongly acidic, e.g. Kilauea steam condensate of 2N HCl (see Anderson and Grew, 1977). At shallow crustal depths these corrosive fluids may exert a profound influence on crack propagation (see earlier sections).

There are several weaknesses in the so-called 'hot-spot' theory that accounts for the alignment of volcanic islands, such as the Hawaiian chain, by invoking the existence of centres of volcanic activity that are overridden by the

lithospheric plates. Anderson and Grew (1977) point to some of these and suggest that stress corrosion crack propagation may be a better explanation. The most obvious objection to the 'hot-spot' theory is that direction and the rate of plate movements deduced from the assumption of fixed hot spots are inconsistent with plate motions deduced by other means (Jackson, 1976). This has led to the proposition that the 'hot-spots' are not fixed but migrate. The simpler and more elegant proposition of Anderson and Grew (1977) and others is that a linear volcanic chain is related to the growth of a slowly propagating crack in the plate. The rate of propagation of volcanic chains can attain velocities of from 1 - 30 cm. yr^{-1}. (Jackson, 1976; Anguita and Hernan, 1975). The apparent rate of propagation is controlled by the bending moment in the plate and only indirectly by the plate velocity. Thus, as is observed, the direction and rate of plate movements can be different to that deduced from the assumption of fixed hot spots. Moreover, the non linear rates of propagation in some volcanic chains can be accounted for by noting that even for a continuous crack volcanoes still will be rare because magma will only reach the surface along the crack in those few spots where all the conditions for magma intrusion to the surface are satisfied. Magmas might rise repeatedly through older weakened, previously cracked, portions of the lithosphere or at the advancing portion of the crack (see Vogt, 1974). Propagating fractures need not be collinear with plate motions nor proceed at the same velocity as the plates.

An objection based on fracture mechanics can be raised

against this hypothesis of propagating lithosphere fractures controlling magma transport. The rock at crack tips in contact with magma or its volatiles is likely to be under pressure and to be extremely hot ($\sim$ 600°C or higher). Under these conditions the crack tip material is likely to be highly susceptible to plastic flow. This will blunt the cracks and inhibit the rate of crack propagation by stress corrosion. To maintain the same rate of crack propagation would require that the stress be raised. If it were possible to so raise the stress then eventually crack growth may occur more rapidly by a process involving nucleation, growth and coalescence of microcracks controlled by stress concentrations arising from heterogeneous plastic flow. For example, stresses due to dislocation pile-ups at grain boundaries (see earlier sections). Thus, the environmental conditions of magma transport might favour mechanisms of subcritical growth of cracks other than stress corrosion.

Relaxation of Internal Stresses in Rock

It is a relatively common observation that strains as large as 10^{-3} occur in silicate rocks that are removed from quarries or drill holes or that are disturbed by sawing, drilling or loading. The spectacular experiments of Price (1966) provide experimental evidence of stress relaxation in sedimentary rocks (siltstone) during cyclical loading. These strains accumulate in periods of a few hours to several months and have been attributed to the relaxation of internal

stresses by some unknown mechanism.

Bruner(1980) has proposed that the most likely mechanism for this stress relaxation is stress corrosion. He discounts intragranular creep as a possible mechanism because the mean internal stresses in exhumed granite and other silicate rocks are probably two orders of magnitude lower than the strengths of their constituent minerals at room temperature. Bruner simulated the cycle of exhuming, unloading and relaxation for a two-dimensional model of a rock in which grain scale stresses arise from the thermal and mechanical anistropy of the polygonal grains. The nucleation of flat cracks at highly stressed grain boundary junctions and their growth by stress corrosion across the interior of grains can readily account for the observed strain relaxation and its time dependence.

CONCLUSIONS

I have outlined some of the complexities of subcritical tensile failure in materials and presented a large body of experimental evidence to show that the subcritical growth of pre-existing cracks in rocks by stress corrosion is a common phenomena under laboratory conditions. With few exceptions, however, the range of conditions explored in the laboratory represents only extremely shallow depths in the earth's crust. The extent to which stress corrosion is an important mechanism of rock deformation must still remain an open question. Nevertheless, a wide range of geophysical phenomena can plausibly be explained by invoking stress corrosion crack growth, and some important examples are given. Under appropriate environmental conditions, some form of subcritical crack growth other than stress corrosion may occur which has approximately the same stress intensity factor/crack velocity relationship. This area has yet to be explored. Data on the influence of pressure on stress corrosion are urgently needed.

Unfortunately, the physical interpretation of crack propagation and static fatigue theories is hampered because with the sort of data that is readily available an unequivocal distinction between different theories cannot be reached. As Wiederhorn (1978) has pointed out, the same set of data is often used to justify fracture theories that have very different

starting assumptions and physical bases.

Two factors cause most of the problems; the stress dependence of crack growth rate and the activation enthalpy for crack propagation. Because in a static fatigue test on rock one order of magnitude change in stress can only be covered by between 20 and 35 orders of magnitude in time, a variety of theories will adequately fit the same data. The activation enthalpies for crack propagation are generally rather low (ca. 50 - 100 $kJ.mole^{-1}$). Not only are these low values of activation enthalpy intrinsically hard to measure (Swanson, 1980), but their determination by an empirical fit of experimental data depends on the form of the equation chosen for the fit, and hence on the physical model of crack propagation adopted. Furthermore, the activation enthalpies for competing deformation mechanisms are often rather similar (e.g. for quartz, Atkinson, 1979).

Finally, this article has concentrated to a large extent on mode I crack propagation. This was inevitable as no data were available for rock on subcritical crack propagation in other modes. It was implicit, however, in much of the discussion on applications of stress corrosion theory that this mechanism does occur in modes II and III (shear modes). Moreover, it was assumed that the form of equations describing stress corrosion in mode II and III should be the same as that for mode I crack propagation, even if the values of parameters in these equations differed. These assumptions urgently need experimental verification under simulated crustal conditions.

APPENDIX - Construction of fracture mechanism map for quartz.

This diagram was constructed on the assumption that quartz can deform plastically under high partial pressures of water in a "hydrolytically" weakened state and that diffusion of oxygen is the rate controlling step in diffusion-dependent deformation mechanism. This assumption is based on the implications of Kröger-Vink diagrams constructed by P. Dennis (personal communication, 1980). The values of all unreferenced constants in constitutive equations presented below also derive from P. Dennis (personal communication, 1980).

The fracture mechanism map for quartz (Figure 1) is truncated at its top by the ideal strength which is given by equation 4. In this equation Young's modulus for quartz is 97 GPa (Birch, 1966) at 293°K. The temperature dependence of Young's modulus is taken to be the same as that of the shear modulus and is given by

$$E_T = E_o \ (1 - \alpha T) \qquad (A.1)$$

where E_T and E_o are respectively Young's modulus at temperature T°K and 0°K and α is $2.17 \times 10^{-4} {}^{o}K^{-1}$ (Bäeta and Ashbee, 1970).

The upper boundary to the cleavage (brittle intergranular fracture) fields 2 and 3 is given by the tensile flow stress corresponding to a strain rate of $10^{6} s^{-1}$. At loading rates

faster than this dynamic effects become important.

The lower boundary to the field of cleavage 2 is given by equation 3. In this equation the grain size is arbitrarily taken to be 100 micrometres. G_c is taken to be 24 $J.m^{-2}$ from the data of Atkinson (1980) on a fine-grained pure quartz rock. The temperature-dependence of G_c is estimated from the temperature-dependence of G_c for single crystals of quartz (Atkinson and Avdis, 1980).

The boundary between the fields of cleavage 3 and cleavage 1 and between intergranular creep fracture and cleavage 1 is given by the stress required for a plastic strain rate of $10^{-10}s^{-1}$.

The boundary between the fields of cleavage 3 and intergranular creep fracture is the transition stress between conditions where respectively dislocation glide and dislocation creep are the dominant mechanisms of plastic flow, i.e. $\simeq 10^{-3}$ of the shear modulus (Weertman, 1968). Fracture and flow stresses that are taken from results of compression tests are divided by 8 to get equivalent tensile stresses (Gandhi and Ashby, 1979).

The melting temperature of quartz is 1470°C (1743°K) (Kracek and Clark, 1966).

To construct fracture mechanism field boundaries that depend on rates of plastic flow it was first necessary to

calculate the conditions under which dislocation glide, dislocation creep and diffusion creep are dominant and then to calculate the corresponding tensile stresses.

Dislocation creep rates were calculated using

$$\dot{e} = \frac{AD_v Gb}{kT} \left(\frac{\sigma}{G} \right)^n \qquad (A.2)$$

where A = 1610, n = 4, b (the Burger's vector) = 5×10^{-10}m, k is Boltzmann's constant, G (shear modulus) = $G_o(1-\alpha T)$ where G_o is shear modulus at 0^oK (44.7 GPa, derived from Birch, 1966), α is as previously defined and T is the temperature in degrees Kelvin. D_v is the volume diffusion coefficient given by $D_v = D_o \exp(-\Delta H_v/RT)$ where D_o = $4 \times 10^{-18} m^2 s^{-1}$, ΔH_v = 84 kJ.mole^{-1}. The strain rate is $\dot{e}$ and the stress is σ.

Dislocation glide deformation rates were estimated by linearly extrapolating the intersection of the dislocation creep strain rate contours with the boundary between dislocation creep and dislocation glide (10^{-3}G, Weertman (1968)) to the yield stress at absolute zero, $\sigma^o y$. From the data of Rutter (1976), $\sigma^o y$ was estimated to be 0.97 GPa in tension.

Diffusion creep rates were calculated from

$$\dot{e} = \frac{21\Omega D_v \sigma}{kTd^2} \left(1 + \frac{\pi W}{d} \frac{D_b}{D_v} \right) \qquad (A.3)$$

where Ω is the molar volume = 22 x 10^{-6} $m^3.mole^{-1}$, D_v, $\dot{e}$, σ, T, k are as previously defined, d is the grain size, W is the grain boundary width = 100 nanometres, D_b is the grain boundary diffusion coefficient = $D_o \exp(-\Delta H_b/RT)$ where ΔH_b = 56 $kJ.mole^{-1}$.

Acknowledgements

Financial support for much of the work reported here was provided by the U.S. Geological Survey in the form of contract numbers 14-08-0001-17662 and 14-08-0001-18325. This study forms part of the U.S. National Earthquake Hazards Reduction Programme. Additional funds were provided by the British Natural Environment Research Council under grant GR3/3716.

The assistance of Paul Dennis and Philip Meredith in the preparation of this paper is gratefully acknowledged. Some of the experimental work described here was undertaken with facilities provided by Paul Ewing and Rees Rawlings of Imperial College. Michael Ashby of Cambridge University has continued to influence strongly my view of the mechanics of materials. I wish to thank him for the provision of numerous reprints of his work.

REFERENCES

Anderson, D.L. and Hanks, T.C. 1972. Is the moon hot or cold? Science 178, 1245-1249.

Anderson, O.L. and Grew, P.C. 1977. Stress corrosion theory of crack propagation with application to geophysics. Rev. Geophysics. Space Physics 15, 77-104.

Anderson, O.L. and Tiernan, M.F. 1980. Stress corrosion cracking in premonitory earthquake events. Final Technical report to managers of U.S. National Earthquake Hazards Reduction Program, Contract No.: 14-08-0001-16798.

Anguita, F. and Hernan, F. 1975. A propagating fracture model versus a hot spot origin for the Canary Islands. Earth Planet Sci. Lett. 27, 11-19.

Ashby, M.F., Gandhi, C. and Taplin, D.M.R. 1979. Fracture-mechanism maps and their construction for F.C.C. metals and alloys. Acta Metallurgica 27, 699-729.

Atkinson, B.K. 1979. A fracture mechanics study of sub-critical tensile cracking of quartz in wet environments. Pure Applied Geophysics 117, 1011-1024.

Atkinson, B.K. 1980. Stress corrosion and the rate-dependent tensile failure of a fine-grained quartz rock. Tectonophysics 65, 281-290.

Atkinson, B.K. 1981. Review of experimental methods in fracture mechanics (in preparation)

Atkinson, B.K. and Avdis, V. 1980. Fracture mechanics parameters for some rock-forming minerals determined using an indentation technique. Int. J. Rock Mech. Min. Sci. and Geomech. Abstr. (in press).

Atkinson, B.K. and Meredith, P.G. 1981. Stress corrosion cracking of quartz: A note on the influence of chemical environment. Tectonophysics (in review)

Atkinson, B.K. and Rawlings, R.D. 1979a. Acoustic emission characteristics of subcritical and fast tensile cracking in rock. Proc. Institute of Acoustics (London). (in press).

Atkinson, B.K. and Rawlings, R.D. 1979b. Acoustic emission during subcritical and fast tensile cracking of Westerley granite and a gabbro. EOS, Transactions American Geophysical Union 60, 740.

Atkinson, B.K. and Rawlings, R.D. 1981. Acoustic emission during stress corrosion cracking in rocks. In: Earthquake Prediction, Third Maurice Ewing Symposium, New York, 1980 (in press).

Atkinson, B.K., Price, N.J., Dennis, S.M., Meredith, P.G. and Holloway, R.F. 1980. Mechanisms of fracture and friction of crustal rock in simulated geologic environments. Semi-annual technical report to managers of U.S. National

Earthquake Hazards Reduction Program, Contract No.: 14-08-0001-18325.

Bäeta, R.D. and Ashbee, K.H.G. 1970. Mechanical deformation of quartz. 2. Stress relaxation and thermal activation parameters. Phil. Mag. 22, 624-635.

Birch, F. 1966. Elastic constants and compressibility. In: Handbook of Physical Constants (ed. S.P. Clark, Jr.) Mem. Geol. Soc. Am. 97, 97-173.

Bonafede, M., Fazio, D., Mulargia, F. and Boschi, E. 1976. Stress corrosion theory of crack propagation applied to the earthquake mechanism. A possible basis to explain the occurrence of two or more large seismic shocks in a geologically short time interval. Bolletino di Geofisica, teorica ed applicata, XIX, 377-403.

Brown, S.D. 1979. Multibarrier kinetics of brittle fracture: I. Stress dependence of the subcritical crack velocity. J.Am. Ceramic Soc. 62, 515-524.

Bruner, W.M. 1979. Unpublished Ph.D. thesis, University of California, Los Angeles.

Bruner, W.M. 1980. Relaxation of internal stresses in rocks by time-dependent crack growth. EOS, Transactions American Geophysical Union, 61, 372.

Byerlee, J.D. and Peselnick, L. 1970. Elastic shocks and earthquakes. Naturwissenschaften, 57, 82-85.

Charles, R.J. 1958. Dynamic fatigue of glass. J.Applied Phys. 29, 1657-1662.

Charles, R.J. and Hillig, W.B. 1962. Kinetics of glass failure of stress corrosion. In: Symposium sur la Résistance Mécanique du Verre et les Moyens de l'Améliorer. Union Scientifique Continentale du Verre, Charleroi, Belgium, 511-27.

Cruden, D.M. 1970. A theory of brittle creep in rock under uniaxial compression. J. Geophys. Res. 75, 3431-3442.

Das, S. and Aki, K. 1977. Fault plane with barriers: A versatile earthquake model. J. Geophys. Res. 82, 5658-5670

Das, S. and Scholz, C.H. 1980. Theory of time-dependent rupture in the earth. J.Geophys.Res. (in press).

Dehart, R.C. and Liebowitz, H. 1968. The influence of ambient pressure on the stress corrosion susceptibility of metals. Eng. Fract. Mech. 1, 129-135.

Demarest, H.H. Jr. 1976. Application of stress corrosion to geothermal reservoirs. Informal Report LA-6148-ms, Los Alamos Scientific Laboratory, 4pp.

Duba, A., Heard, H.C. and Schock, R.N. 1976. Electrical conductivity of orthopyroxene to 1400°C and the resulting selenotheny. Proc.Lunar.Sci.Conf. 7th, 3173-3181.

Dunning, J.D., Lewis, W.L. and Dunn, D.E. 1980. Chemo-mechanical weakening of synthetic quartz and sandstone in the presence of surfactants. J.Geophys.Res. (in press).

Evans, A.G. 1972. A method for evaluating the time-dependent failure characteristics of brittle materials - and its application to polycrystalline alumina. J.Mater.Sci. 7, 1137-1146.

Evans, A.G. and Graham, L.J. 1975. A model for crack propagation in polycrystalline ceramics. Acta Metallurgica, 23, 1303-1312.

Evans, A.G. and Johnson, H. 1975. The fracture stress and its dependence on slow crack growth. J.Mater.Sci. 10, 214-222.

Evans, A.G. and Linzer, M. 1973. Failure prediction in structural ceramics using acoustic emission. J.Amer.Ceram.Soc. 56, 575-581.

Fuller, E.R., Jr. and Thompson, R. 1980. Theory of chemically assisted fracture. Part 2. Atomic models of crack growth. J.Mat.Sci. 15, 1027-1034.

Gandhi, C. and Ashby, M.F. 1979. Fracture mechanism maps for materials which cleave: F.C.C., B.C.C. and H.C.P. metals and ceramics. Acta Metallurgica 27, 1565-1602.

Gerberich, W.W. 1974. On the pressure dependence of threshold stress intensity. Eng.Fract.Mech. 6, 405-407.

Granryd, L.A., Sondergeld, C.H. and Estey, L.H. 1980. Precursory changes in acoustic emissions prior to the uniaxial failure of rock. EOS, Transactions American Geophysical Union, 61, 372.

Henry, J.P. 1978. Mécanique lineaire de la rupture appliquee a l'etude de la fissuration et de la fracture de roches calcaires. Unpublished Ph.D. thesis, Université des Sciences et Techniques de Lille, 182 pp.

Henry, J.P. and Paquet, J. 1976. Mécanique de la rupture de roches calcitiques. Bull.Soc.géol.France. XVIII, 1573-82.

Irwin, G.R. 1958. Fracture. In: Handbuch der Physik, vol. 6 (ed. by S. Flügge) Springer, Berlin, 551-590.

Jackson, E.D. 1976. Linear volcanic chains on the Pacific plate. In: The Geophysics of the Pacific Ocean Basin and its Margin, Geophys. Monogr. Ser., vol. 19. (ed. by G.P. Woolard, G.H. Sutton, M.H. Manghnani and R. Moberly) American Geophysical Union, Washington, D.C. 319-335.

Kracek, F.C. and Clark, S.P., Jr., 1966. Melting and transformation points in oxide and silicate systems at low pressure. In: Handbook of Physical Constants (ed. S.P. Clark, Jr.) Mem. Geol.Soc.Am. 97, 301-322.

Kranz, R.L. 1980. The effects of confining pressure and stress difference on static fatigue of granite. J.Geophys. Res. 85, 1854-1866.

Krausz, A.S. 1978. The deformation and fracture kinetics of stress corrosion cracking. Int.J.Fracture 14, 5-15.

Lawn, B.R. 1975. An atomistic model of kinetic crack growth in brittle solids. J.Mat.Sci. 10, 469-480.

Lawn, B.R. and Wilshaw, T.R. 1975. Fracture of Brittle Solids Cambridge Univ. Press, Cambridge, 204 pp.

Marsh, D.M. 1964. Plastic flow in glass. Proc.RoyalSoc.Lond. A279, 420-435.

Martin, R.J. III, 1972. Time-dependent crack growth in quartz and its application to the creep of rocks. J.Geophys. Res. 77, 1406-1419.

Martin, R.J. III and Durham, W.B. 1975. Mechanisms of crack growth in quartz. J.Geophys. Res. 80, 4837-4844.

Meredith, P.G. and Atkinson, B.K. 1981. Acoustic response and stress corrosion of Whin Sill dolerite (in preparation).

Mizutani, H., Spetzler, H., Getting, I., Martin, R.J. III and Soga, N. 1977. The effect of outgassing upon the closure of cracks and the strength of lunar analogues. Proc.Lunar Sci.Conf. 8th, 1235-1248.

Norton, M.G. and Atkinson, B.K. 1981. Stress-dependent morphological features on fracture surfaces of quartz and glass. Tectonophysics (in press).

Peck, L. 1980. Stress corrosion cracking of quartzite. EOS, Transactions American Geophysical Union, 61, 361.

Price, N.J. 1966. Fault and joint development in brittle and semi-brittle rock. Pergamon, Oxford, 176 pp.

Ramsay, J.G. 1980. The crack-seal mechanism of rock deformation. Nature 284, 135-139.

Rice, J.R. 1979. Theory of precursory processes in the inception of earthquake rupture. Gerlands. Beitr. Geophysik, Leipzig 88, 91-127.

Rudnicki, J.W. 1980. Fracture mechanics applied to the earth's crust. Annual Rev. Earth Planet Sci. (ed. F.A. Donath), Annual Reviews Inc. vol. 8, 489-525.

Rutter, E.H. 1976. The kinetics of rock deformation by pressure solution. Phil.Trans.Roy.Soc.Lond. A283, 203-219.

Sano, O. and Ogino, S. 1980. Acoustic emission during slow crack growth. Tech.Rept.Yamaguchi Univ. 2 (in press).

Schmidt, R.A. 1976. Fracture mechanics of oil shale - unconfined fracture toughness, stress corrosion cracking and tension test results. Proc. 18th U.S. Symposium Rock Mechanics, Keystone, Colorado, 2A2-1-2A2-6.

Scholz, C.H. 1972. Static fatigue of quartz. J.Geophys.Res. 77, 2104-2114.

Scholz, C.H. 1968. Mechanism of creep in brittle rock. J.Geophys.Res. 73, 3295-3302.

Shuck, L.Z. and Keach, T.W. 1977. Monitoring acoustic emission from propagating fractures in petroleum reservoir rocks. In: Proc. First Conference on Acoustic emission/ Microseismic activity in Geological Structures and Materials (ed. by H.R. Hardy, Jr. and F.W. Leighton) Trans.Tech. Publications, Clausthal, Germany, 309-338.

Sibson, R.H. 1980. Low stress hydrofracture dilatancy; controls on its development in thrust, strike-slip and normal fault terrains. Nature (in review).

Schwartz, M.W. and Mukherjee, A.K. 1974. The migration of point defects in crack tip stress fields. Mat.Sci.Engineering 13, 175-179.

Söderberg, R. 1972. On the growth of intercrystalline wedge-cracks during creep-deformation. J.Mat.Sci. 7, 1373-1378.

Soga, N., Spetzler, H. and Mizutani, H. 1979. Comparison of single crack propagation in lunar analogue glass and the failure strength of rocks. Proc.Lunar Sci. Conf, 10th(in press)

Stevens, R.N. and Dutton, R. 1971. The propagation of Griffith cracks at high temperatures by mass transport processes. Mat. Sci. Engineering, 8, 220-234.

Swain, M.V., Williams, J.S., Lawn, B.R. and Beek, J.J.H. 1973. A comparative study of the fracture of various silica modifications using the Hertzian test. J.Mater.Sci. 8, 1153-1164.

Teng, T. and Henyey, T.L. 1981. Acoustic emission as a possible earthquake precursor. Proc.Third Ewing Symposium on Earthquake Prediction (in press)AGU, Washington, D.C.

Thomson, R. 1980. Theory of chemically assisted fracture. Part 1. General reaction rate theory and thermodynamics. J.Mater.Sci. 15, 1014-1026.

Tittman, B.R., Housley, R.M. and Cirlin, E.H. 1973. Internal friction of rocks and volatiles on the moon. Proc. Lunar Sci. Conf. 4th. 2631-2637.

Verrall, R.A. and O'Connell, R.J. 1979. Creep and fracture in the moon. Proc. Lunar Sci. Conf. 10th (in press).

Vogt, P.R. 1974. Volcano spacing, fractures, and thickness of the lithosphere. Earth Planet Sci. Lett.21, 235-252.

Waza, T., Kurita, K. and Mizutani, H. 1980. The effect of water on the subcritical crack growth in silicate rocks. Tectonophysics 67, 25-34.

Weeks, J.D., Lockner, D. and Byerlee, J. 1978. Change in b-values during movement on cut surfaces in granite. Bull. Seism. Soc. Am. 68, 333-341.

Weertman, J. 1968. Dislocation climb theory of steady-state creep. Am.Soc.Metals Trans. 61, 681-694.

Wiederhorn, S.M. 1968. Moisture assisted crack growth in ceramics. Int.J. Fracture Mechanics 4, 171-177.

Wiederhorn, S.M. 1974. Subcritical crack growth in ceramics. In: Fracture Mechanics of Ceramics, vol.2 (ed. by R.C. Bradt, D.P.H. Hasselman and F.F. Lange) Plenum Press, N.York, 613-646.

Wiederhorn, S.M. 1978. Mechanisms of subcritical crack growth in glass. In: Fracture Mechanics of Ceramics, vol. 4 (ed. by R.C. Bradt, D.P.H. Hasselman, and F.F. Lange) Plenum Press, N. York, 549-580.

Wiederhorn, S.M. and Bolz, L.H. 1970. Stress corrosion and static fatigue of glass. J.Am.Ceram.Soc. 53, 543-548.

Wiedmann, G.W. and Holloway, D.G. 1974. Plastic flow - slow crack propagation and static fatigue in glass. Phys. Chem. Glasses 15, 68-75.

Wilkins, B.J.S. 1980. Slow crack growth and delayed failure of granite. Int.J.Rock Mech.Min.Sci. and Geomech.Abstr. (in press).

Williams, D.P. and Evans, A.G. 1973. A simple method for studying slow crack growth. J.Testing and Evaluation 1, 264-270.

Williams, J.G. and Marshall, G.P. 1975. Environmental crack and craze growth phenomena in polymers. Proc.Royal Soc.Lond. A342, 55-77.

TABLE 1 Compilation of stress corrosion parameters (n-stress corrosion index, and activation enthalpy for crack propagation) in geological materials.

TABLE 1. Stress corrosion data for geological materials

MATERIAL	CONDITIONS	ACTIVATION ENTHALPY ($kJ.mole^{-1}$)	STRESS CORROSION INDEX (n)	REFERENCE
Quartz				
a plane $\perp$ r	air, 30% R.H., 20°C		19.1	ATKINSON (1979)
a plane $\perp$ z	water, 20°-80°C	52.5	12.0	ATKINSON (1979)
	2N NaOH, 20°C		9.5	ATKINSON/MEREDITH(1980)
	2N HCl, 20°C		19.3	ATKINSON/MEREDITH(1980)
5° to $[0\bar{1}10]$	water vapour, 90°-240°C	108		MARTIN (1972)
	water vapour, 20°-250°C	63		MARTIN/DURHAM (1975)
<c>	water vapour, 20°C-50°C	46-100		SCHOLZ (1972)
Arkansas Novaculite	water, 20°-80°C	69.5	25.1	ATKINSON (1980)
Falerans	air, 20°C		130	HENRY/PAQUET (1976)
Micrite	water+$CaCO_3$, 20°C		26	HENRY/PAQUET (1976)
	water+$CaCO_3$, 20°-85°C	63-147		HENRY (1978)
St.Pons Marble	water+$CaCO_3$, 20°C		26-29	HENRY/PAQUET (1976)
Black Gabbro	air, 30% R.H., 20°C		32.1	ATKINSON/RAWLINGS (1979a 1979b, 1981)
	water, 20°C		36.1(region 3)	op.cit.
			28.6(region 1)	op.cit.
Murata Basalt	air, 20°C		22	SANO/OGINO (1980)

TABLE 1.(continued)

MATERIAL	CONDITIONS	ACTIVATION ENTHALPY ($kJ.mole^{-1}$)	STRESS CORROSION INDEX(n)	REFERENCE
Ralston	air,28%R.H.,20°C		44.4	ATKINSON et al.(1980)
Intrusive	water,20°C		23.5	ATKINSON et al.(1980)
Kinosaki	air,30°C		~ 34	WAZA et al.(1980)
Basalt	water,25°C		~ 33	WAZA et al.(1980)
Whin Sill	air,30%R.H.,20°C			MEREDITH/ATKINSON(1981)
Dolerite	water,20°-80°C			MEREDITH/ATKINSON(1981)
Westerley	air,30%R.H.,20°C		39.1	ATKINSON/RAWLINGS(1981)
Granite	water,20°C		34.8	ATKINSON/RAWLINGS(1981)
	air,30%R.H.,20°C		35.9	ATKINSON et al.(1980)
	water,20°C		33.7	ATKINSON et al.(1980)
	toluene,11.3%R.H.		51	SWANSON(1980)
	water,20°C		53	SWANSON(1980)
Oshima	air,20°C		30	SANO/OGINO(1980)
Granite				
Yugawara	air,25°C		~ 31	WAZA et al.(1980)
Andesite	water,25°C		~ 26	WAZA et al.(1980)
Lac du Bonnet	air,20°C		58.5	WILKINS(1980)
Granite	air,20°C		55.9	WILKINS(1980)

FIGURE CAPTIONS

FIGURE 1. Fracture mechanism map for quartz. Normalized tensile stress is plotted against homologous temperature. Grain size is 100 micrometres.

FIGURE 2. Schematic stress intensity factor (K_I) - crack velocity (v) curves. The threshold stress intensity factor (K_{Io}) and the critical stress intensity factor (K_{Ic}) are shown. For an explanation of the significance of regions 1, 2, and 3 see text.

FIGURE 3. Synoptic diagram showing the influence of crystallographic orientation on stress corrosion in quartz. Stress intensity factor is plotted against $\log_{10}$ of crack velocity. After Bruner (1979). Solid and open circles are for crack growth on $\underline{r}$ in the direction $[10\bar{1}2]$ for 2 specimens of natural quartz at 62.5% R.H. (Bruner, 1979). Solid triangles are for crack growth perpendicular to $\underline{z}$ on $\underline{a}$ in synthetic quartz in liquid water (Atkinson, 1979). Open triangles are for crack growth perpendicular to $\underline{r}$ on $\underline{a}$ in synthetic quartz at 68% R.H. (Atkinson, 1979).

FIGURE 4. Influence of environment chemistry (pH) on crack propagation in synthetic quartz. Crack growth occurs on the $\underline{a}$ plane in a direction normal to $\underline{z}$. Log_{10} of stress intensity factor is plotted against $\log_{10}$ of crack velocity. After Atkinson and Meredith (1981).

FIGURE 5. Synoptic K_I-v diagram for rocks of basaltic composition. Note discontinuous stress intensity factor scale. All tests at 20°C unless otherwise indicated.

FIGURE 6. Synoptic K_I-v diagram for rocks of granitic composition. All tests at 20°C.

FIGURE 7. Plot of crack velocity (v) and acoustic emission event rate (dN_E/dt) gainst mode I stress intensity factor (K_I) for Westerley granite in liquid water at 20°C.

FIGURE 8. Influence of stress intensity factor (normalized with respect to K_{Ic}) on the b-value (the amplitude distribution parameter) for Westerley granite and Black gabbro in air of 30% R.H. and in liquid water. Horizontal bars denote the stress range of these data.

FIGURE 9. An example of the likely trend in the growth of an earthquake rupture controlled by stress corrosion. After Das and Scholz (1980). Note discontinuous and non-uniform time scale. Star denotes initial radius of rupture. Other relevant conditions are given on the figure.

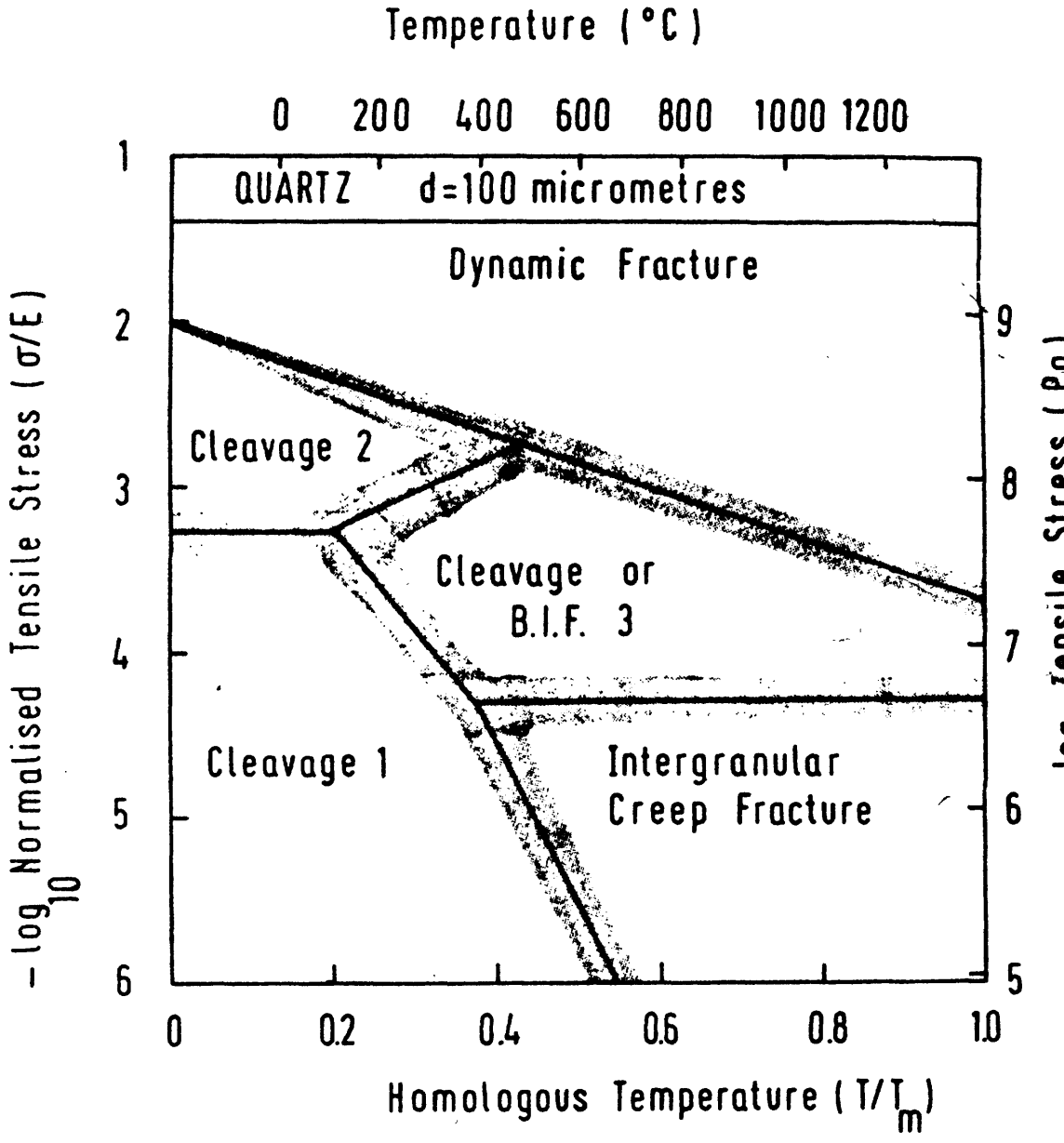
Temperature (°C)
0 200 400 600 800 1000 1200
QUARTZ d=100 micrometres
Dynamic Fracture
Cleavage 2
Cleavage or
B.I.F. 3
Cleavage 1
Intergranular
Creep Fracture
$-\log_{10}$ Normalised Tensile Stress (σ/E)
$\log_{10}$ Tensile Stress (Pa)
1 2 3 4 5 6
9 8 7 6 5
0 0.2 0.4 0.6 0.8 1.0
Homologous Temperature (T/T_m)

Fig. 1

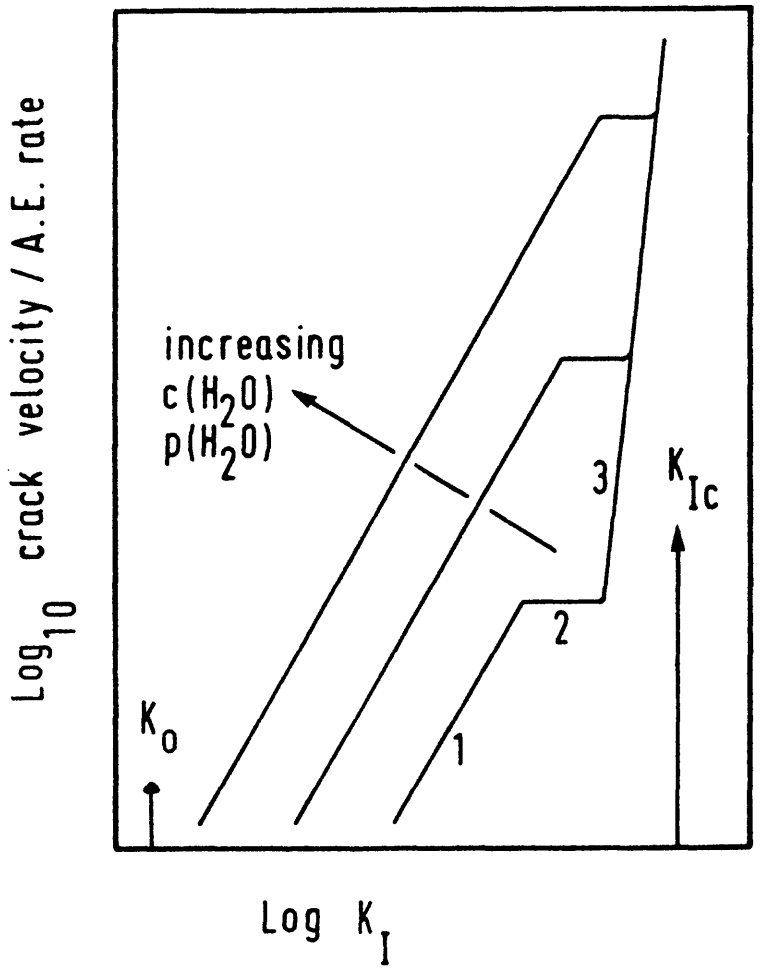
Log10 crack velocity / A.E. rate
increasing
c(H2O)
p(H2O)
3
KIc
2
1
K0
Log KI

FIG. 2.

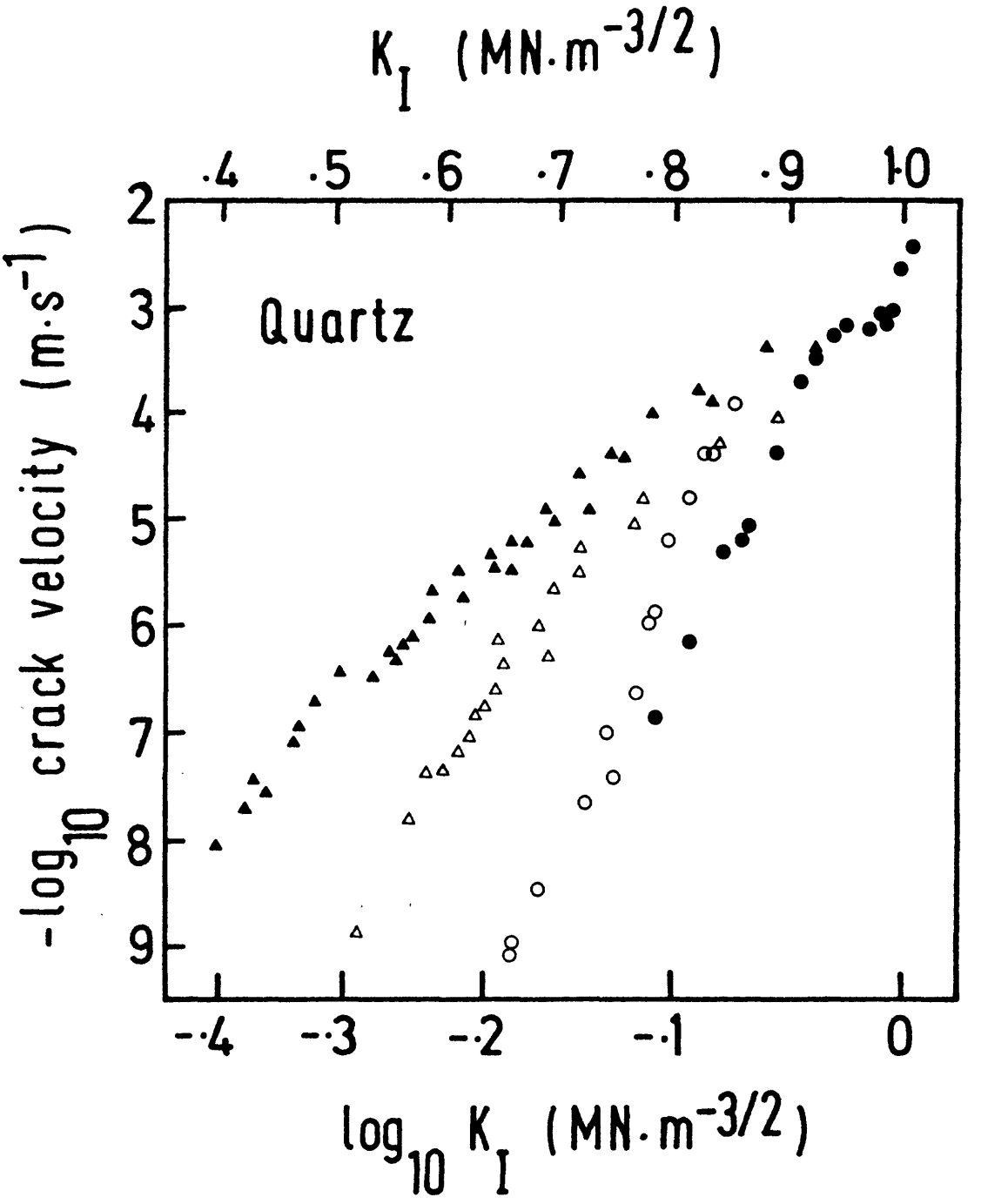
K_I (MN.m$^{-3/2}$)
.4
.5
.6
.7
.8
.9
1.0
Quartz
$-\log_{10}$ crack velocity (m.s^{-1})
2
3
4
5
6
7
8
9
-.4
-.3
-.2
-.1
0
$\log_{10} K_I$ (MN.m$^{-3/2}$)

FIG. 3.

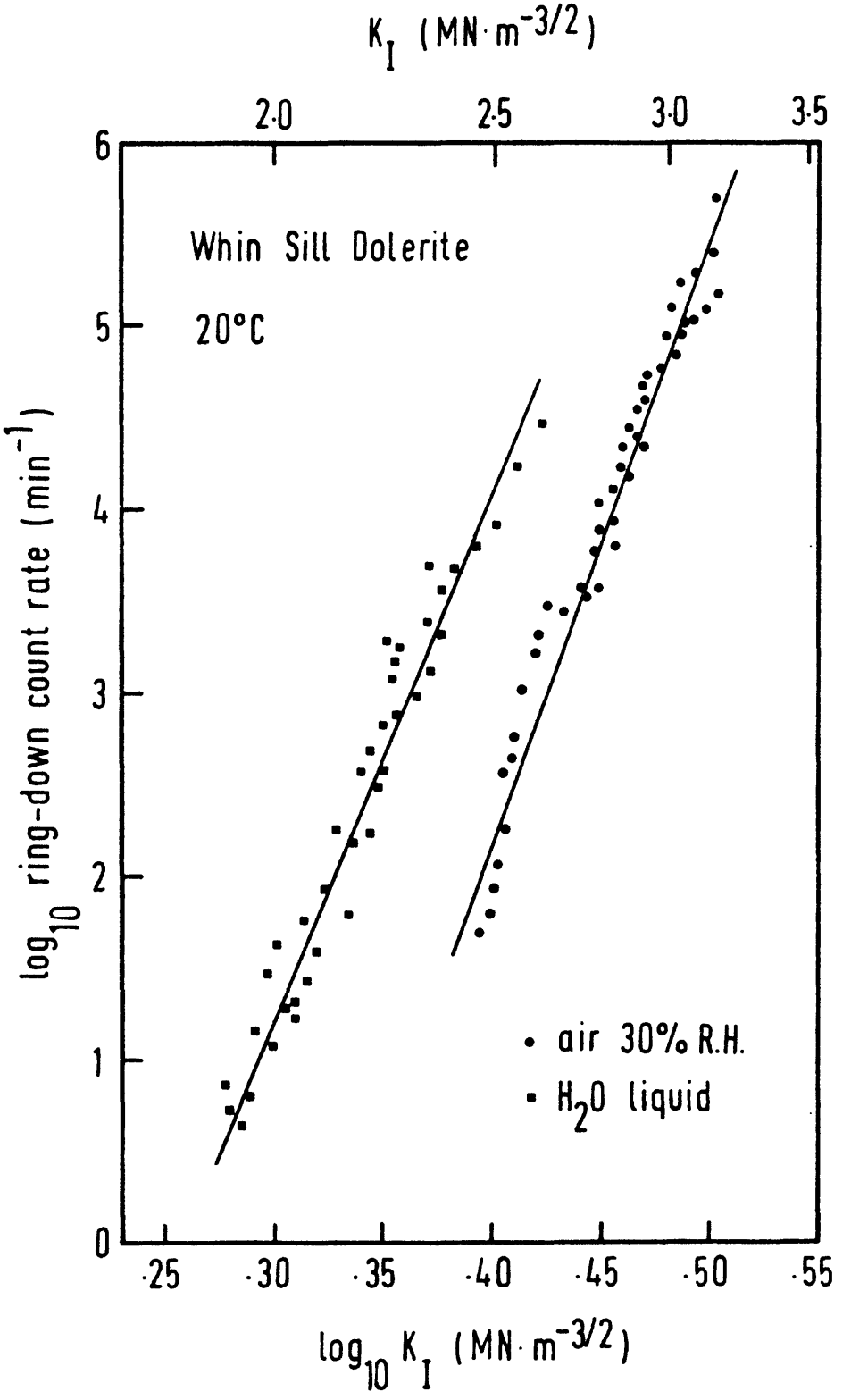
K_I (MN·m$^{-3/2}$)
2·0
2·5
3·0
3·5
Whin Sill Dolerite
20°C
$\log_{10}$ ring-down count rate (min^{-1})
0
1
2
3
4
5
6
• air 30% R.H.
▪ H_2O liquid
·25
·30
·35
·40
·45
·50
·55
$\log_{10} K_I$ (MN·m$^{-3/2}$)

FIG. 4

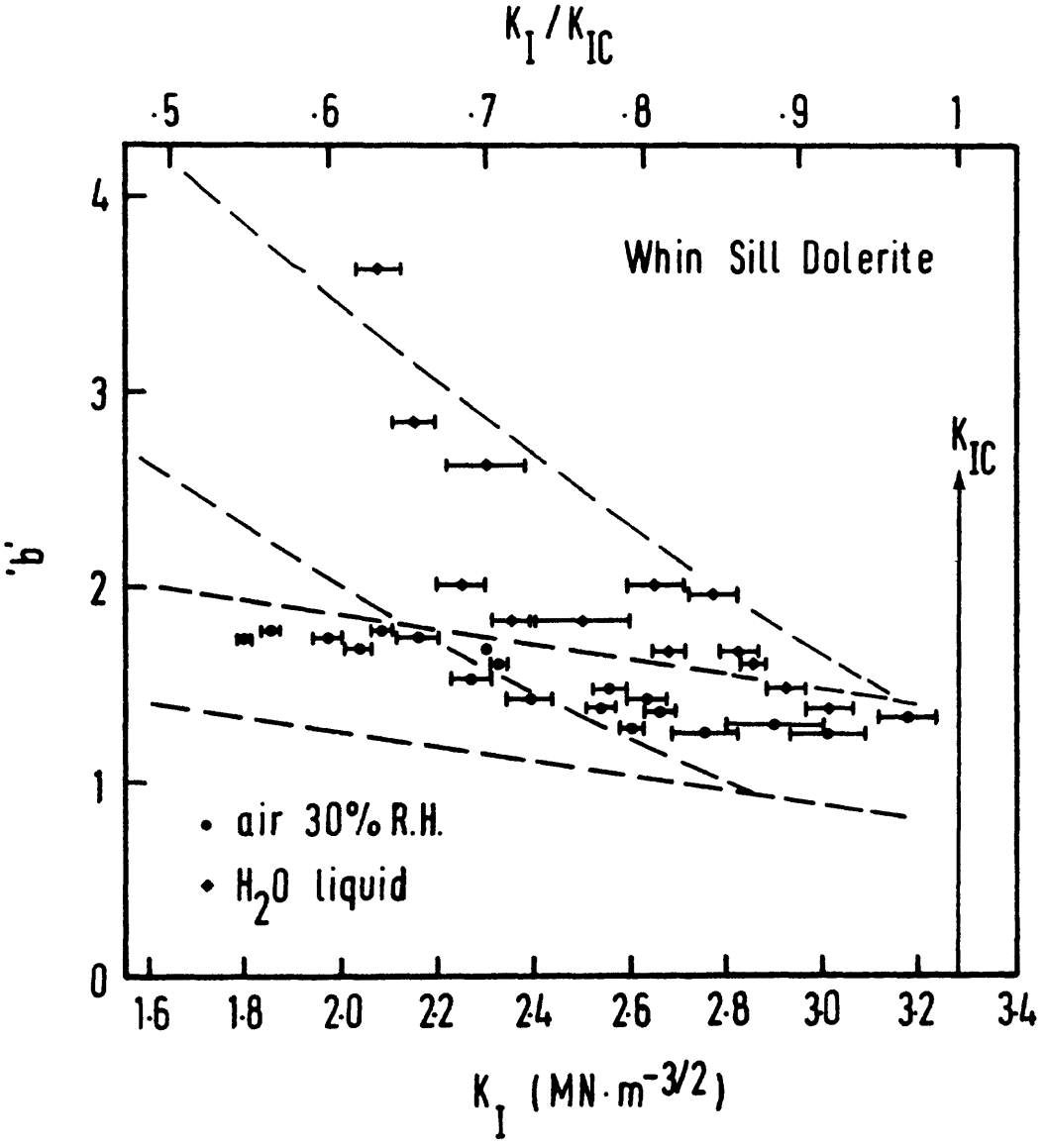
K_I / K_{IC}
·5
·6
·7
·8
·9
1
Whin Sill Dolerite
K_{IC}
• air 30% R.H.
• H_2O liquid
0
1
2
3
4
1·6
1·8
2·0
2·2
2·4
2·6
2·8
3·0
3·2
3·4
K_I (MN·m$^{-3/2}$)

FIG. 5

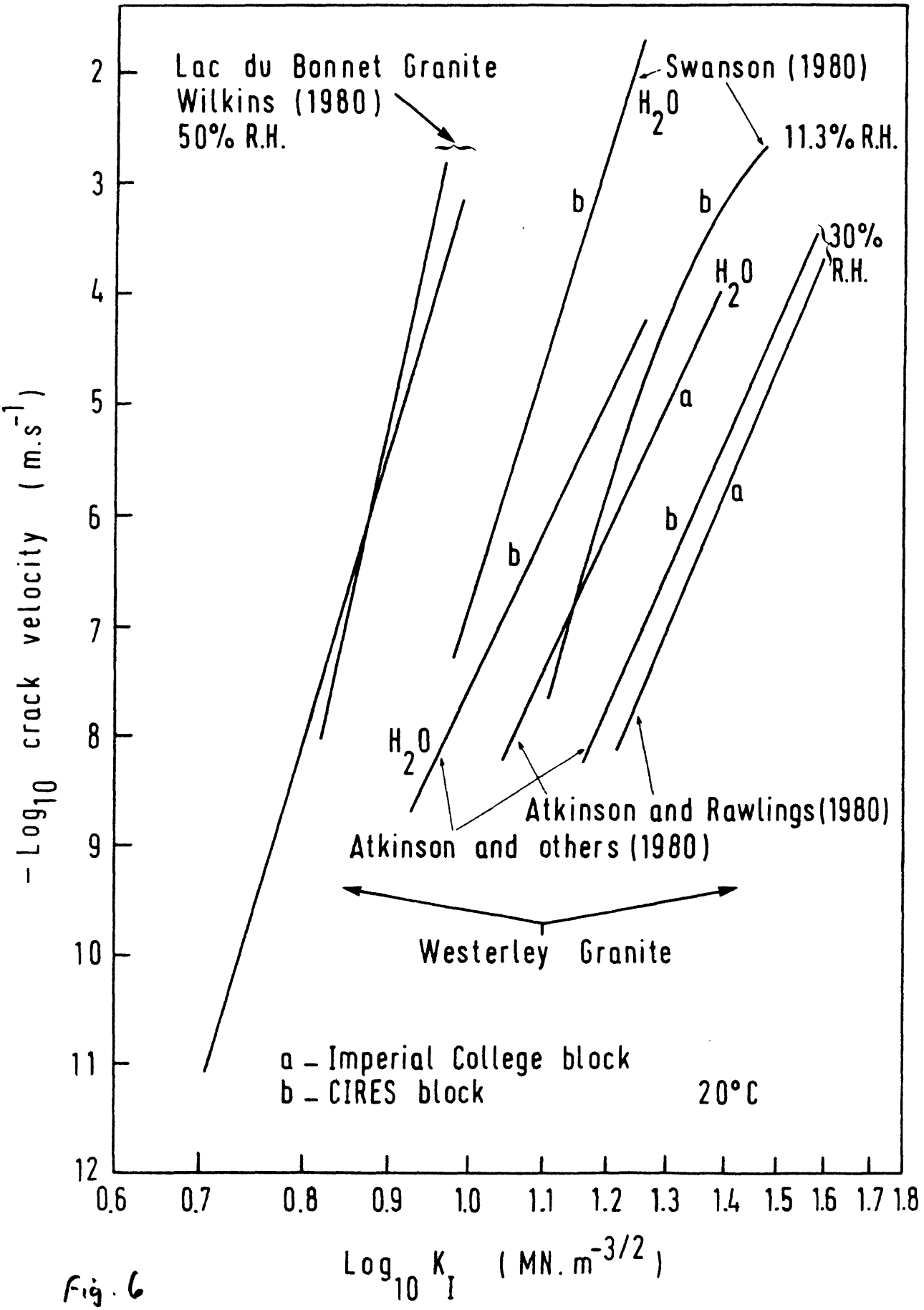
Lac du Bonnet Granite
Wilkins (1980)
50% R.H.
Swanson (1980)
H_2O
11.3% R.H.
30%
R.H.
H_2O
H_2O
a
b
Atkinson and Rawlings(1980)
Atkinson and others (1980)
Westerley Granite
a – Imperial College block
b – CIRES block
20°C
$-\text{Log}_{10}$ crack velocity (m.s^{-1})
Log_{10} K_I (MN.m$^{-3/2}$)
2
3
4
5
6
7
8
9
10
11
12
0.6
0.7
0.8
0.9
1.0
1.1
1.2
1.3
1.4
1.5
1.6
1.7
1.8

Fig. 6

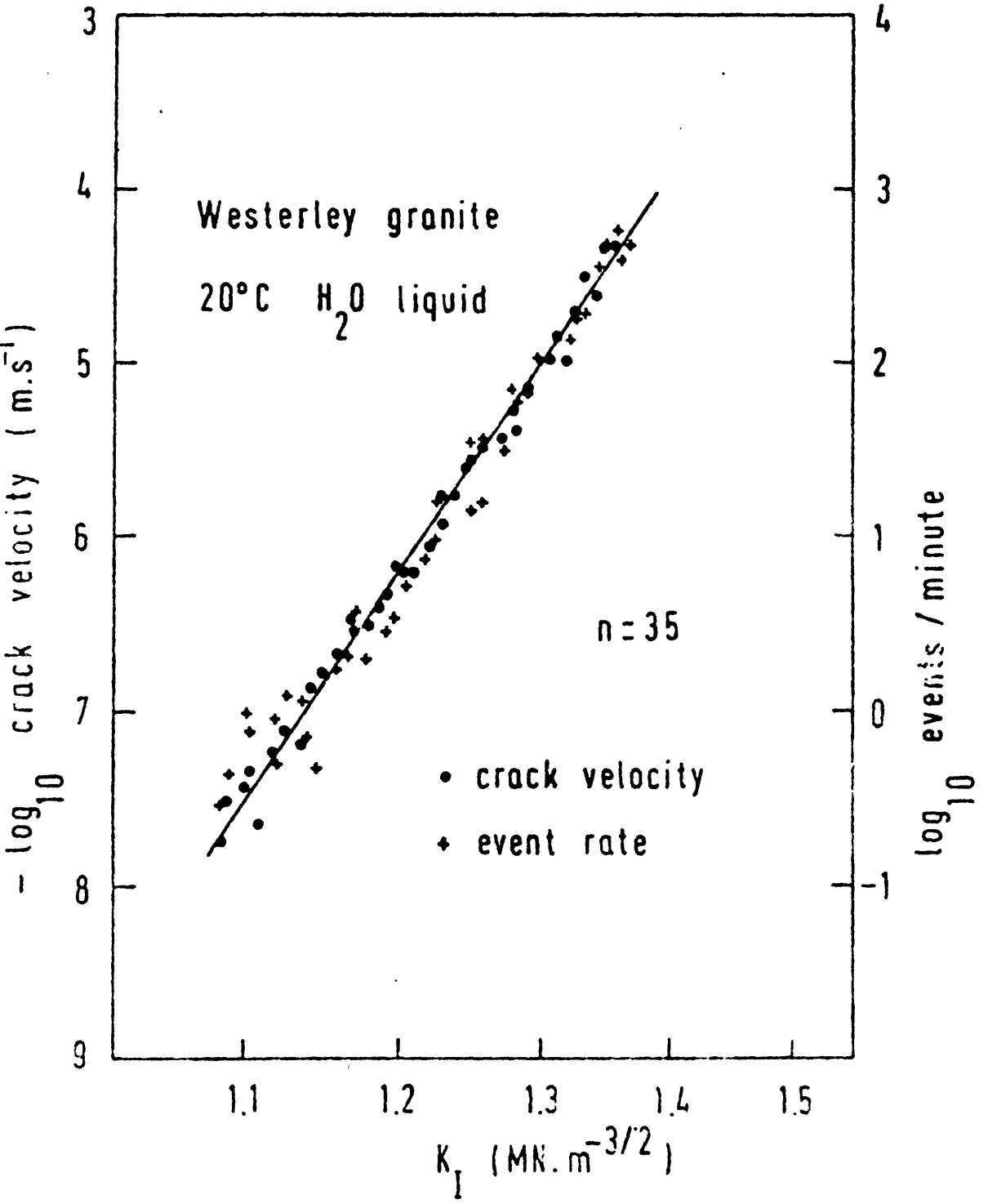
Westerley granite
20°C H2O liquid
n = 35
• crack velocity
+ event rate
- log10 crack velocity (m.s-1)
log10 events / minute
KI (MN.m-3/2)
3
4
5
6
7
8
9
4
3
2
1
0
-1
1.1
1.2
1.3
1.4
1.5

FIG. 7.

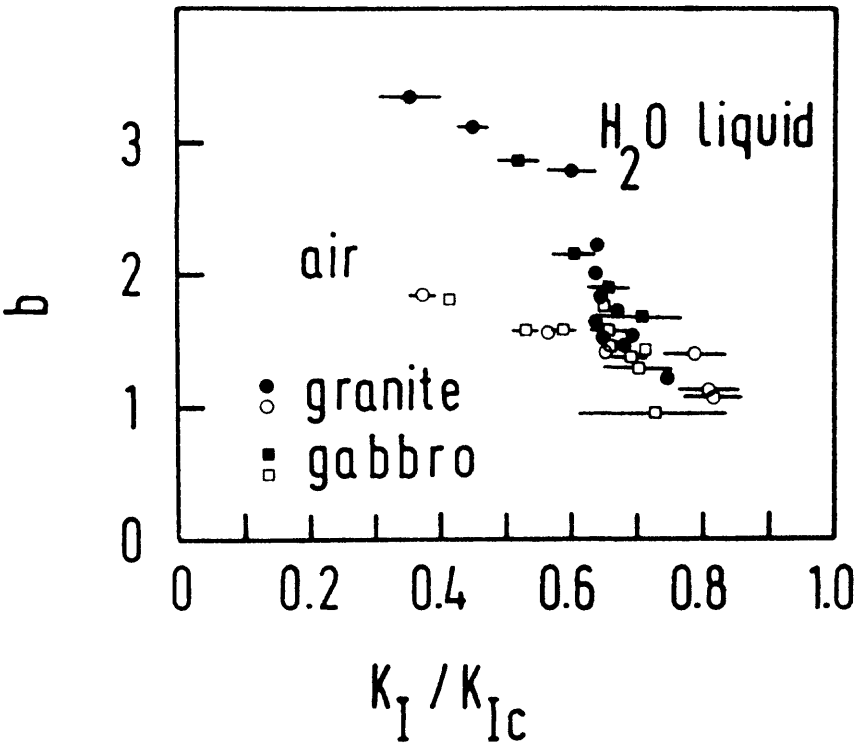

FIG. 8.

FIG. 9.

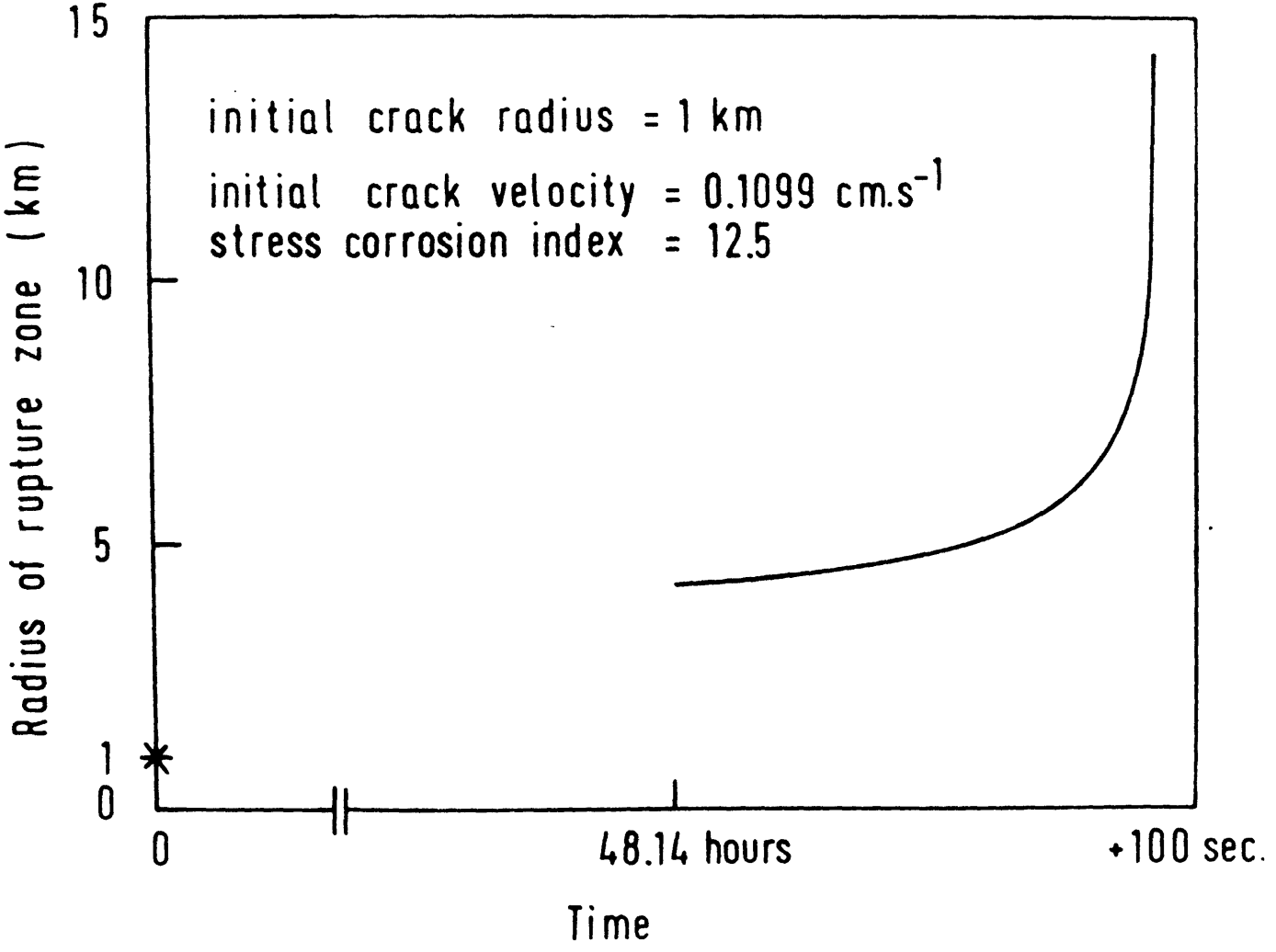
15
10
5
1
0
initial crack radius = 1 km
initial crack velocity = 0.1099 cm.s^{-1}
stress corrosion index = 12.5
Radius of rupture zone (km)
0
48.14 hours
+100 sec.
Time

3. ACOUSTIC EMISSION AND STRESS CORROSION OF WHIN SILL DOLERITE.

P.G. Meredith and B.K. Atkinson

Introduction.

Double torsion tests have been run on plates of Whin Sill dolerite to establish K_{Ic}, and K_I-v diagrams for specimens in air and liquid water. Acoustic response was monitored during the deformation experiments.

Theoretical considerations

K_I values were determined from the expression

$$K_I = PW_m \left[3(1+\nu)/Wt^3 t_n\right]^{\frac{1}{2}} \qquad (1)$$

where P is the load, W_m is the moment arm, ν is Poisson's ratio, W is the width, t the thickness and t_n a reduced thickness of the specimen.

Crack velocity was measured from load relaxation curves using

$$V = -\phi\ a_f P_f (1/P^2)(dP/dt) \qquad (2)$$

where ϕ is a constant, a_f and P_f are the crack length and load at the end of a test, P is the load and dP/dt is the rate of load relaxation.

Activation enthalpies (ΔH) for crack propagation were

calculated from

$$\Delta H = \frac{RT_1T_2}{(T_2-T_1)} (n+1) \ln {}^{K_{I_1}}/_{K_{I_2}} \quad (3)$$

where R is the gas constant, n is the stress corrosion index and T is the temperature.

K_I-v data were fitted to an equation of the form

$$V = \alpha K_I^n \quad (4)$$

Acoustic emission data were fitted to equations such as

$$dN_E/dt = \beta K_I^{n_E} \quad (5)$$

and

$$dN_R/dt = \gamma K_I^{n_R} \quad (6)$$

where α, β, γ are constants, as are n, n_E and n_R; dN_E/dt is the rate of events and dN_R/dt is the rate of ring-down counts.

Amplitude distributions were described by

$$n(a) = (a/a_o)^{-b} \quad (7)$$

where n(a) is the fraction of the emission population whose peak amplitude exceeds amplitude a and a_o is the lowest detectable amplitude. b is the amplitude distribution parameter.

Results

K_{Ic} for Whin Sill dolerite was found to be 3.28 ± 0.10 MN.m$^{-3/2}$ The values of n, n_E and n_R as in equations 4, 5 and 6 are given below (see Figs. 1, 2 and 3).

	Air, 20°C, 30% RH	H_2O 20°C	H_2O 75°C
n	31.2 (0.990)	29.0 (0.992)	28.4 (0.995)
n_E	31.1 (0.984)	29.1 (0.977)	
n_R	32.9 (0.981)	29.9 (0.973)	

Figures in brackets are correlation coefficients.

Note of close similarity of n_E, n_R, and n, as found for Westerley granite and Black gabbro in earlier studies.

The activation enthalpy between 20°C and 75°C was found to be 30.4 ± 1.9 kJ.mole^{-1} using a constant loading rate technique and 34 to 47.6 kJ.mole^{-1} using the data of K_I-v diagrams.

Amplitude distribution b-values shown in Figure 4 show the same trend as found for granite and gabbro, i.e. the b-values depend strongly on the "humidity" of the crack tip environment and K_I values. The dashed lines in Figure 4 are the limits of data obtained wet and "dry" for earlier experiments on granite and gabbro. Examples of amplitude distribution

nique used to obtain b-value data at high fractions of K_{Ic}. It is based on capturing emission and ring-down count rate data on a storage oscilloscope. The slope of Figure 7 is a measure of the b-parameter.

FIGURE CAPTIONS

FIGURE 1. K_I - v diagram for Whin Sill dolerite.

FIGURE 2. dN_E/dt - K_I diagram for Whin Sill dolerite.

FIGURE 3. dN_R/dt - K_I diagram for Whin Sill dolerite.

FIGURE 4. Amplitude distribution parameter vs K_I for Whin Sill dolerite. Horizontal bars denote stress range. Dashes denote data for Westerley granite and Black gabbro.

FIGURE 5. Amplitude distribution data for "dry" Whin Sill dolerite.

FIGURE 6. Amplitude distribution data for "wet" Whin Sill dolerite.

FIGURE 7. Plot of cumulative events vs cumulative ring-down counts for "dry" Whin Sill dolerite. Inset shows load/time trace for test. Points on load trace with letters correspond to points with same letter on emission plot.

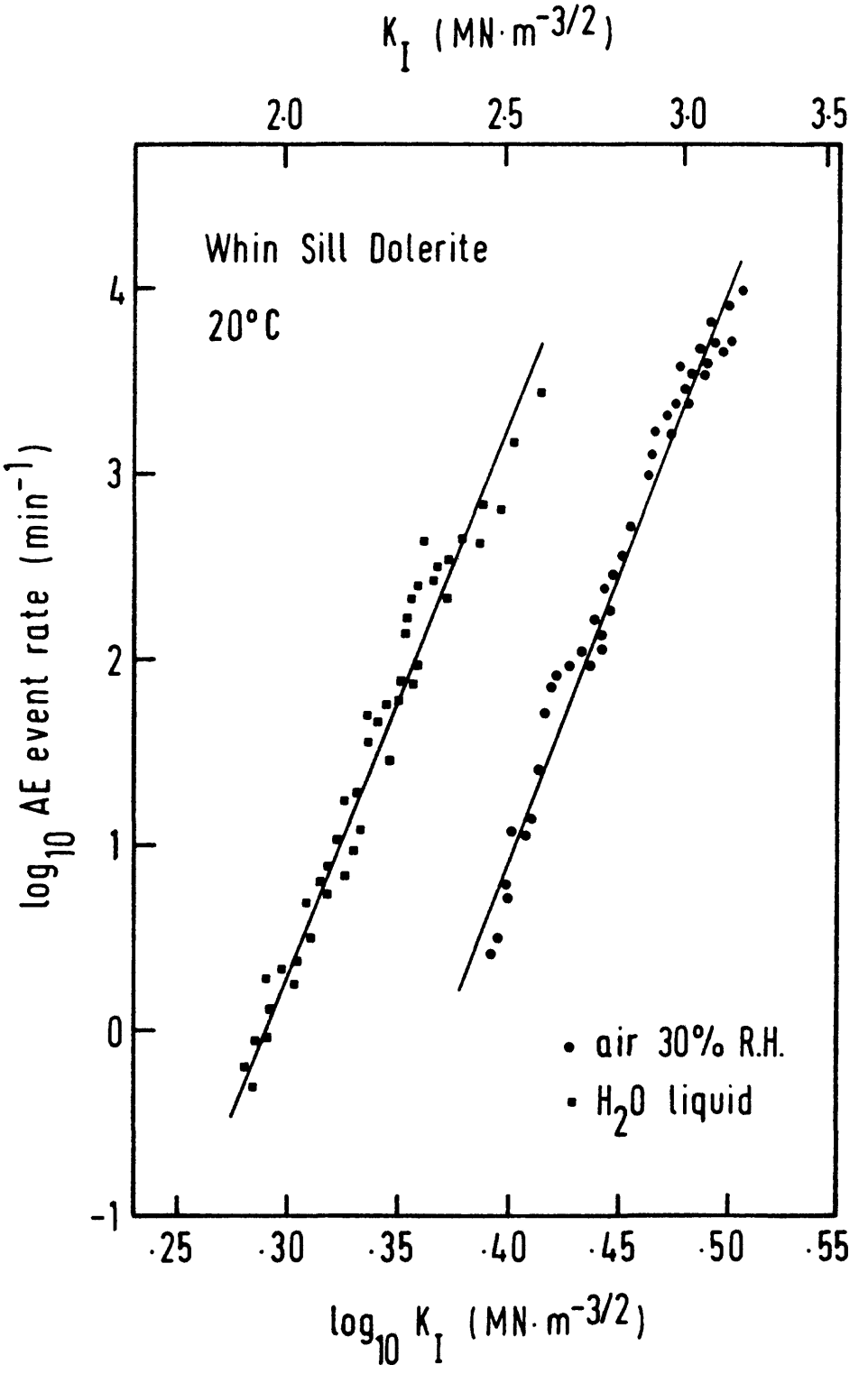
K_I (MN·m$^{-3/2}$)
2·0
2·5
3·0
3·5
Whin Sill Dolerite
20°C
4
3
2
1
0
-1
$\log_{10}$ AE event rate (min^{-1})
• air 30% R.H.
• H_2O liquid
·25
·30
·35
·40
·45
·50
·55
$\log_{10}$ K_I (MN·m$^{-3/2}$)

FIG. 2.

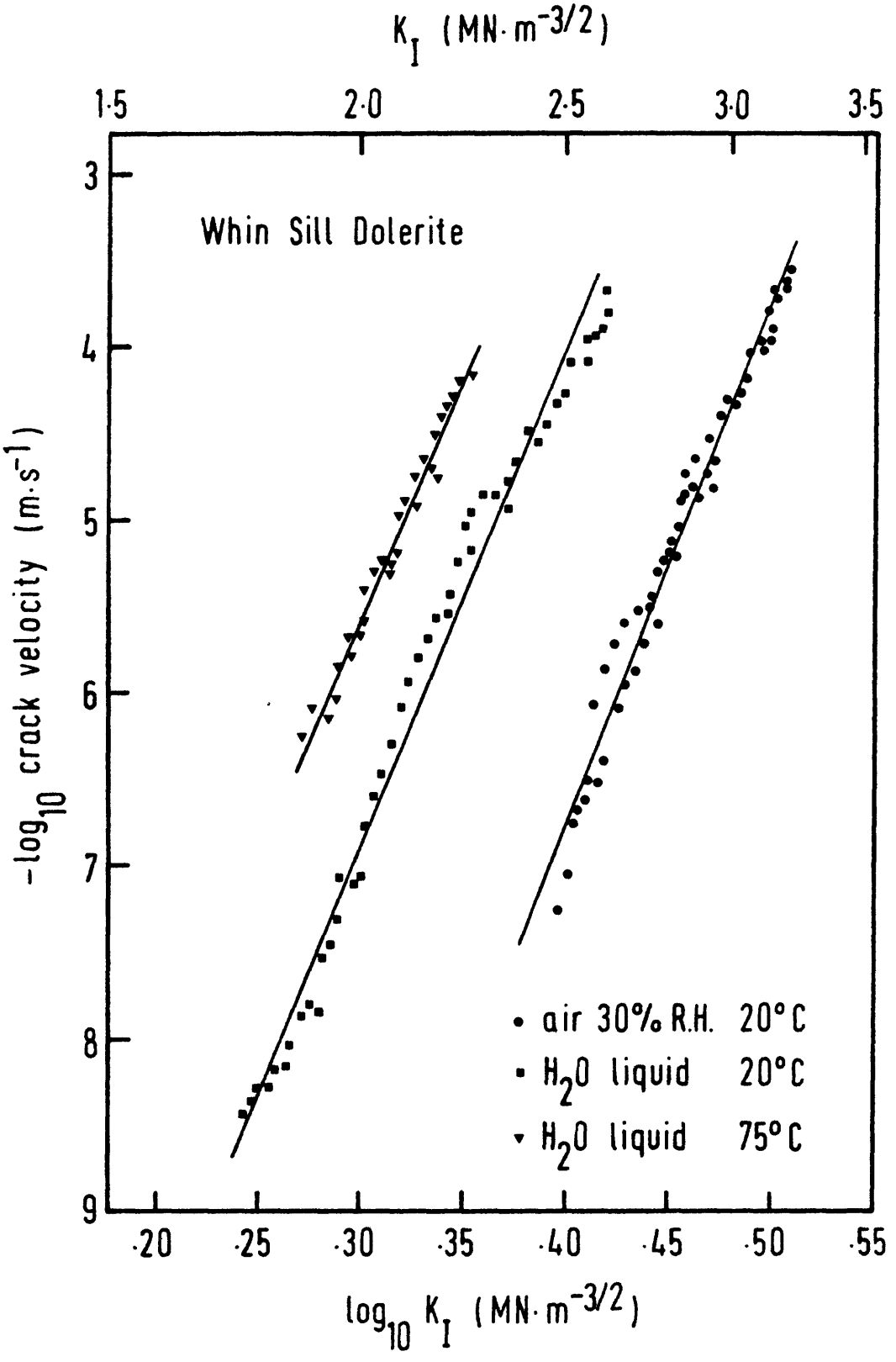
K_I (MN·m$^{-3/2}$)
1·5
2·0
2·5
3·0
3·5
Whin Sill Dolerite
$-\log_{10}$ crack velocity (m·s^{-1})
3
4
5
6
7
8
9
• air 30% R.H. 20°C
▪ H_2O liquid 20°C
▾ H_2O liquid 75°C
·20
·25
·30
·35
·40
·45
·50
·55
$\log_{10} K_I$ (MN·m$^{-3/2}$)

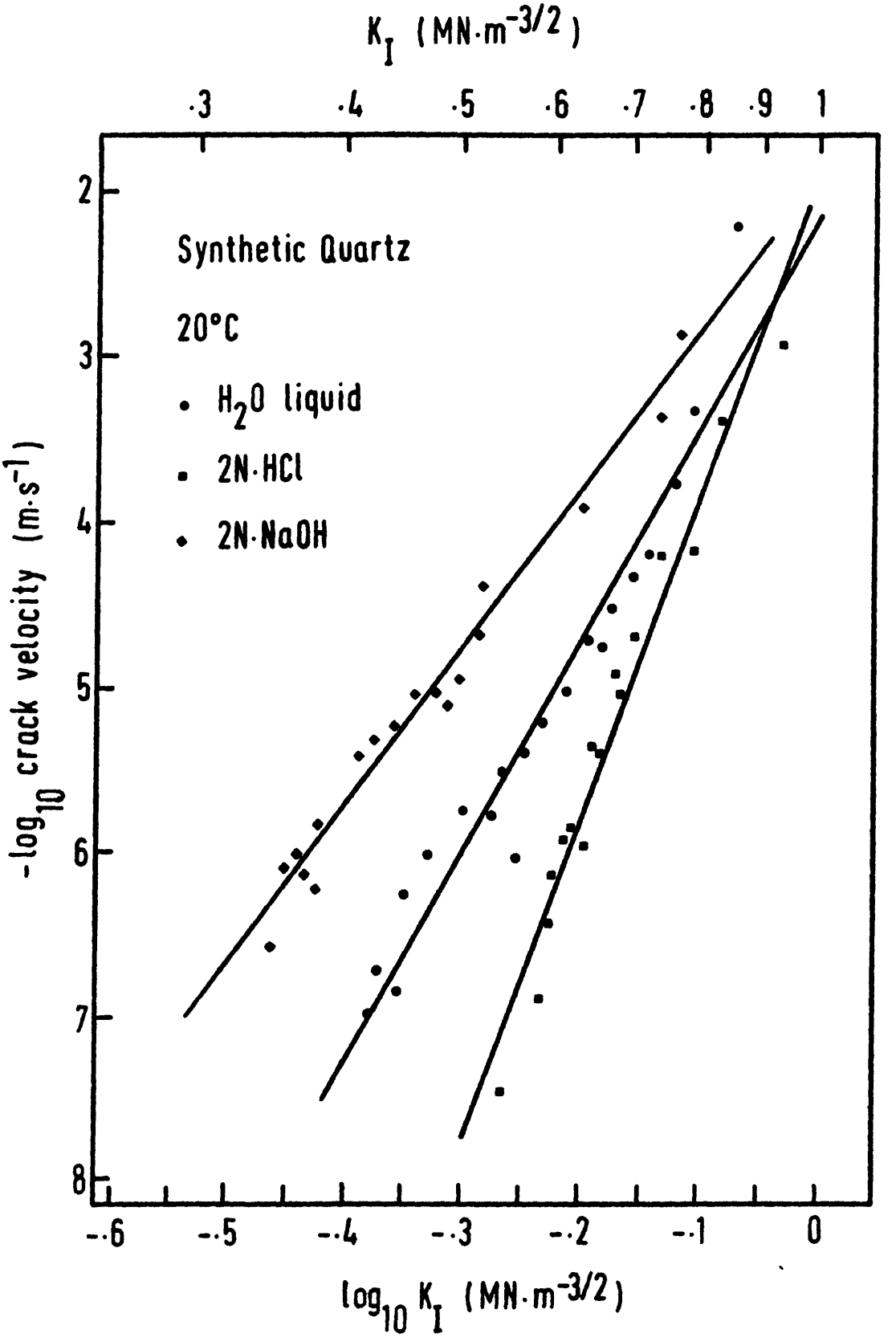
K_I (MN·m$^{-3/2}$)
·3
·4
·5
·6
·7
·8
·9
1
Synthetic Quartz
20°C
• H_2O liquid
▪ 2N·HCl
• 2N·NaOH
$-\log_{10}$ crack velocity (m·s^{-1})
2
3
4
5
6
7
8
-·6
-·5
-·4
-·3
-·2
-·1
0
$\log_{10} K_I$ (MN·m$^{-3/2}$)

FIG. 4.

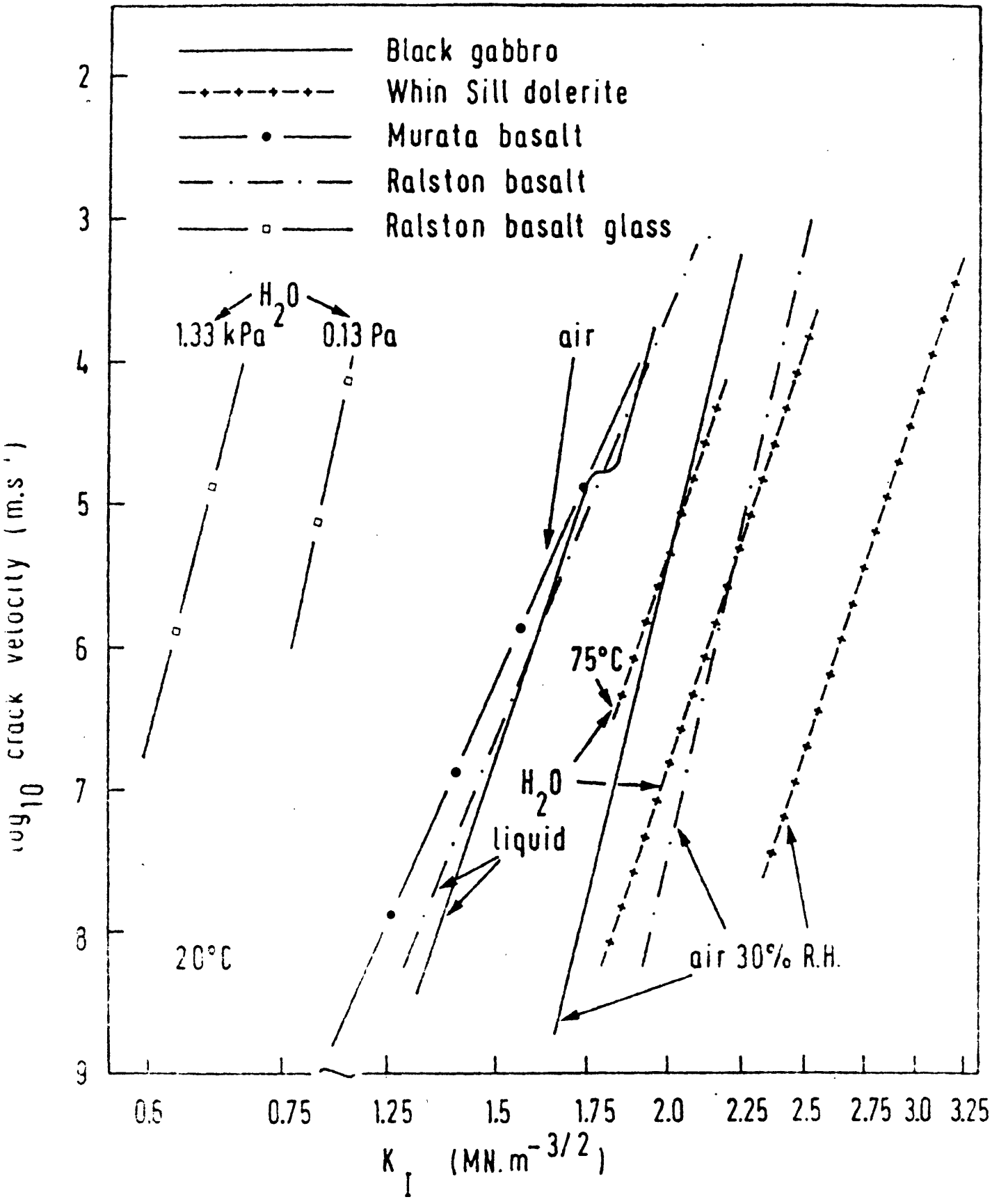
Black gabbro
Whin Sill dolerite
Murata basalt
Ralston basalt
Ralston basalt glass
H_2O
1.33 kPa
0.13 Pa
air
75°C
H_2O
liquid
20°C
air 30% R.H.
$\log_{10}$ crack velocity (m.s^{-1})
K_I (MN.m$^{-3/2}$)
2
3
4
5
6
7
8
9
0.6
0.75
1.25
1.5
1.75
2.0
2.25
2.5
2.75
3.0
3.25

FIG. 5.

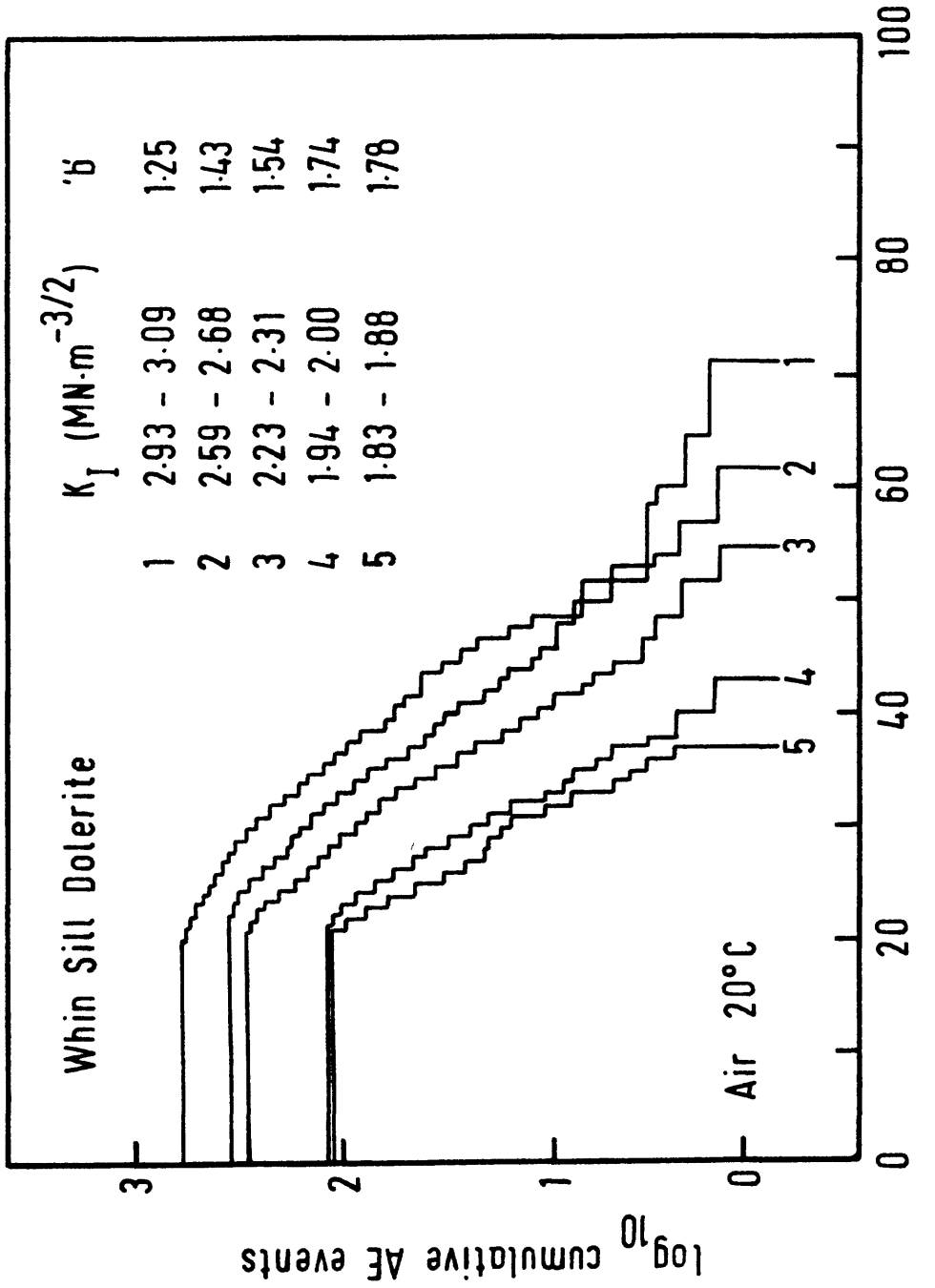
Whin Sill Dolerite
K_I (MN·m$^{-3/2}$)
'b'
1 2·93 - 3·09 1·25
2 2·59 - 2·68 1·43
3 2·23 - 2·31 1·54
4 1·94 - 2·00 1·74
5 1·83 - 1·88 1·78
Air 20°C
log$_{10}$ cumulative AE events
Amplitude (dB)
0
1
2
3
20
40
60
80
100

FIG. 5

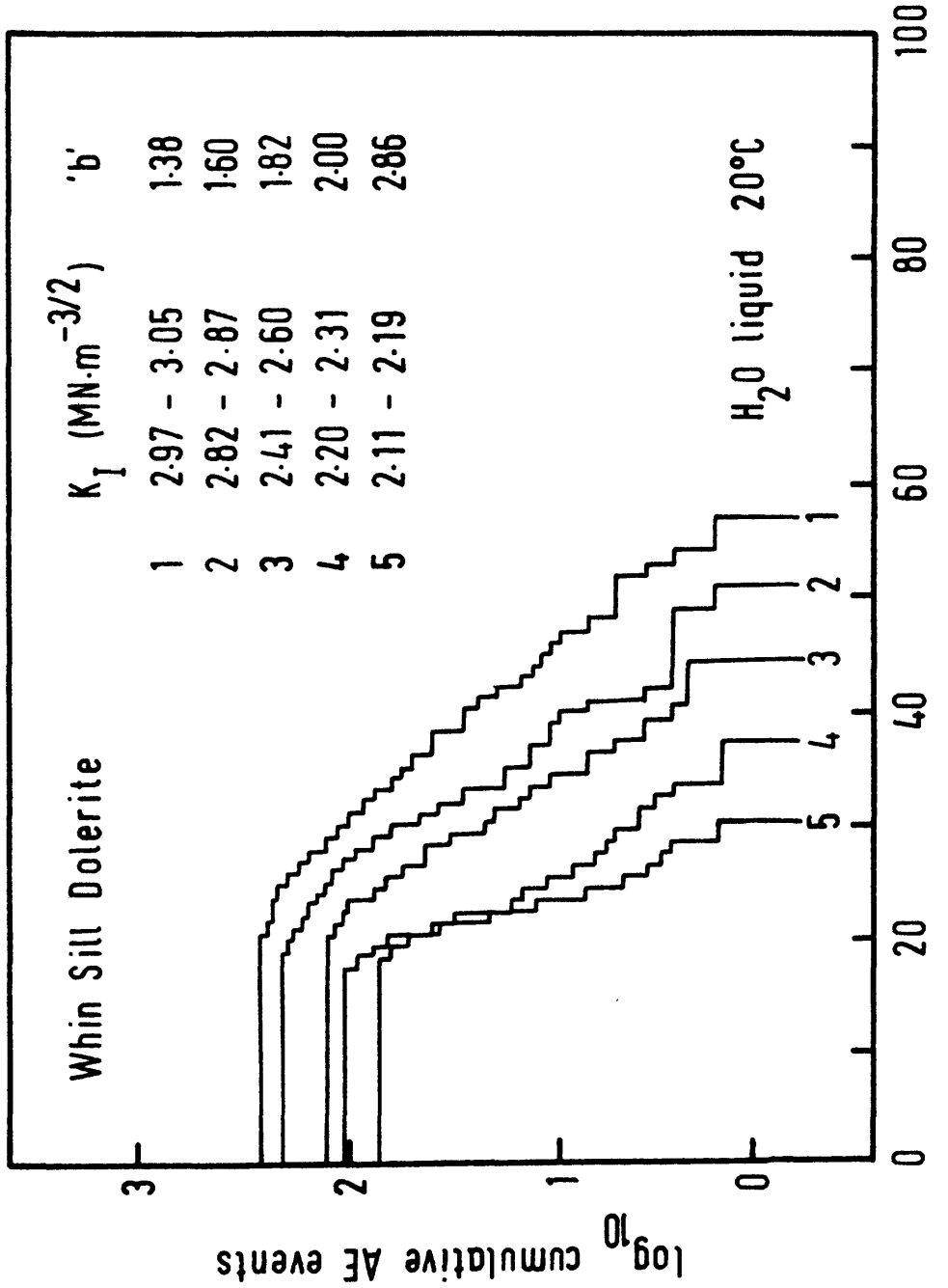
Whin Sill Dolerite
K_I (MN·m$^{-3/2}$)
'b'
1 2·97 - 3·05 1·38
2 2·82 - 2·87 1·60
3 2·41 - 2·60 1·82
4 2·20 - 2·31 2·00
5 2·11 - 2·19 2·86
H_2O liquid 20°C
$\log_{10}$ cumulative AE events
Amplitude (dB)
0
1
2
3
20
40
60
80
100

FIG. 6.

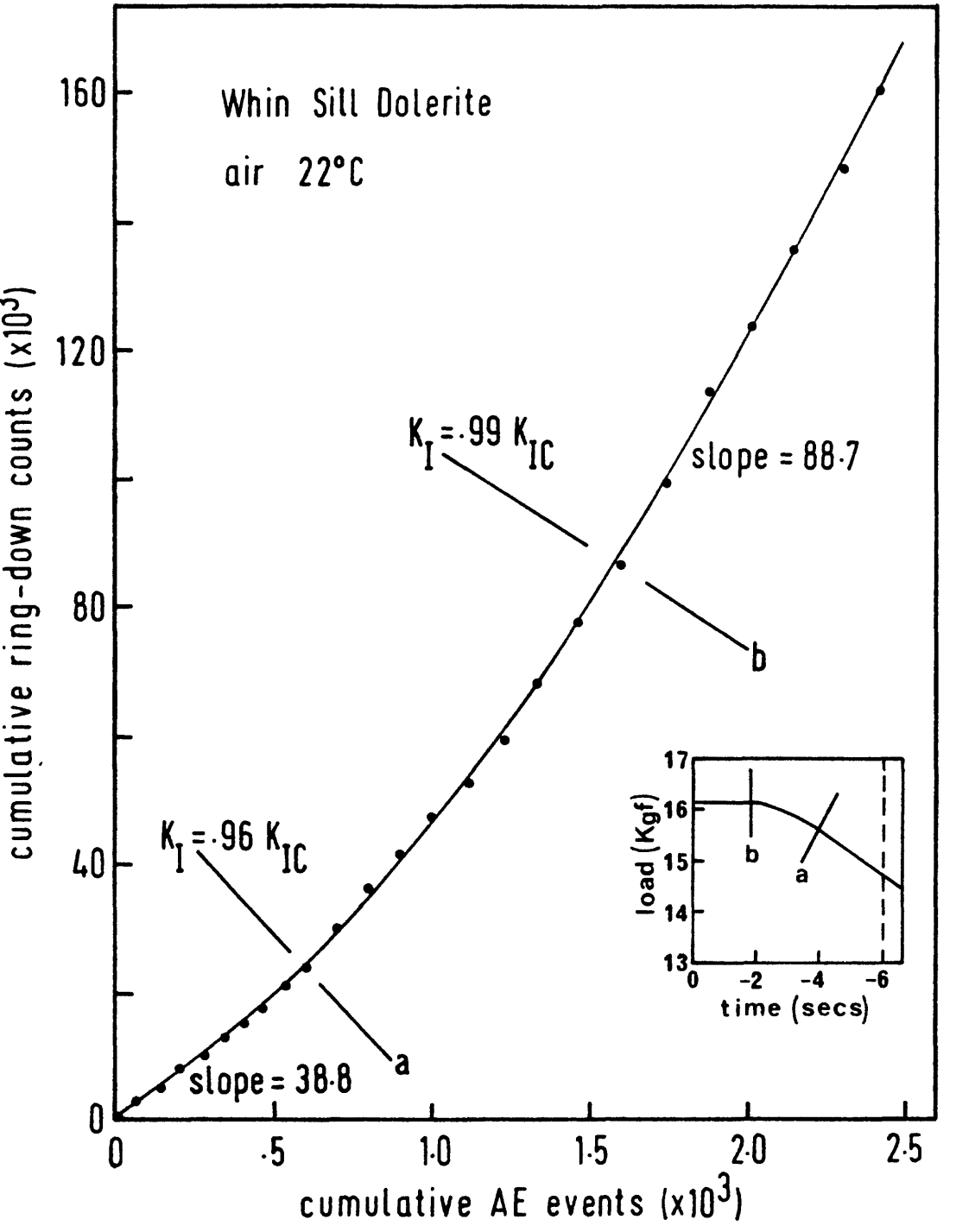
Whin Sill Dolerite
air 22°C
$K_I = .99\ K_{IC}$
slope = 88·7
b
$K_I = .96\ K_{IC}$
slope = 38·8
a
cumulative ring-down counts (x10³)
cumulative AE events (x10³)
0
40
80
120
160
·5
1·0
1·5
2·0
2·5
load (Kgf)
time (secs)
17
16
15
14
13
-2
-4
-6

FIG. 7.

4. INFLUENCE OF THERMAL AND STRESS CYCLING ON THE FRACTURE AND ACOUSTIC RESPONSE OF WESTERLEY GRANITE.

B. K. Atkinson, D. Macdonald and P. G. Meredith

Introduction

A series of thermal cycling and stress cycling experiments have been performed on Westerley granite to determine how such treatment influences fracture mechanics parameters, such as K_{Ic} and the K_I-v relationship. As a guide to the growth and development of microcracks the acoustic response was continuously monitored in all experiments, i.e. event rates, count rates and amplitude distributions.

Thermal cycling experiments

A 2.5 cm cube of granite was placed in a silver steel holder into which a stainless steel waveguide was screwed. The waveguide was screwed down until it exerted a force of approximately 1 Kg on the specimen. The waveguide/specimen assembly was placed in a furnace so that the free end of the wave guide emerged from the furnace. An appropriate transducer was attached by epoxy cement to this free end via a stainless steel cone.

The specimen was heated slowly ($<2.5^{o}C$/min) to a predetermined temperature and then allowed to cool slowly ($<1.5^{o}C$/min) to room temperature. This cycle was repeated. On each subsequent heating cycle the specimen was taken to a temperature of $100^{o}C$ higher than on the previous cycle. A maximum temperature of $500^{o}C$ was studied so as to avoid

complicating factors due to the α-β quartz transition.

Additionally, double torsion specimens were given one cycle of the above heat treatment so that specimens were available that had been heat-treated to a maximum temperature of 20°C, 100°C, 200°C, 300°C, 400°C and 500°C. These specimens were then tested for K_{Ic} and to determine K_I-v relations. Experiments to determine the latter relations also involved measurement of the acoustic response.

Before fracture mechanics tests were performed on these specimens they were stored at 20°C in a dessicator containing silica gel and evacuated to better than 10^{-3} torr.

Stress cycling experiments

A double torsion specimen was loaded to approximately $^1/5$ of the expected K_{Ic} and then unloaded to near zero load again. Acoustic response was monitored only on the loading cycle. This cycle was repeated five times, on each occasion taking the specimen to a maximum load $^1/5K$ greater than in the previous cycle.

Results.

Thin section studies

Thin sections were made of dummy specimens given the same heat treatment as described in the section on thermal cycling.

A general increase in microcrack density with increase in

maximum temperature of heat treatment was observed. The differential expansion of neighbouring quartz and feldspar grains which becomes markedly non linear above 450°C plays the dominant role in thermal crack development and widening during heating.

In specimens heated to 100° and 200°C the intragranular thermal cracks develop mainly as cleavage cracks in the feldspars and as randomly oriented cracks in the quartz grains. Many of the intragranular cracks do not traverse grains. Grain boundary cracking, however, is dominant in these specimens. In the specimens heated to 300°C most intragranular cracks do traverse the grains. In the specimens there is a marked increase in the number of microcracks. Although specimens heated to 400°C and 500°C also show an increase in microcrack density it is not nearly as marked as the increase that occurs between 200° and 300°C.

Bauer and Johnson (1979) obtained a linear increase in the microcrack density with increasing temperature up to the α-β quartz transition of 573°C. This contrasts with our results (Fig. 1). One explanation of this is the anomalous lowering of the Hertzian fracture strength of quartz noted by Swain et al. (1973) in the region 200°-300°C.

But this does not explain why Bauer and Johnson (1979) did not observe the effect. An alternative hypothesis, which does not preclude the existence of the effect noted in Hertzian studies, is that residual strains locked in the specimen are released when a sufficient density of microcracks is attained,

which happens to result after heat treatment to 300°C. Such strains may not have been released in the Bauer and Johnson experiments or were not present in these specimens.

Acoustic emission during thermal cycling tests

The acoustic response during heating and cooling stages of each cycle is well illustrated by the data of Figures 2 and 3. These show ring-down counts as a function of temperature. Note that on heating very little acoustic emission occurs until the maximum temperature in the previous cycle is reached. At this point there is a substantial increase in the rate of emission. This can be viewed as a sort of thermal equivalent to the Kaiser effect. Note also that heating above 300°C induces a dramatic increase in the level of acoustic emissions. The increase in ring-down counts at about the previous cycle's maximum temperature is thought to reflect the extension and widening of previously formed microcracks and the formation of new microcracks. The uniform b-values found for these emissions argue for a constant source for the emissions.

On cooling there is a rapid drop in ring-down count rate for a few tens of degrees and then all emission/cooling curves follow a similar trend. Once more b-values are relatively constant, except at 500°C. The rapid change in emission rate is thought to result from grain readjustment and the steady change to microcrack healing.

K_{Ic} tests

Two sets of double torsion specimens were used in this

work. Small specimens were 0.23 x 2.9 x 10 cm. Larger specimens were 0.4 x 6 x 10 cm.

After heat treatment, their K_{Ic} values were determined and are given in Figure 4. Note the substantial change in the rate of strength reduction around 200°-300°C, but that heating to 100°C has little influence on K_{Ic}. The small specimens gave a maximum value of K_{Ic} as 2.37 $MN.m^{-3/2}$ and the larger ones gave a value of 1.69 $MN.m^{-3/2}$. It is not clear at this time why the discrepancy in the two sets of data arose.

Crack velocity/stress intensity factor data

K_I-v curves were obtained by stress relaxation tests on heat-treated double torsion specimens. Specimens that were heated to a maximum of 20°C, 100°C, 300°C and 500°C were treated at 20°C in air of 30% R.H.

Stress relaxation tests and acoustic emission monitoring

Ring-down count rates and event rates were recorded and are plotted against stress intensity factor as well as crack velocity in Figures 5, 6 and 7.

The acoustic emission and crack velocity data were fitted to expressions of the form of equations 4, 5 and 6 in section 3, where n, n_E, n_R are constants.

Values of n, n_E and n_R are given in Table 1.

Table 1: Values of n, n_E and n_R for heat-treated Westerley granite tested at 20°C.

	20°C	100°C	300°C	500°C
n	39.1	38.5(0.998)	39.1(0.99)	38.6(0.972)
n_E	39.6	40.4(0.996)	41.2(0.982)	39.5(0.990)
n_R	38.8	41.4(0.998)	40.0(0.971)	37.4(0.992)

Figures in brackets are correlation coefficients.

The most notable feature of the data in Table 1 is that heat treating does not significantly influence the values of n, n_E or n_R. b-values for the specimen heat-treated to 100°C decrease as K_I is raised, but those for specimens heated to 300° and 500°C lie close to 1.3 independent of K_I.

Stress-cycling and acoustic emission monitoring

Data from these experiments are plotted in Figure 8. For the first 4 loading cycles the acoustic response illustrates what has become known as the Kaiser effect, i.e. Only after the maximum stress attained in a previous cycle has been exceeded will there be any significant acoustic emission. Cycles 5 and 6 ignore this principle, however, and show substantial emission at much lower stresses than were attained in the previous cycles.

This is interpreted to show that residual strain energy is being released by the stress cycling process. Other evi-

dence supporting the presence of residual strains in these specimens are: anomalous increase in microcrack density between 200° and 300°C, marked lowering of K_{Ic} values between 200° and 300°C.

Conclusions and recommendations for further work

Heat treatment can markedly influence the fracture mechanics properties of Westerley granite, but drying in ovens to 100°C (a common practice in many laboratories) does not significantly affect fracture properties, although some influence is discernible.

Our specimen of Westerley granite probably contains residual strains which influence fracture behaviour.

The influence of confining pressure on the effects of heat-treating should be studied as a next stage in this work.

References

Atkinson, B.K., Rutter, E.H., Sibson, R.H., and White, S.H. 1980. Specific experimental and field studies pertaining directly to the mechanisms of seismic and aseismic faulting. Final technical report to NEHRP, USGS, 1980. Contract:- 14-08-0001-17662.

Rutter, E.H. and Mainprice, D.H. 1978. The effect of water on stress relaxation of faulted and unfaulted sandstone. Pure and Applied Geophysics, 116, 634-654.

Rutter, E.H., Atkinson, B.K., Mainprice, D.H. 1978. On the use of the stress relaxation testing method in studies of the mechanical behaviour of geologic materials. Geophys. J. R. Astr. Soc. 55, 155-170.

obtain larger displacements. These experiments will be carried out in Hoek-Franklin cells (Fig. 10) at room temperature and moderate confining pressure (up to 50 MPa (.5Kb.)). It is also hoped to carry out creep experiments to obtain creep laws for various gouges.

PRESHAL MORE BASALT

Stress relaxation and long term constant strain rate experiments are to be carried out to determine the effects of a varying mineralogy and rock chemistry on deformation mechanisms along faults at low strain rates. The Tertiary Preshal More basalt from Skye, N.W. Scotland, was chosen as it is reasonably unaltered and contains few vesicles and cracks.

Characterisation of basalt.

Preliminary characterisation experiments have been completed under similar conditions to Westerley granite (Fig.11). Dry basalt shows similar or slightly lower fracture and sliding stress to dry Westerley granite. However, a larger reduction in fracture stress is observed on wetting, and therefore Rehbinder effects seem to be more important than in Westerley granite. Stick-slip occurs frequently and is the dominant sliding behaviour at confining pressures greater than 100 MPa (1 Kb). From these experiments it would seem that 200 MPa (2 Kb) is a suitable confining pressure for pre-fracturing for stress relaxation and long term constant strain rate tests, as a single through going fracture is produced.

Figure Captions

Figure 1 Plot of total number of microcracks (solid circles) and the number of intragranular microcracks (open circles) as a function of temperature; from microscopic studies of Westerley granite.

Figure 2 Cumulative ring-down counts on slow heating Westerley granite to successively higher temperatures.

Figure 3 Cumulative ring-down counts on slow cooling of Westerley granite from successively higher temperatures.

Figure 4 K_{Ic} values for Westerley granite after heat-treatment. Open triangles - small specimens. Solid triangles - large specimens.

Figure 5 Crack velocity (solid squares), event rate (open squares) and ring-down counts (open circles) vs K_I for Westerley granite heat-treated to 100°C (large specimens).

Figure 6 As for Fig. 5, but heat-treated to 300°C (large specimens)

Figure 7 As for Fig. 5, but heat-treated to 500°C (large specimens)

Figure 8 Ring-down counts as a function of loading cycle for double torsion specimens of Westerley granite.

References

Bauer, S.J. and Johnson, B. 1979. Effects of slow heating on the physical properties of Westerley and Charcoal granites. 20th US Symposium on Rock Mechanics, Austin, Texas.

Swain, M.V., Williams, J.S., Lawn, B.R. and Beek, J.J.H., 1973. A comparative study of the fracture of various silica modifications using the Hertzian test. J. Mater. Science 8, 1153-1164.

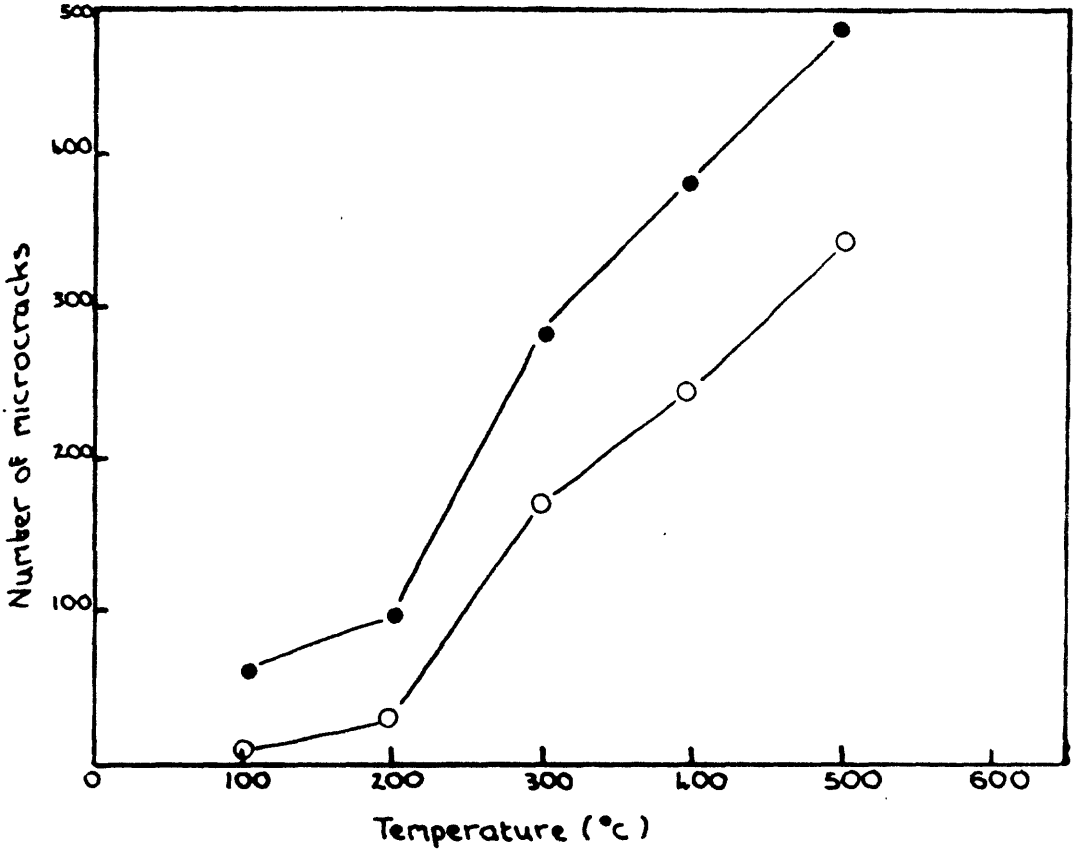
Number of microcracks
500
600
300
200
100
0
100
200
300
400
500
600
Temperature (°C)

Fig. 1

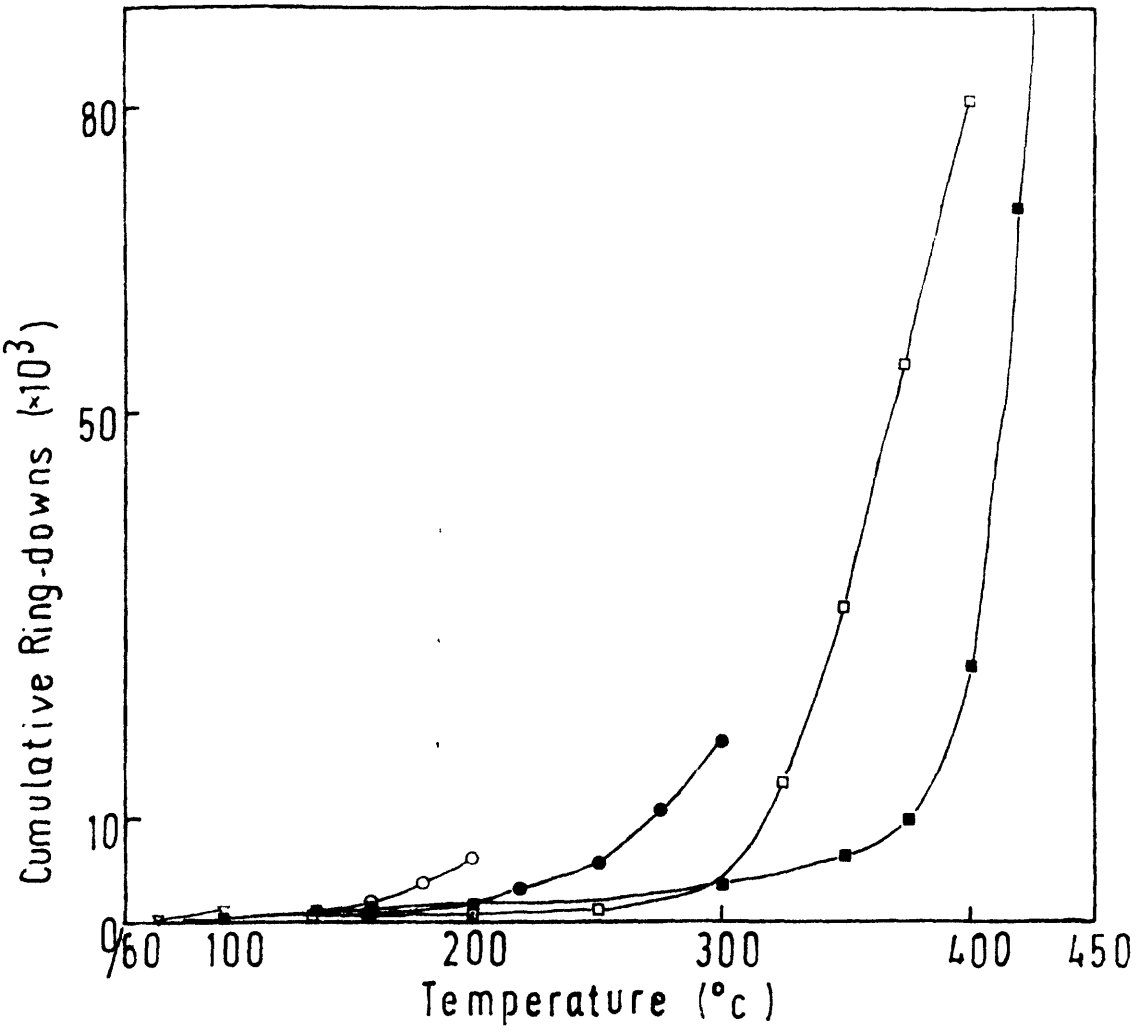
80
50
10
0
60
100
200
300
400
450
Cumulative Ring-downs (×10³)
Temperature (°C)

Fig. 2

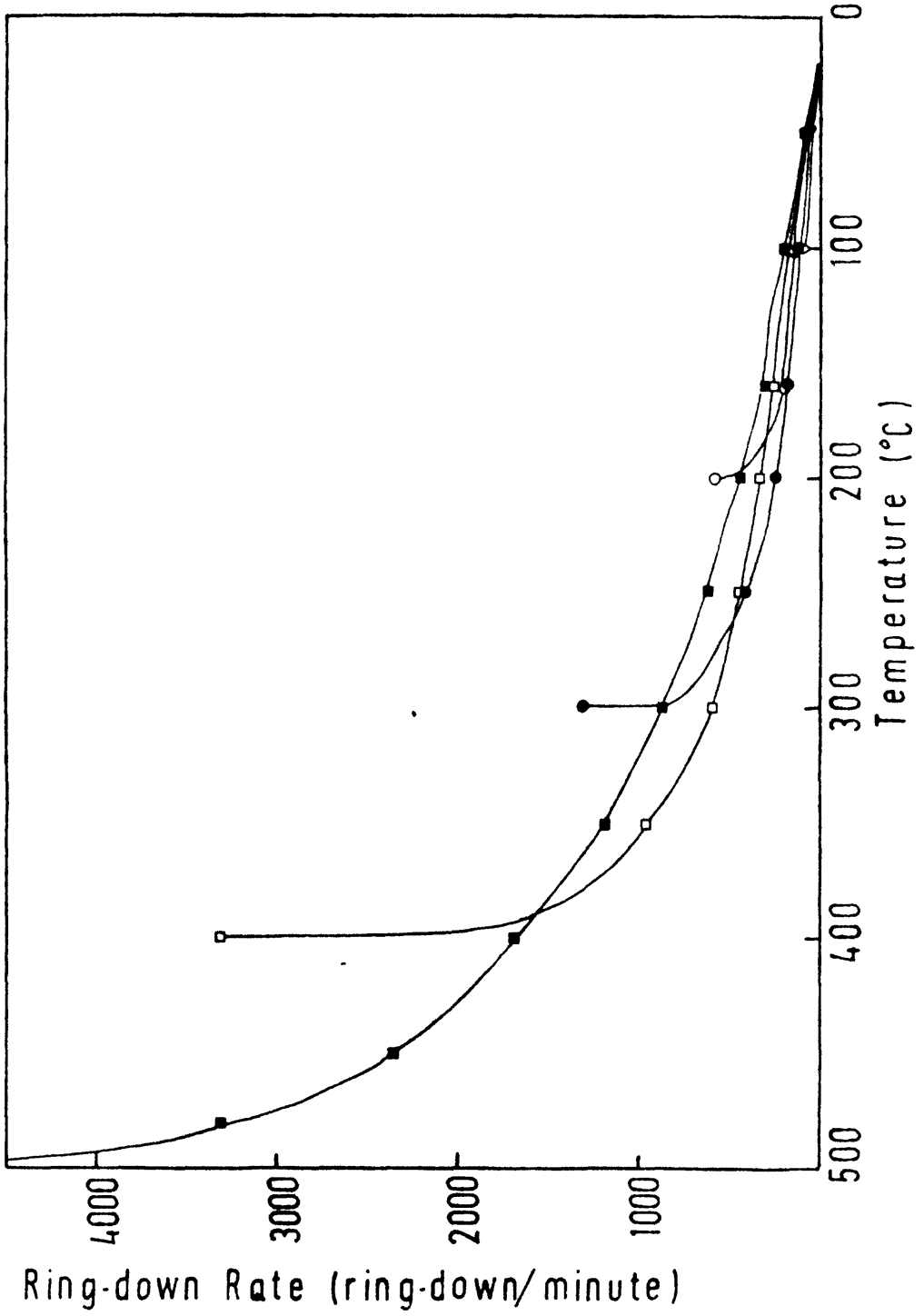
Ring-down Rate (ring-down/minute)
4000
3000
2000
1000
0
100
200
300
400
500
Temperature (°C)

Fig. 3

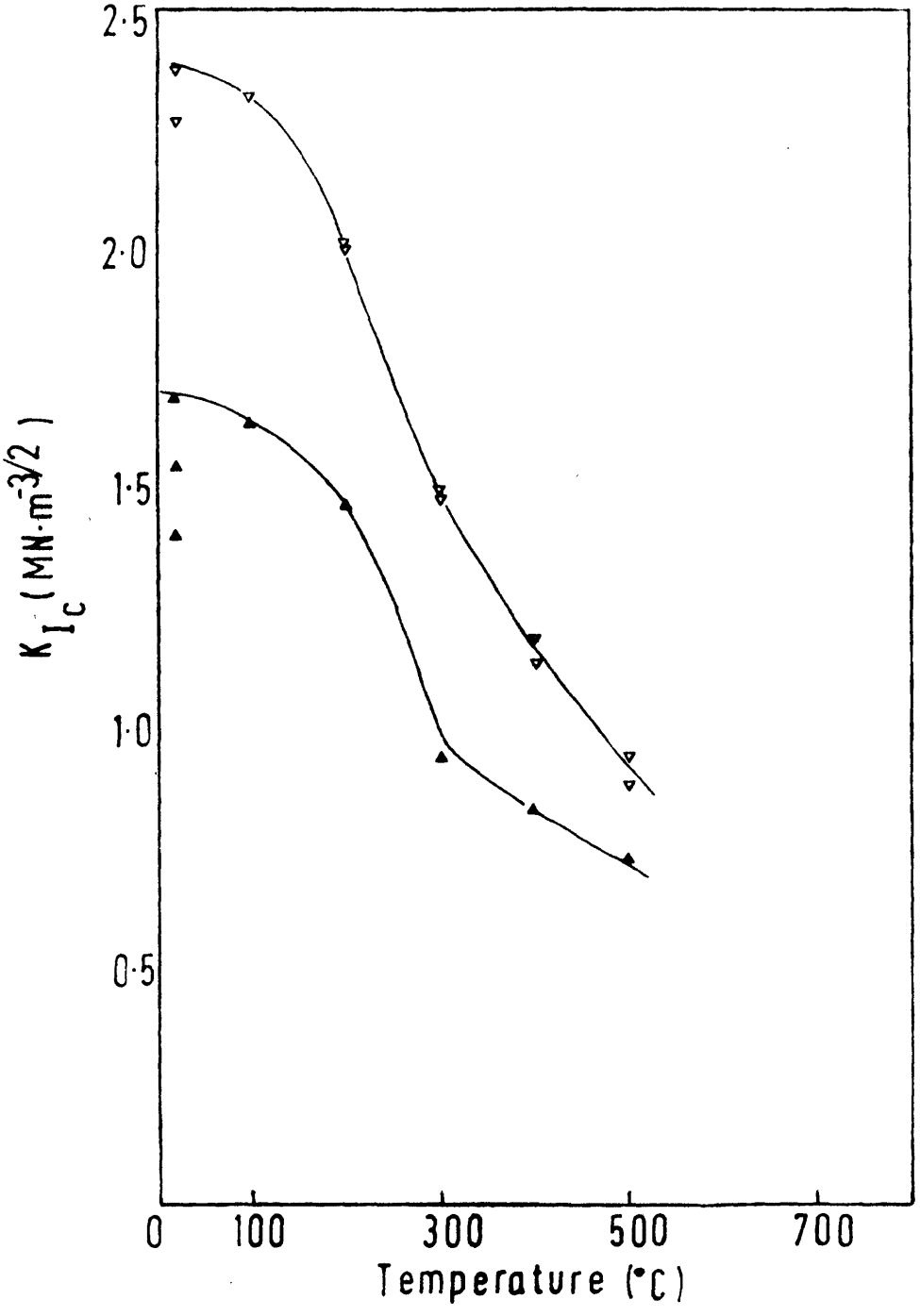

Fig. 4

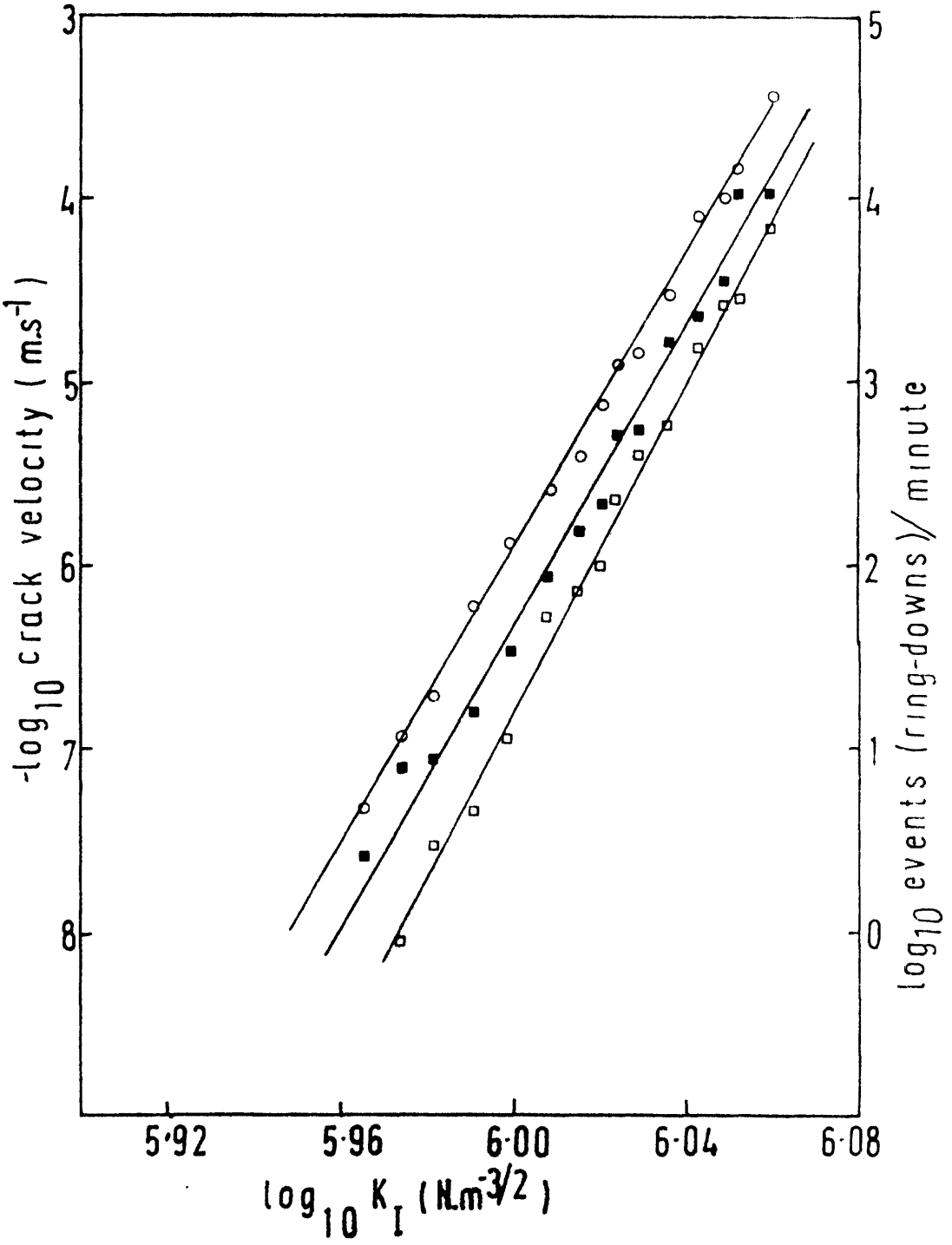
3
4
5
6
7
8
-log10 crack velocity (m.s-1)
5
4
3
2
1
0
log10 events (ring-downs)/ minute
5·92
5·96
6·00
6·04
6·08
log10 KI (N.m-3/2)

Fig. 5

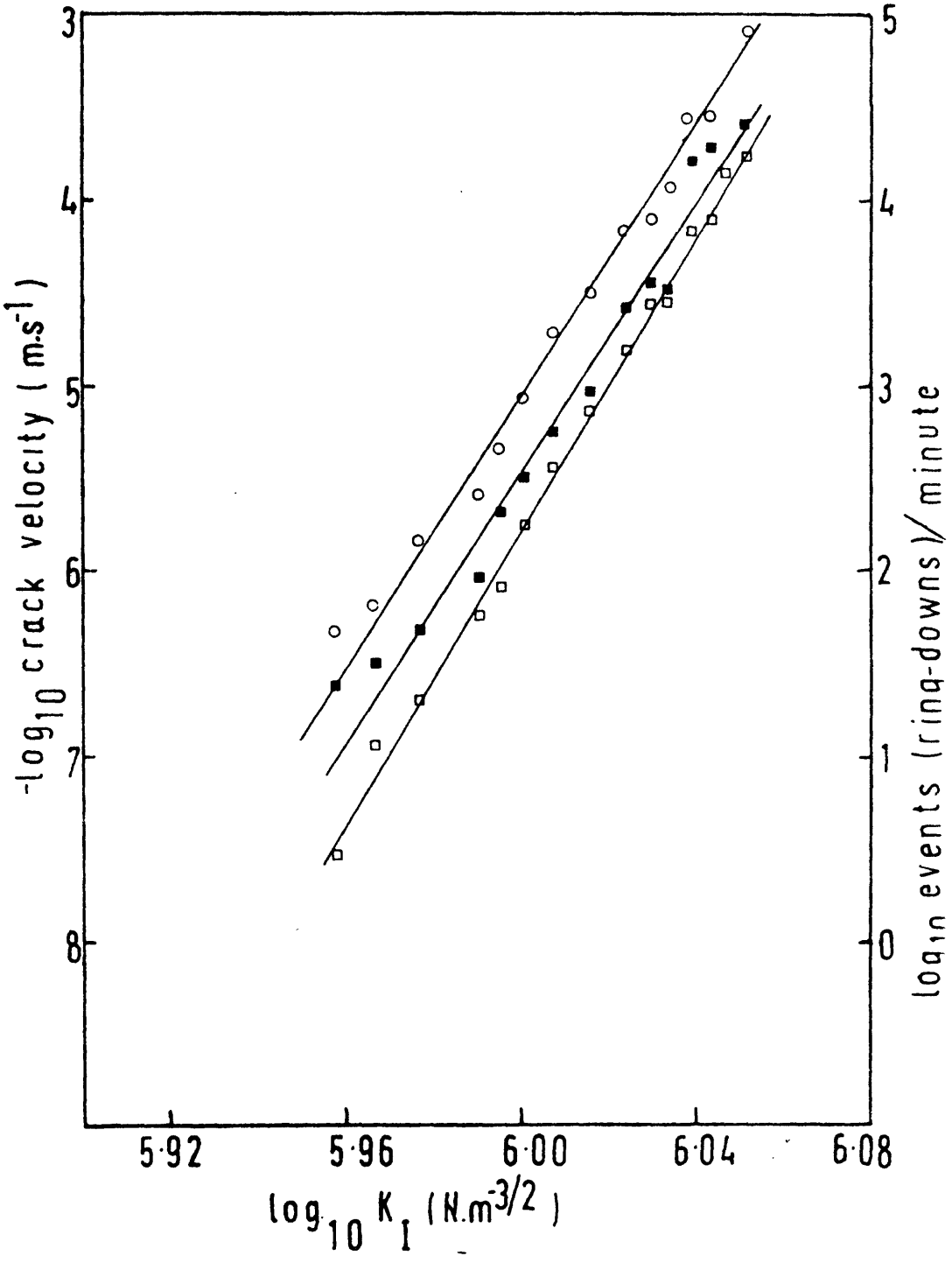
3
4
5
6
7
8
5
4
3
2
1
0
-log10 crack velocity (m.s-1)
log10 events (ring-downs)/ minute
5·92
5·96
6·00
6·04
6·08
log10 KI (N.m-3/2)

Fig. 6

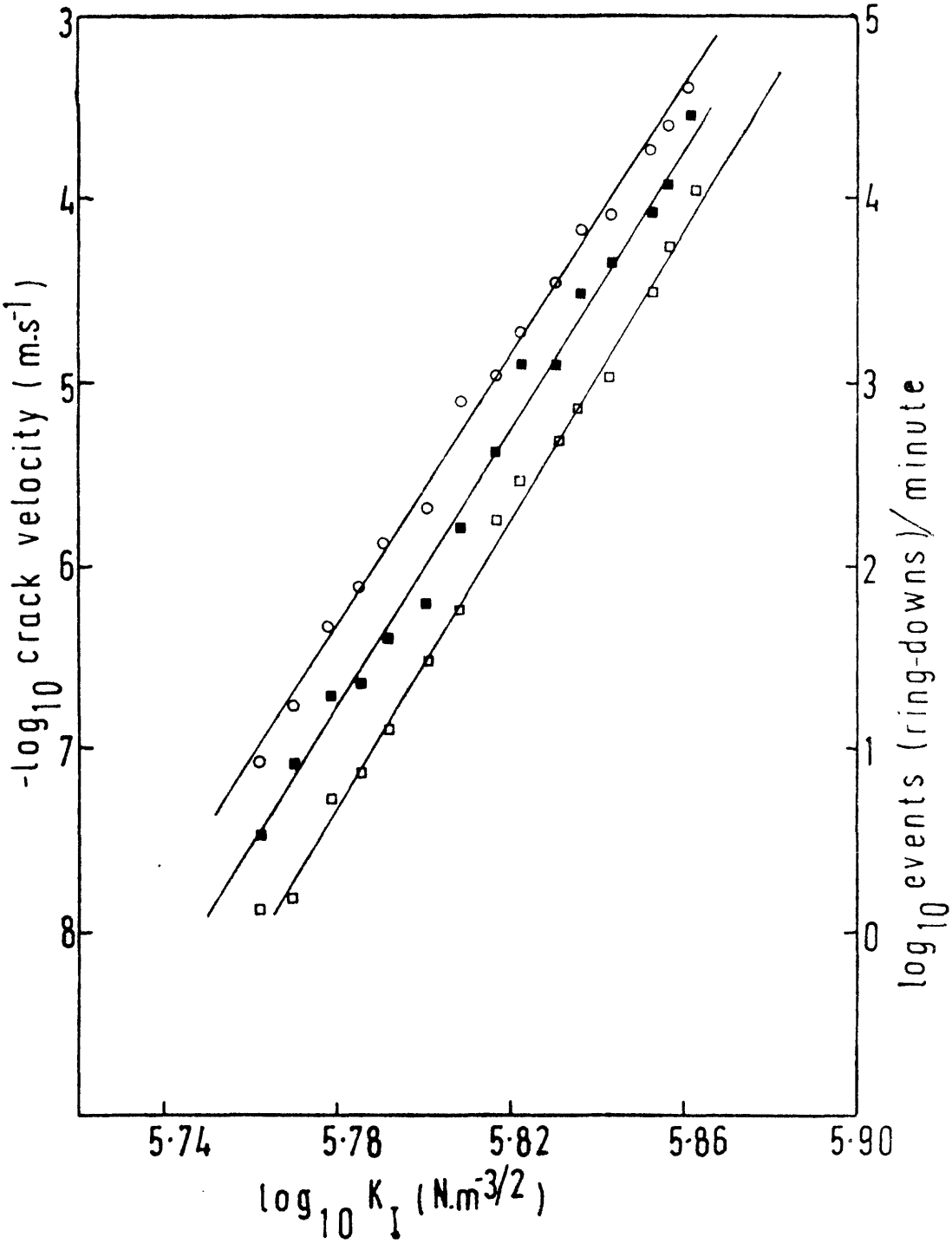
3
4
5
6
7
8
5
4
3
2
1
0
-log10 crack velocity (m.s-1)
log10 events (ring-downs)/ minute
5·74
5·78
5·82
5·86
5·90
log10 KI (N.m-3/2)

Fig. 7

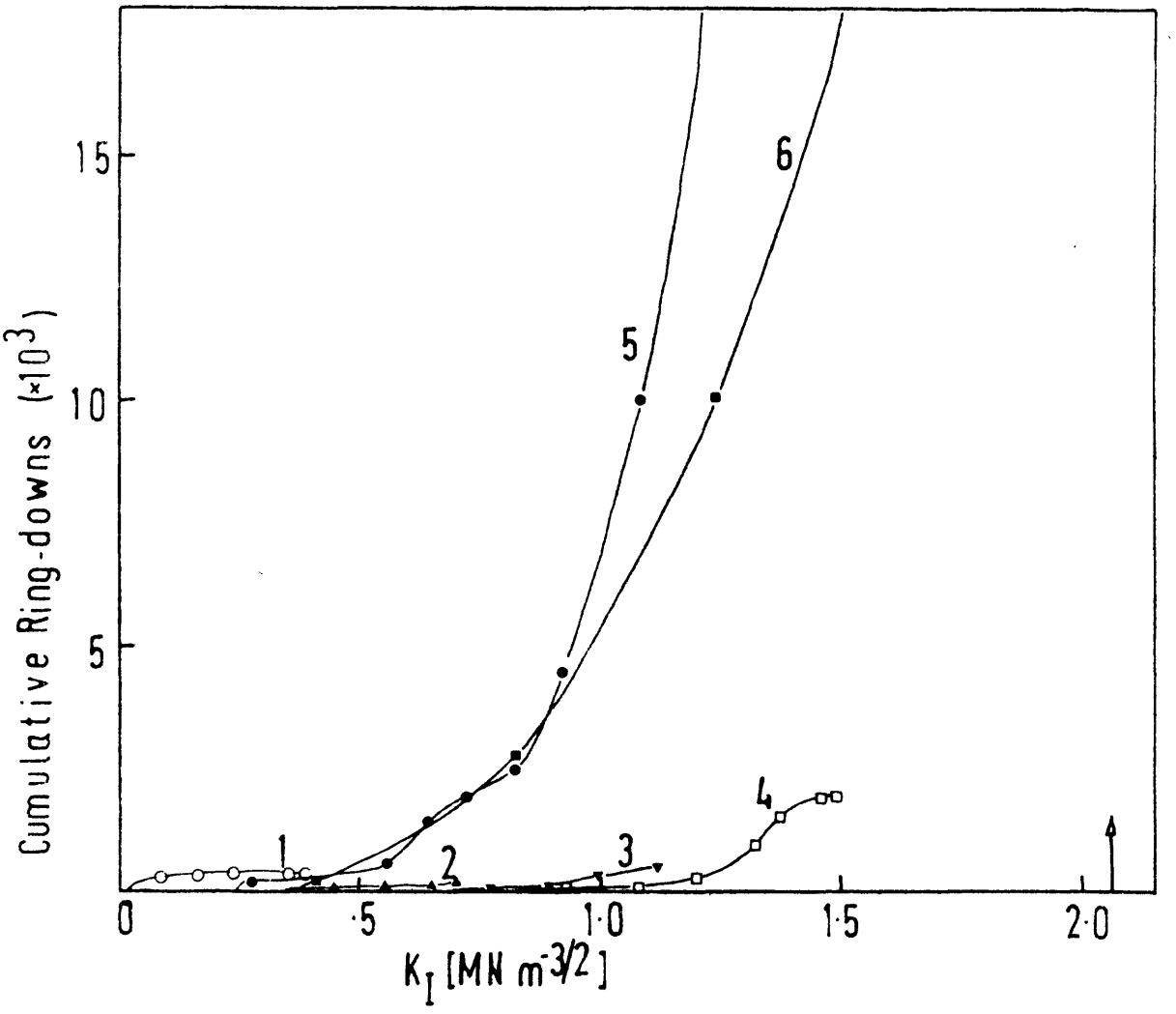

Fig. 8

5. INFLUENCE OF PORE WATER ON THE SLIDING OF FAULTS IN EXPERIMENTALLY DEFORMED WESTERLEY GRANITE AND PRESHAL MORE BASALT

S.M. Dennis and B.K. Atkinson

WESTERLEY GRANITE

The first part of this study into fault slip at low strain rates has concentrated on Westerley granite.

Experiments were carried out in fluid medium Heard type deformation rigs using 0.25" diameter cores.

Characterisation of Granite

The rock was first characterised by deforming wet and dry samples to failure at a constant strain rate of $10^{-5}sec^{-1}$, confining pressures from 0.1 MPa (1b) to 300 MPa (3Kb) and 250^{o}C (Fig.1).

The behaviour of the rock varies considerably with confining pressures: at low confining pressures failure is usually slow followed by stable sliding. At high confining pressures failure is sudden, often with a loud noise, followed by a rise in stress to a constant sliding stress (stable/stick-slip transition). Sudden failure and stable/stick-slip sliding are also commoner in wet samples.

Two main results are obtained from the confining pressure/strength relationships: i) our samples behaved in a similar way to those reported in the literature (Fig.2) and ii) water has little effect on the rock's strength (Fig.1) i.e. Rehbinder effects are not very important.

Microscopically the rocks seem to show little effect of confining pressure or whether they are wet or dry. The wet samples appear to have a narrower zone with widespread fracturing. There also appears to be more fine grained gouge of quartz and feldspar above 150 MPa (1.5 Kb). In general biotite is preserved, quartz develops some fractures and feldspar is most fractured. Through going fractures are usually anastamosing and intergranular. Extension fractures parallel to σ_1 are seen in some higher confining pressure samples.

Stress relaxation

Stress relaxation tests were carried out to establish the effects of the presence and pressure of pore fluids on sliding stress at low strain rates. Samples were prefractured at confining pressures of 200 MPa (2 Kb), strain rates of $10^{-5}sec^{-1}$ and temperatures of $25^{o}C$. They were then unloaded and pore fluid pressure added to 20 MPa (.2 Kb) or 100 MPa (1 Kb). Effective confining pressure was adjusted to 150 MPa (1.5 Kb), temperature to $300^{o}C$ and samples were reloaded to sliding. Relaxation was started and continued for several months or until no further relaxation was observed.

Results were as follows: 1) Dry granite shows no reduction in sliding stress at strain rates down to $10^{-11}sec^{-1}$ (Fig.3 WG 40); 2) The rock is weakened by wetting at strain rates less than $10^{-6.5}$-$10^{-8}sec^{-1}$, but not as much as Tennessee sandstone or Mojave quartzite (Rutter and Mainprice, 1978;

Atkinson et al., 1979) (Fig. 3, WG 30); 3) Increasing the pore fluid pressure (P_f) with effective pressure held constant results in a substantial increase in the rate of stress relaxation, (Fig. 3, WG 35).

Values of stress exponent 'n', where $\dot{e}$ and σ^n, were obtained from linear regression on the data showing significant strength reduction (Fig. 5). For P_f = 20 MPa (.2Kb) $n \simeq 25$, and for 100 MPa (1 Kb) $n \simeq 6$, although WG 35 showed a step with $n \simeq 17$ at strain rates less than $10^{-9}sec^{-1}$. This could be due to a change in the dominant deformation mechanism. Pressure solution, a possible deformation mechanism, gives $n = 1$, but stress corrosion gives higher values and seems more likely.

A relaxation test was also carried out using an unfractured specimen which had been brought to$\sim$ 80% of its fracture stress (Fig. 3, WG 37). Although P_f = 20 MPa (.2 Kb), no significant relaxation was observed at 300^{o}C and 150 MPa (1.5 Kb) effective pressure. This again suggests that pressure solution is not a viable mechanism as it would cause relaxation in unfractured samples.

A preliminary temperature cycling stress relaxation experiment was carried out to obtain an estimate of the activation enthalpy (H) for sliding in wet granite (Fig.4). The sample was relaxed at 400^{o}C, then at 300^{o}C with P_f (20 MPa) and effective pressure (150 MPa)held constant H can be calculated from the equation:

$$\dot{e} = G\ \sigma^{n} \exp.\ (-H/RT) \quad \text{(Rutter et al, 1978)}$$

Figures of 20 - 35 kJ. $mole^{-1}$ are obtained, but more experiments are needed to verify this.

Reproducibility

Values of 'n' are similar for experiments using similar conditions (Figs. 5 and 6). However, the initial stress varies considerably; this is probably due to specimen variability.

Long term constant strain rate experiments ($10^{-8} sec^{-1}$)

One long term experiment (WG 39) at 150 MPa (1.5 Kb) confining pressure, 20 MPa (.2 Kb) pore fluid pressure and 300°C has now been completed. Microscopic analysis is in progress. However, a slight leak developed during the test which meant it could only be run for 2 months and therefore a large enough strain may not have accumulated for easy microscope analysis. A repeat experiment (WG 42) is now in progress and stress-strain plots of both are shown in Fig. 7.

WG 39 shows stick-slip behaviour, although some of the variation in stress supported may be due to fluctuations in pressure. WG 42 is similar, but with much less variation in stress, except where the stress dropped due to furnace failure.

Another long term constant strain rate test (WG 43)

under similar conditions, but using O^{18} enriched pore fluid has just commenced. The deformed sample will be examined using the ion microprobe within the Royal School of Mines. Pressure solution should be identifiable by distinct overgrowth of O^{18} enriched minerals within the gouge zone. It should be possible to estimate values for the amount of material transferred during deformation and hence check the validity of the current phenomenological model of pressure solution.

O^{18} enriched water is separated from normal fluid using a diaphragm separator (Fig. 8 and 9). The system is first evacuated with valves 1 and 2 open. A microsyringe containing enough O^{18} enriched water is then connected to valve 2; when this is opened the water fills the system. Once the required temperature is reached, the normal pore fluid system is pressurized. This pressure is transmitted to the O^{18} enriched system by flexing of the diaphragm. Valve 1 is kept shut during the experiment to prevent contamination of O^{18} enriched water if the diaphragm should break. Pressure is monitored using the pressure transducer.

Artificial gouge Experiments

Microstructural development of artificial gouges (e.g. kaolinite) in faults and saw-cuts in Westerley granite is to be studied.

Larger cores (1 - 1½" diameter) are to be used so as to

Figure Captions

Figure 1. Ultimate stress (sliding stress)/confining pressure data for Westerley granite.

Figure 2. Synoptic diagram of previous work on Westerley granite.

Figure 3. Stress relaxation data for wet and dry Westerley granite.

Figure 4. Influence of temperature on stress relaxation of Westerley granite.

Figure 5. Synoptic diagram of stress relaxation data for Westerley granite.

Figure 6. Repeat experiments on stress relaxation of Westerley granite.

Figure 7. Stress/strain curves at low strain rates for faulted Westerley granite.

Figure 8. Schematic separator system for O^{18} enriched isotope exchange experiments.

Figure 9. O^{18}/normal water separator.

Figure 10. Schematic diagram of Hoek-Franklin cell.

Figure 11. Ultimate stress (sliding stress)/confining pressure data for Preshal More basalt.

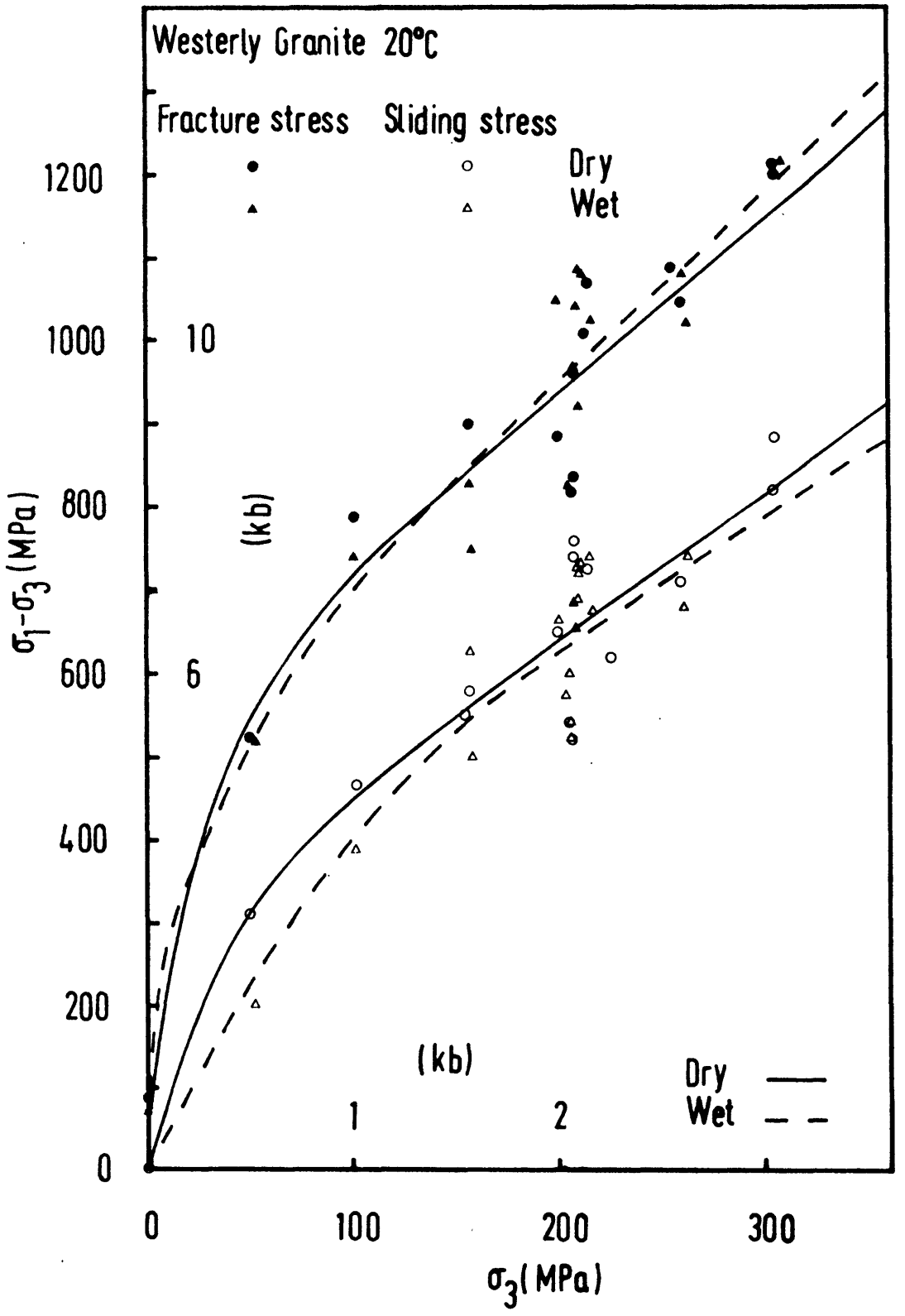
Westerly Granite 20°C
Fracture stress
Sliding stress
Dry
Wet
1200
1000
800
600
400
200
0
10
6
(kb)
$\sigma_1-\sigma_3$ (MPa)
(kb)
1
2
Dry
Wet
0
100
200
300
σ_3 (MPa)

FIG. 1.

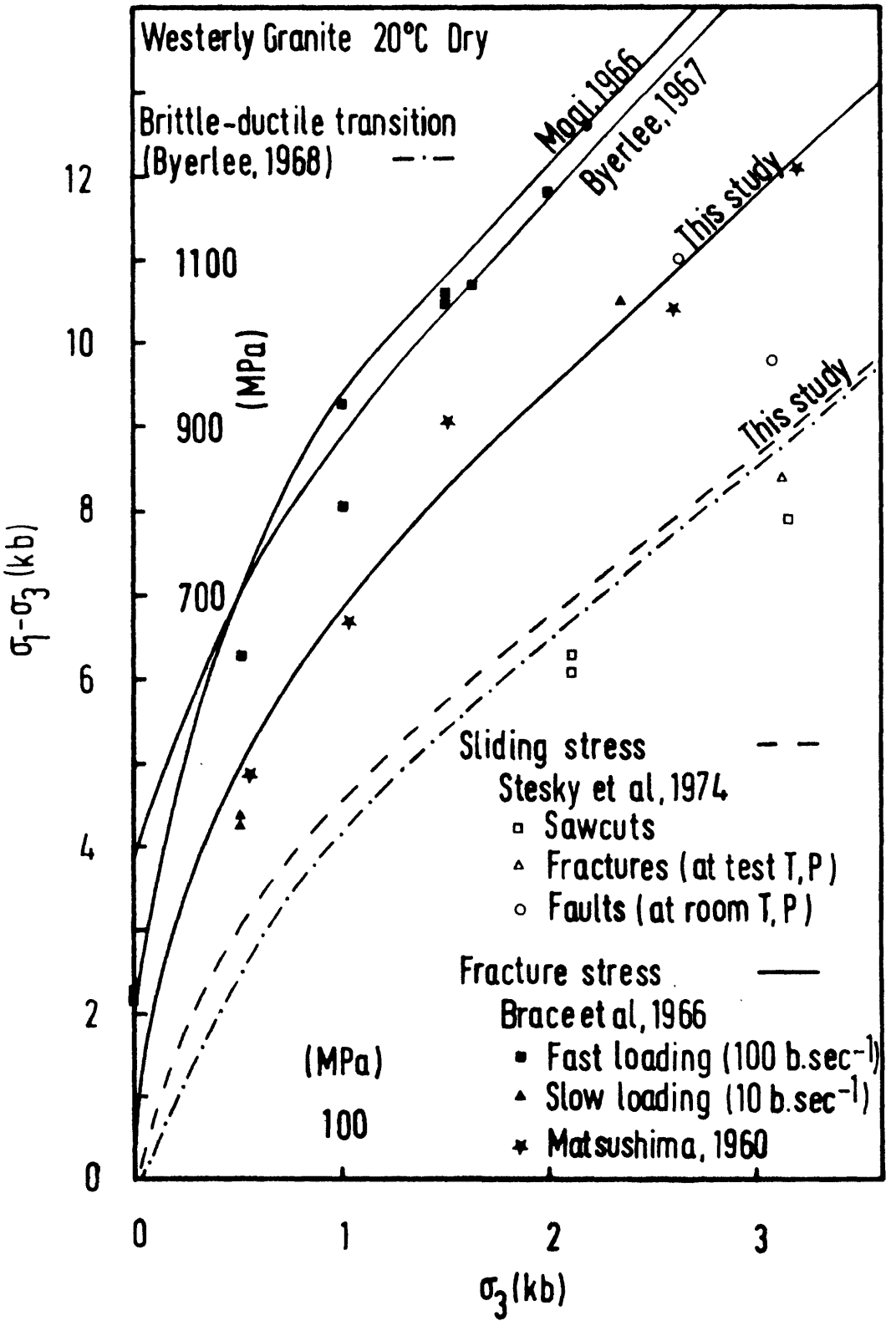
Westerly Granite 20°C Dry
Brittle-ductile transition
(Byerlee, 1968)
Mogi, 1966
Byerlee, 1967
This study
This study
1100
900
700
(MPa)
100
(MPa)
Sliding stress
Stesky et al, 1974
Sawcuts
Fractures (at test T, P)
Faults (at room T, P)
Fracture stress
Brace et al, 1966
Fast loading (100 b.sec⁻¹)
Slow loading (10 b.sec⁻¹)
Matsushima, 1960
σ1-σ3 (kb)
σ3 (kb)
0
2
4
6
8
10
12
0
1
2
3

FIG. 2.

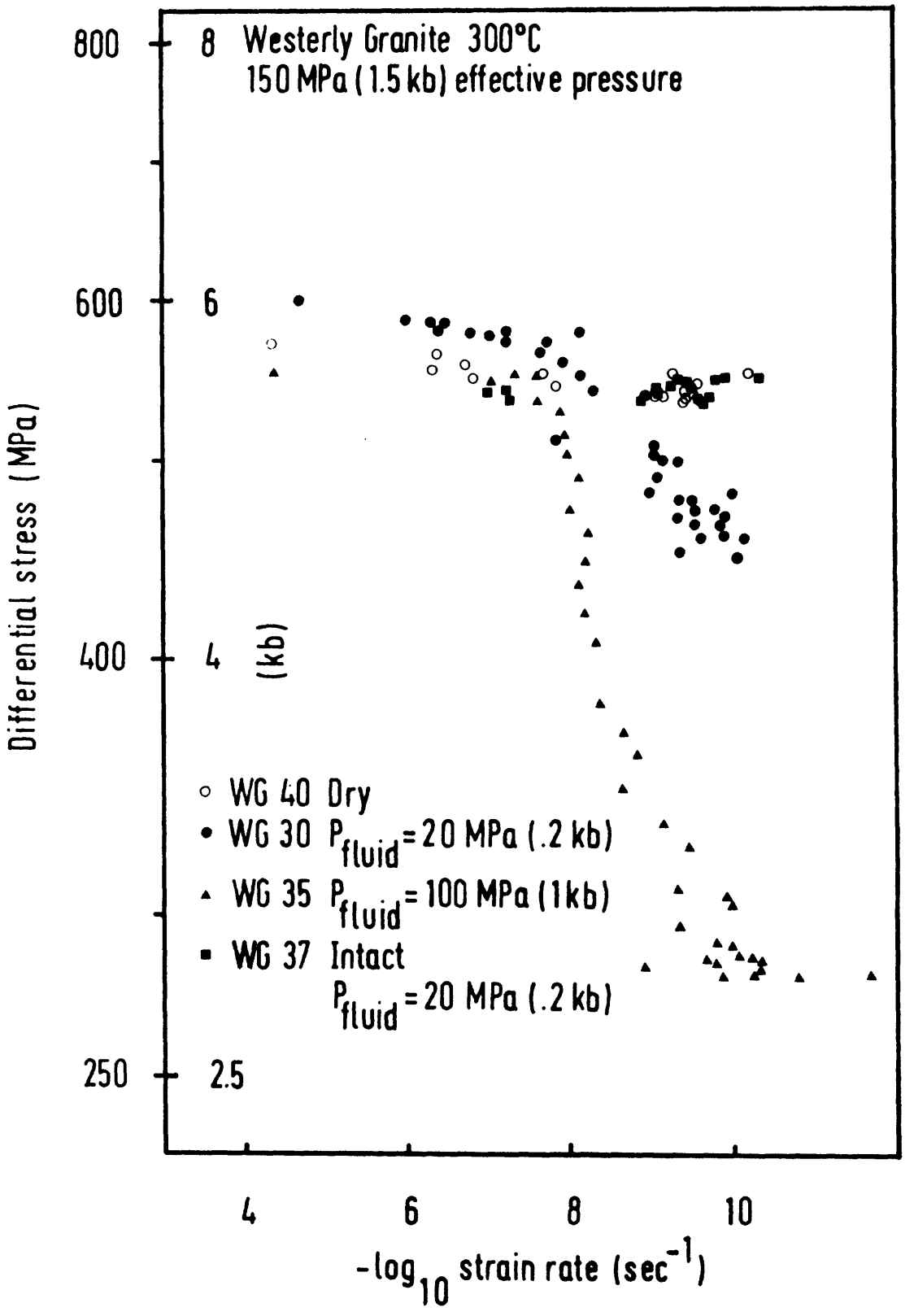
800
600
400
250
8
6
4
2.5
(kb)
Westerly Granite 300°C
150 MPa (1.5 kb) effective pressure
Differential stress (MPa)
WG 40 Dry
WG 30 P_{fluid} = 20 MPa (.2 kb)
WG 35 P_{fluid} = 100 MPa (1 kb)
WG 37 Intact
P_{fluid} = 20 MPa (.2 kb)
4
6
8
10
$-\log_{10}$ strain rate (sec^{-1})

FIG. 3.

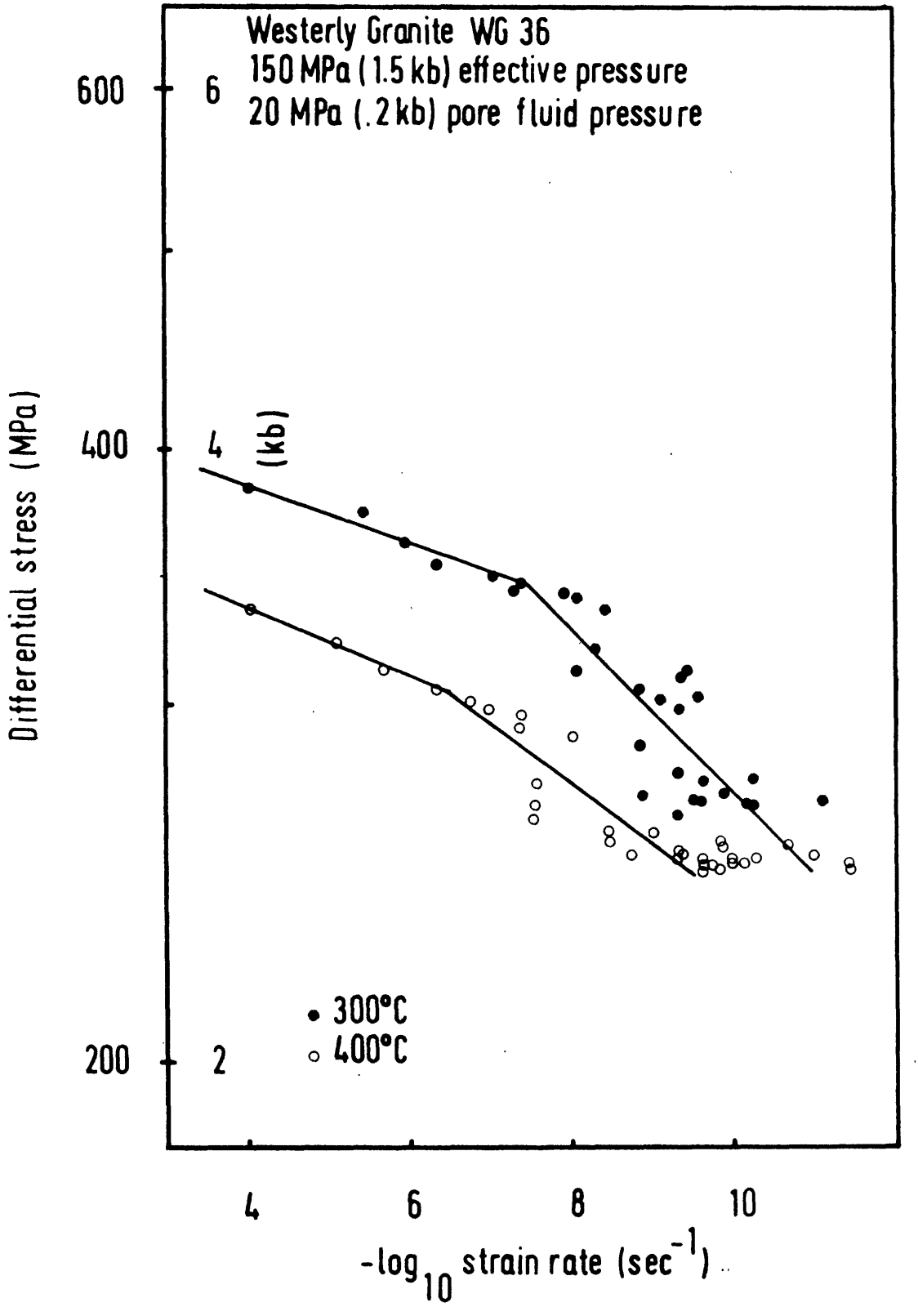
Westerly Granite WG 36
150 MPa (1.5 kb) effective pressure
20 MPa (.2 kb) pore fluid pressure
600
6
400
4
(kb)
200
2
• 300°C
○ 400°C
Differential stress (MPa)
4
6
8
10
-log10 strain rate (sec-1)

FIG. 4.

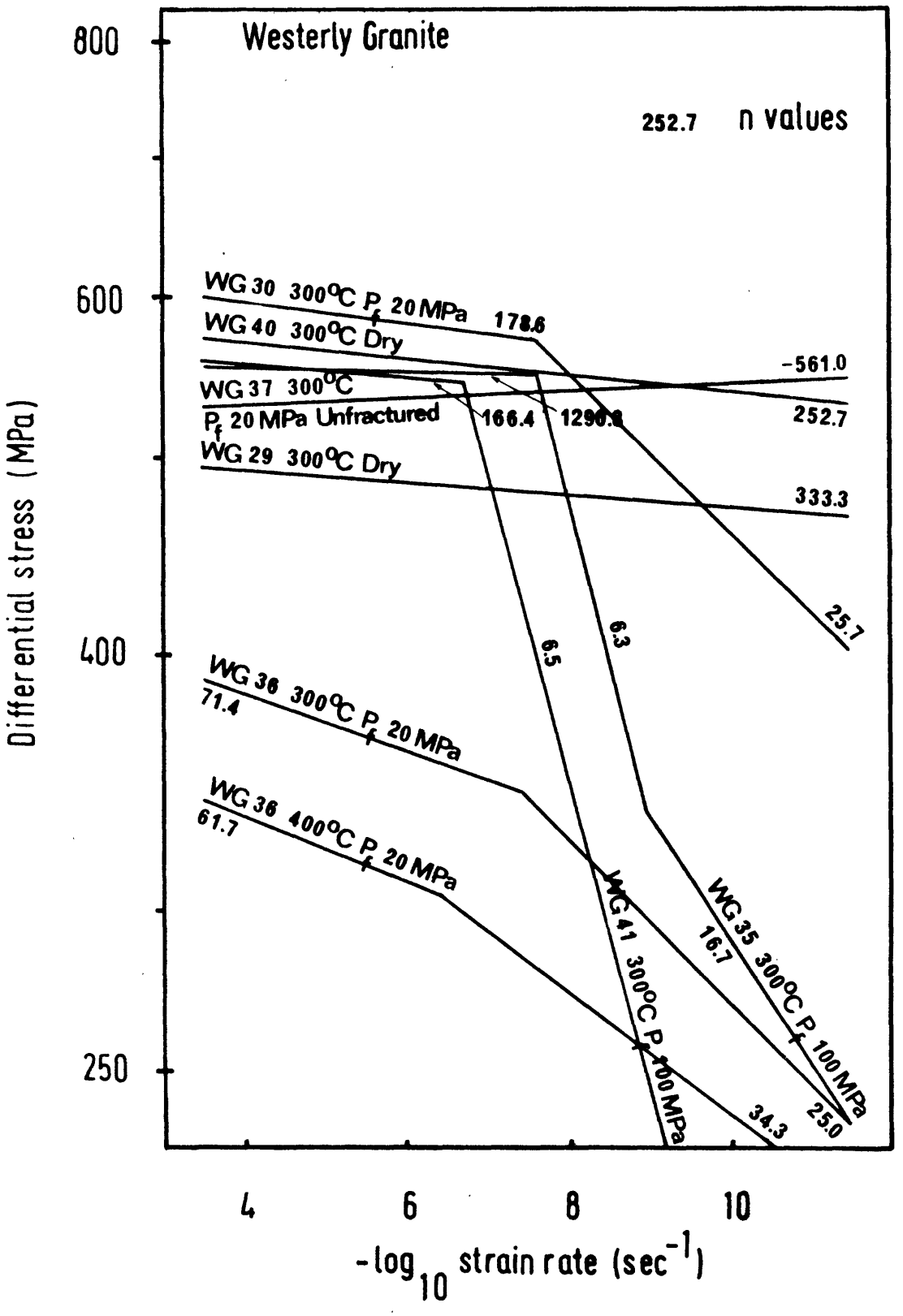
Westerly Granite
n values
800
600
400
250
Differential stress (MPa)
WG 30 300°C Pf 20 MPa
178.6
WG 40 300°C Dry
WG 37 300°C
Pf 20 MPa Unfractured
166.4
1290.8
WG 29 300°C Dry
252.7
-561.0
333.3
25.1
6.5
6.3
WG 36 300°C Pf 20 MPa
71.4
WG 36 400°C Pf 20 MPa
61.7
WG 41 300°C Pf 100 MPa
34.3
WG 35 300°C Pf 100 MPa
16.7
25.0
4
6
8
10
-log10 strain rate (sec-1)

FIG. 5.

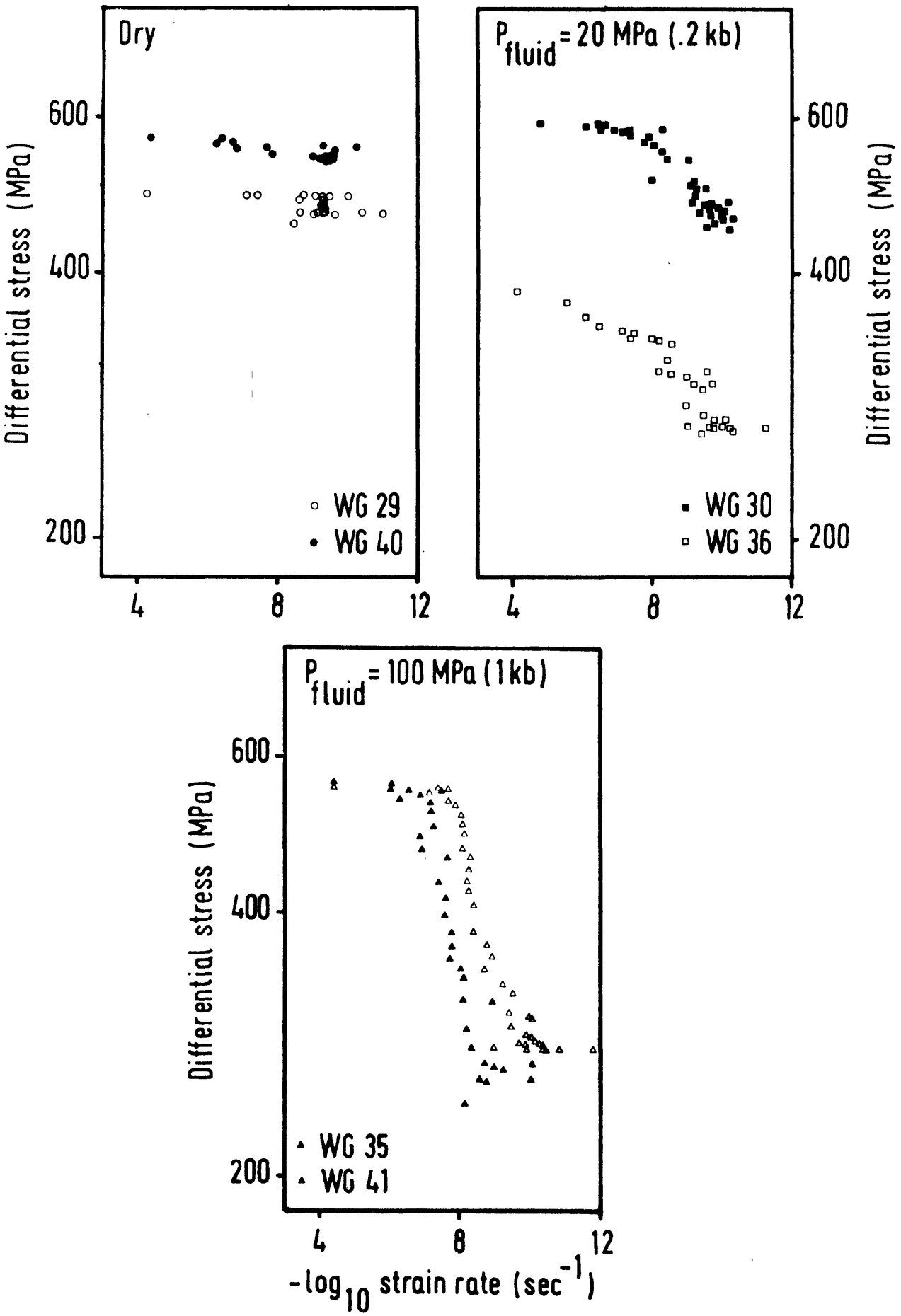
Dry
P_{fluid} = 20 MPa (.2 kb)
P_{fluid} = 100 MPa (1 kb)
Differential stress (MPa)
600
400
200
4
8
12
WG 29
WG 40
WG 30
WG 36
WG 35
WG 41
$-\log_{10}$ strain rate (sec^{-1})

FIG. 6

FIG. 7.

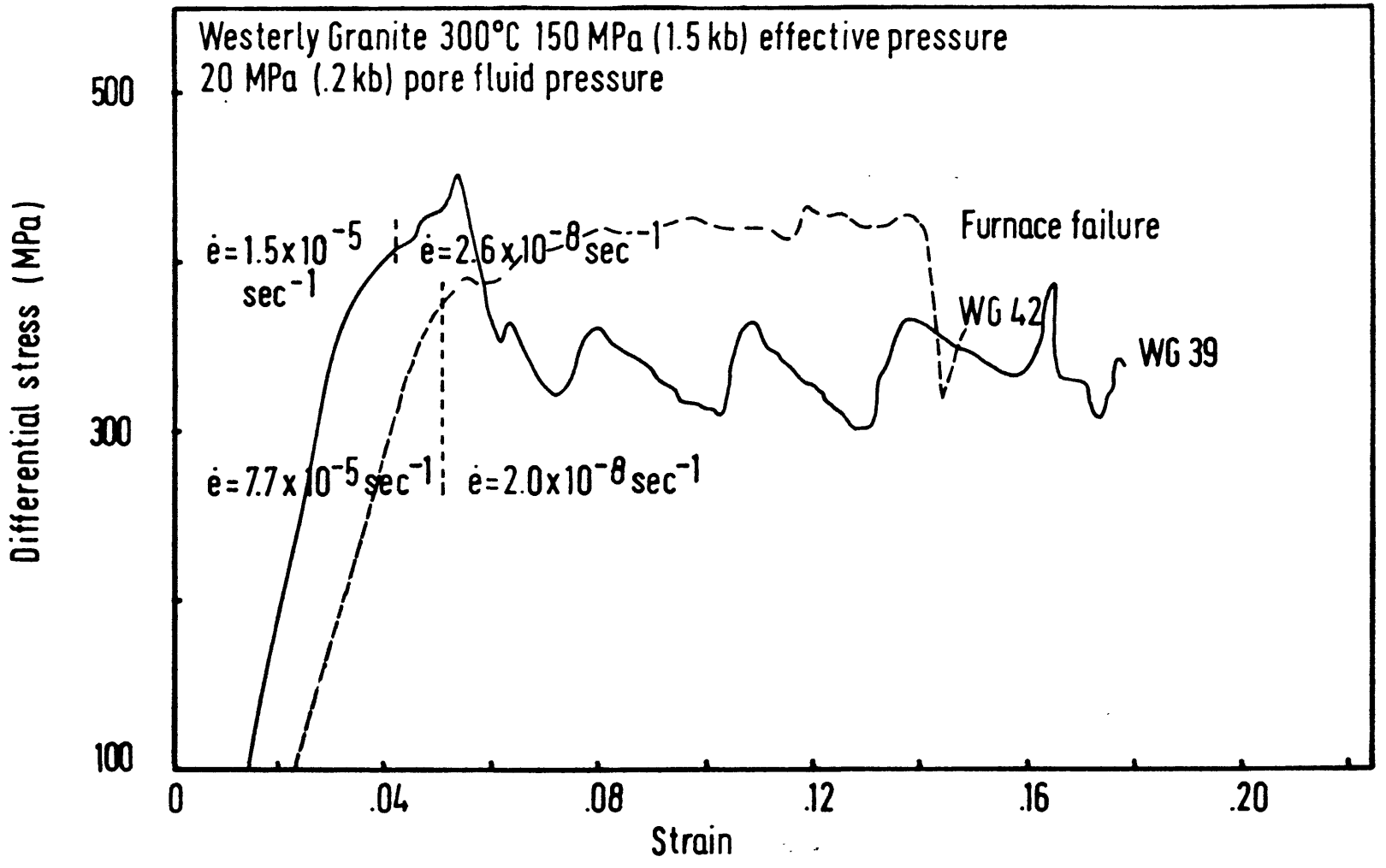
Westerly Granite 300°C 150 MPa (1.5 kb) effective pressure
20 MPa (.2 kb) pore fluid pressure
Differential stress (MPa)
500
300
100
0
.04
.08
.12
.16
.20
Strain
ė=1.5x10⁻⁵ sec⁻¹
ė=2.6x10⁻⁸ sec⁻¹
ė=7.7x10⁻⁵ sec⁻¹
ė=2.0x10⁻⁸ sec⁻¹
Furnace failure
WG 42
WG 39

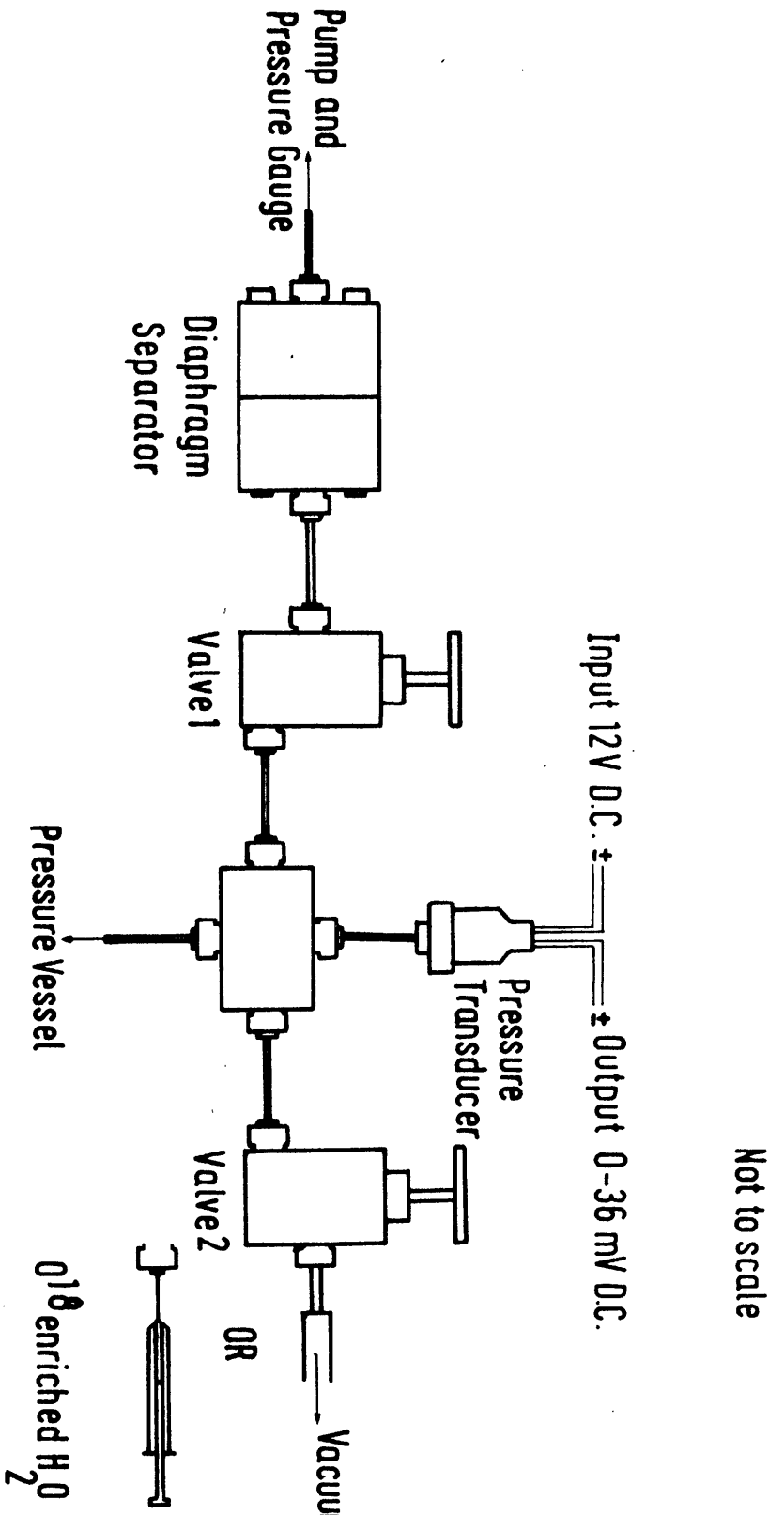
Not to scale
Input 12V D.C. ±
± Output 0-36 mV D.C.
Pump and Pressure Gauge
Diaphragm Separator
Valve 1
Pressure Transducer
Pressure Vessel
Valve 2
OR
Vacuum Pump
O18 enriched H2O

FIG. 8.

Not to scale

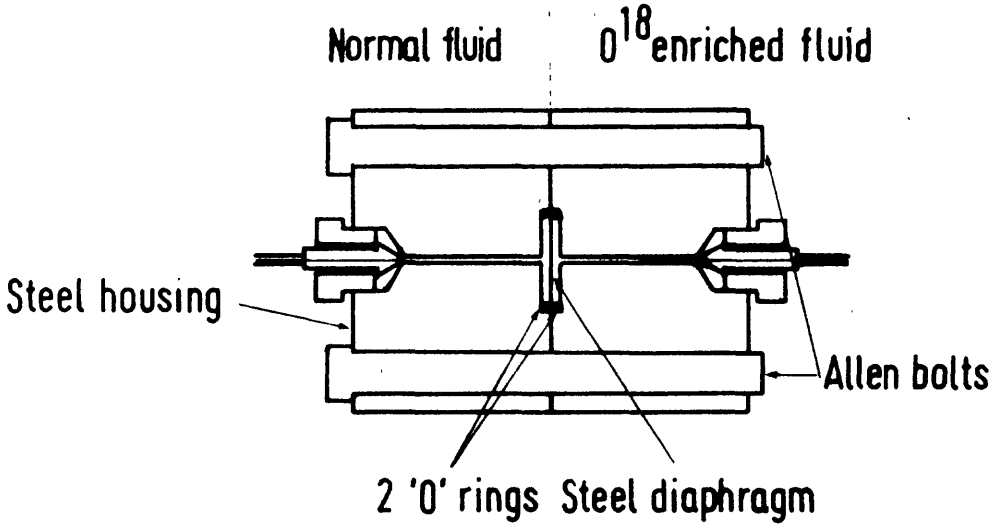

FIG. 9.

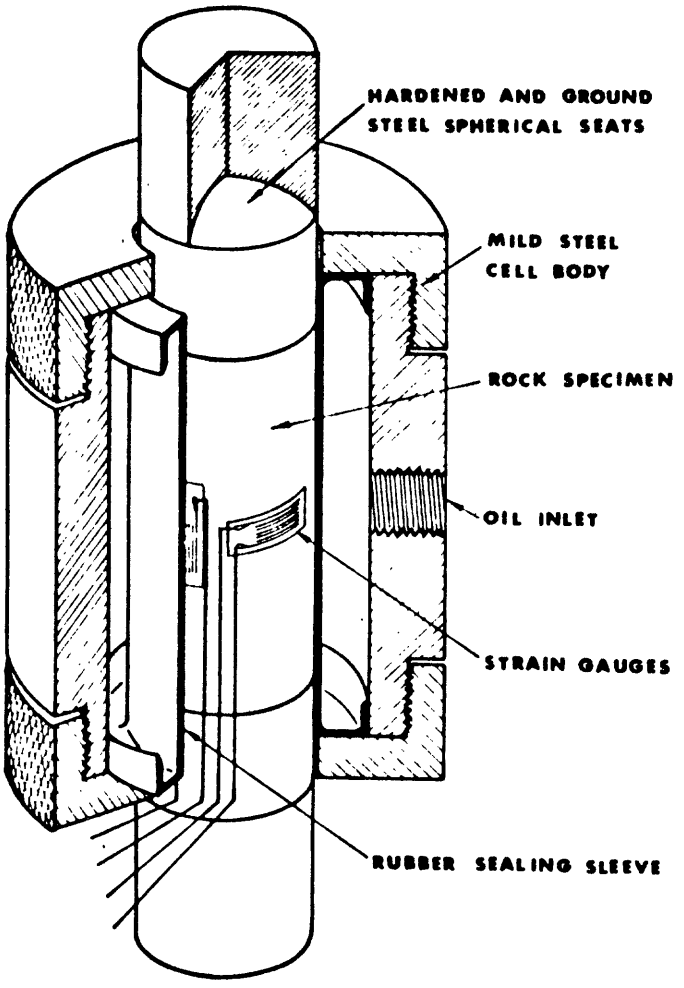
HARDENED AND GROUND
STEEL SPHERICAL SEATS
MILD STEEL
CELL BODY
ROCK SPECIMEN
OIL INLET
STRAIN GAUGES
RUBBER SEALING SLEEVE

FIG. 10.

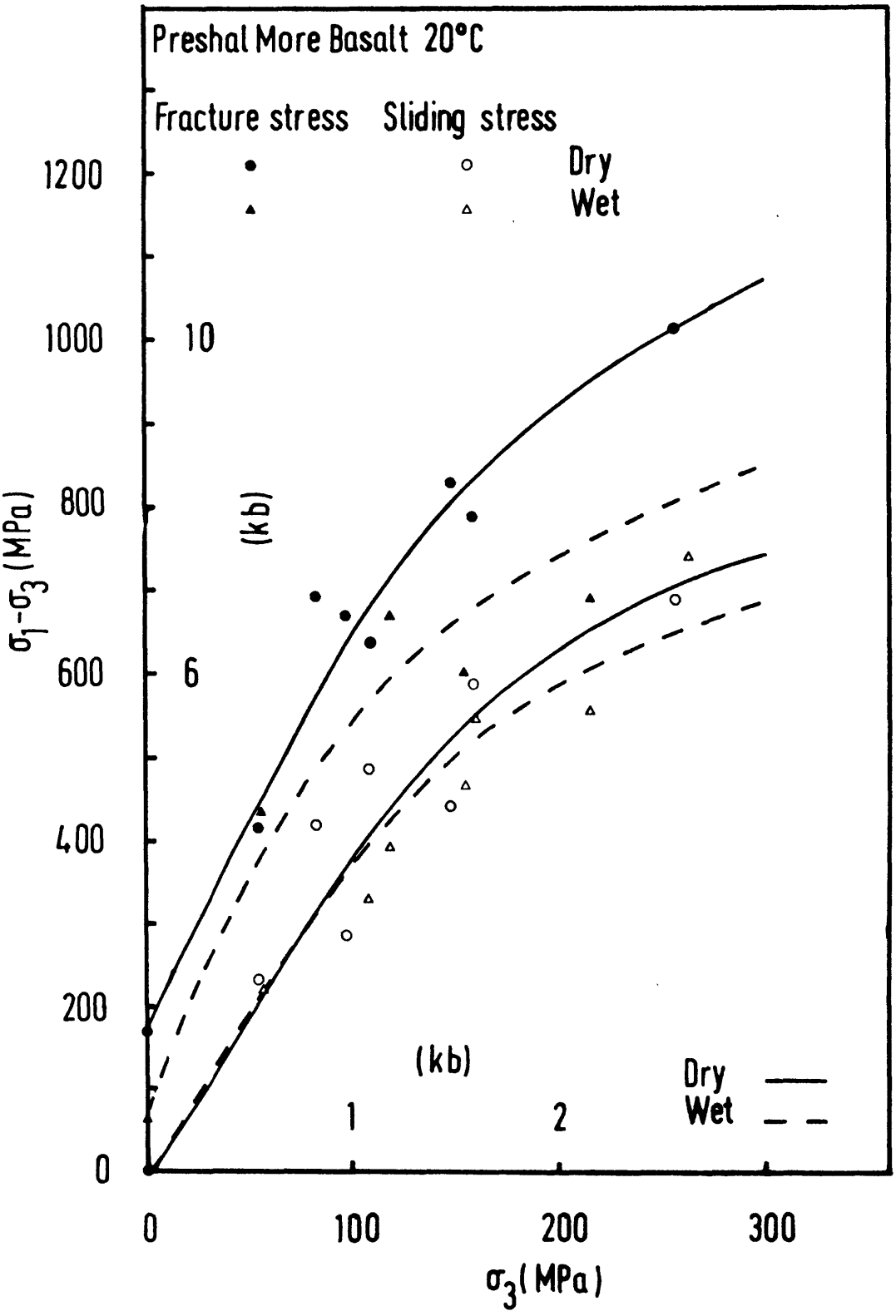
Preshal More Basalt 20°C
Fracture stress
Sliding stress
Dry
Wet
1200
1000
800
600
400
200
0
10
6
(kb)
$\sigma_1-\sigma_3$ (MPa)
(kb)
1
2
Dry
Wet
0
100
200
300
σ_3 (MPa)

6. DEVELOPMENT OF TECHNIQUES TO MEASURE MODE II CRACK PROPAGATION PARAMETERS.

B.K. Atkinson, R.F. Holloway

Two methods have been chosen to obtain mode II crack growth parameters.

The first is called the compact shear specimen and is based upon work done by metallurgists (Jones and Chisholm, 1975). This specimen contains two cracks, is fully symmetric about the centre axis, but is fully asymmetric about the crack tips. The mode II stress intensity factor for this specimen is given by

$$K_{II} = (1.08)\sigma\, a^{\frac{1}{2}} \qquad (1)$$

where σ is the applied stress and a is the crack length. Apparatus to allow the use of this specimen in rock testing has been constructed.

The second method is based upon an idea put forward by Rice (1979). In essence, the post-failure region of a stress/displacement curve can be analyzed in the following way to give a value of the critical strain energy release rate (G_{II}) which is related to K_{II} through the elastic constants. The area under a curve describing the post-failure shear stress/displacement behaviour between the peak stress and the post-failure sliding stress is equal to G_{II}. To obtain useful data a rather stiff machine is required.

Preliminary calculations using both these methods suggests that G_{II} is of the order of $10^4 J.m^{-2}$ for granite.

References

Jones, D.L. and Chisholm, D.B. 1975. An investigation of the edge-sliding mode in fracture mechanics. Engineering Fract. Mech. 7, 261-270.

Rice, J.R. 1979. The mechanics of earthquake rupture. Proc. Int. School of Physics 'Enrico Fermi', Course LXXVIII (in press).

7. SHORT ROD K_{Ic} EXPERIMENTS

P.G. Meredith and B.K. Atkinson

Apparatus for running short rod tests on cores of rock to determine K_{Ic} has been constructed and is now in use on a routine basis.

The peak pressure in a flat jack required to propagate an internal wedge-shaped crack in the core is a measure of K_{Ic} through the equation

$$K_{Ic} = AP\sqrt{B} \qquad (1)$$

where P is the peak pressure, B is the specimen diameter and A is a dimensionlesss constant obtained by calibration experiments.

We have calibrated this apparatus using soda-lime glass as a standard and made determinations of K_{Ic} in a number of rocks at room temperature in air. These are compared in the table below with data on K_{Ic} for the same materials, but obtained using the double torsion apparatus.

Material	K_{Ic} ($MN.m^{-3/2}$)	
	SR	DT
Westerley granite	1.62±0.08	1.74
Pink granite	1.53±0.17	1.66
Black gabbro	2.73±0.40	2.88
Whin Sill dolerite	2.96±0.19	3.28
Preshal More basalt	2.50±0.14	
Icelandic tholeiite	0.87±0.06	
Serpentinized dunite	1.39±0.38	
Arkansas novaculite	1.77±0.25	1.34
Oughtibridge gannister	1.39±0.27	
Penant sandstone	1.97±0.06	
Tennessee sandstone	0.79±0.05	0.45
Carrara marble	0.82±0.04	0.64
Solnhofen limestone	1.09±0.06	1.06

8. APPARATUS DEVELOPMENT

P.G. Meredith, S.M. Dennis, B.K. Atkinson, R.F. Holloway

Apparatus required for fracture mechanics tests are largely completed. Newly manufactured apparatus includes short-rod apparatus, high-temperature/high vacuum double torsion apparatus and internally pressurized thick-walled cylinder apparatus. Additionally apparatus development for compact shear measurement of mode II stress intensity factors and post-failure analysis of stress-displacement records is in hand. We are also attempting to design apparatus for mode III, anti-plane shear measurements of stress intensity factors.

Apparatus required for isotopic exchange experiments in slow sliding tests has been built and is described in an earlier section. A number of different techniques are being developed for looking at the textural development of gouge during relatively large-displacement experiments.

We are also building apparatus for creep measurements on gouge and developing ways of looking at scale effects in frictional sliding.

9. FUTURE WORK

We are poised, waiting to begin the extensive measurement stage of our project. Most of the apparatus development is completed or in hand, and we lack only the funds to begin work.

If further delay in funding occurs we will not be able to maintain the scientific momentum of our effort, nor keep our research team together. This would be a cruel waste of our effort and USGS funds.

10. PUBLICATIONS ARISING DURING THIS CONTRACT PERIOD.

Atkinson, B.K., 1980. An outline proposal of some aims, strategies and objectives in earthquake prediction. In Proceedings 2nd Workshop on European Earthquake Prediction Programme jointly organised by European Space Agency and Parliamentary Assembly of the Council of Europe, Strasbourg, 1980, 135-155.

Atkinson, B.K., 1980. Fracture Mechanics modelling of earthquake generating processes. In Proceedings of an Interdisciplinary Conference on Earthquake Prediction Research in the N. Anatolian Fault Zone, Istanbul, 1980 (in press)

Atkinson, B.K. and Avdis, V., 1980. Fracture Mechanics parameters of some rock-forming minerals determined with an indentation technique. Int. J. Rock Mech. Min. Sci. and Geomech. Abstr. (in press).

Norton, M.G. and Atkinson, B.K., 1980. Stress-dependent morphological features on fracture surfaces of quartz and glass. Tectonophysics (in press).

Atkinson, B.K. 1980. Review of subcritical crack propagation in rock. Proc. 26th International Geological Congress, Paris, 1980. (To be published in J. Struct. Geol.).

Atkinson, B.K. and Rawlings, R.D., 1980. Acoustic emission during stress corrosion cracking in rocks. Proc. 3rd Maurice Ewing Symposium on Earthquake Prediction, New York, 1980. Geophysical Union (in press).

Atkinson, B.K. and Meredith, P.G. 1980. Stress corrosion of quartz: Influence of chemical environment. Tectonophysics (in press).

Meredith, P.G. and Atkinson, B.K. 1980. Stress corrosion and acoustic emission of Whin Sill dolerite (in prep.).

Dennis, S.M. and Atkinson, B.K. 1980. The influence of pore fluids on the sliding of faulted surfaces of Westerley granite under simulated geologic environments (in prep.).

Dennis, P.F. and Atkinson, B.K. 1980. Flow and fracture deformation mechanism maps for quartz (in preparation).

Atkinson, B.K. 1981. Earthquake prediction precursors. Physics in Technology 12.

Atkinson, B.K. 1980. How to take the shock out of earthquakes. The Guardian, 25 September.